ABSTRACT

Title of Dissertation: SEQUENTIAL EXPRESSION OF NICOTINIC ACETYLCHOLINE RECEPTOR SUBUNITS SUPPORTS DEVELOPMENT AND PLASTICITY OF A *DROSOPHILA* CENTRAL SYNAPSE

Justin Rosenthal, Doctor of Philosophy, 2021

Dissertation directed by: Dr. Quan Yuan, National Institute of Neurological Disorders and Stroke
&
Dr. Leslie Pick, Department of Entomology

The central nervous system (CNS) of animals is arguably one of the most sophisticated instruments designed by nature, and one its cardinal components is the postsynaptic specialization. Decades of studies on the cholinergic neuromuscular junction and the central glutamatergic synapses in vertebrate organisms has informed us of just how many factors are at play during postsynaptic development. However, despite its importance, the central cholinergic synapse is one system lacking the same knowledge base as the above models. The thesis work presented here was designed with the aim of understanding if and how nicotinic acetylcholine receptor (nAchR) activity at the postsynapse is used by a developing neuron to shape the structural and functional properties of the synapse and its dendrite arbor during normal periods of

maturation. To this end, we employed the ventral lateral neuron (LNv) as a cellular model for *Drosophila* CNS development. This small group of cells are second-order projection neurons which convey visual activity to higher brain centers and are also critical mediators of adjusting the fly's internal circadian clock. We report how nAchRs not only play a role in LNv neurophysiology by the end of larval development but show how in fact they actively participate during the formation and refinement of the LNv postsynapse. Our transcriptomic, morphological and physiological approaches reveal that two functionally distinct nAchR subunit genes, *Dα1* and *Dα6*, are preferentially expressed during separate periods of larval development. Here, young and immature LNvs are characterized by high *Dα6* expression which facilitates synaptic formation. As the animal grows, *Dα6* is downregulated and *Dα1* is upregulated, which is necessary for synaptic stabilization and maturation. We also expand the scope of our primary investigation by identifying promising candidate genes, including transcription factors, molecular chaperones and membrane-associated proteins, that are key to orchestrating the successive stages of nAchR expression, maturation and postsynaptic activity. In summary, our findings will work to clarify *in vivo* subunit-specific functionalities for the insect nAchR and illustrate how individual nAchR subunits in the CNS are coordinately regulated within a single cell through time to actively regulate distinct properties of the synapse during development.

SEQUENTIAL EXPRESSION OF NICOTINIC ACETYLCHOLINE RECEPTOR SUBUNITS SUPPORTS DEVELOPMENT AND PLASTICITY OF A *DROSOPHILA* CENTRAL SYNAPSE

by

Justin Rosenthal

Dissertation submitted to the Faculty of the Graduate School of the
University of Maryland, College Park, in partial fulfillment
of the requirements for the degree of
Doctor of Philosophy
2021

Advisory Committee:
Professor Dr. Leslie Pick, Chair
Dr. Quan Yuan, Co-chair
Dr. Benjamin White
Dr. Quentin Gaudry
Dr. Steve Mount

Dedication

I would firstly like to dedicate this dissertation and all that becomes of it to my wonderful family: Ira, Arlene, Bryan and Sara Rosenthal. From supporting my interest in insects and science as a child to the mental and emotional support they have given me throughout my studies, I absolutely would not have come this far without them. I would also like to thank all the teachers and professors I have had over the past 20-some years, especially my high school chemistry teacher Dr. Mary Cross. Thirdly, all the other graduate students who I've had the pleasure of meeting and learning from. And finally, and perhaps most importantly, the fascinating flies themselves. Where would we be without these humble, magnificent creatures?

Acknowledgements

Much like a developing neuron, a budding scientist needs the proper environment to mature in. I was fortunate enough to have this experience. First and foremost, I am deeply appreciative of my NIH advisor, Dr. Quan Yuan, for all the mentoring and instruction she has given me during the tumultuous past 5 years. I like to think that many of the work-related attributes I gained during my thesis research came from modeling myself after her. In particular, the ability to be propelled into the unknown without losing sight of what you initially set out to achieve. I am also indebted to Jun Yin who I consider, especially my first year, to be an informal co-advisor of sorts. There are also the other stellar members of the Yuan lab: Our lab manager, Jacob Short, former post-doc researchers Chengyu Sheng and Yang Chen and current and former post-bacs Mary Gibbs, Anna Kim, Emma Spillman and Jimmy Lei. All whose selfless attitude and excellent work ethic helped both with my project directly and provided a continuous source of inspiration. I am also grateful for the other labs I've had the privilege of working with: the White lab and Stopfer lab of NIH, the Gaudry lab at UMD and the Hama lab in Kyoto. Although the meetings with my committee members were few and far between, they were dense with direction, feedback and encouragement. Then there is the fly community at large: rom FlyBase, the BDSC, GSA and SFN down to our own DNC. Finally, all of this work is made possible by the excellent funding provided by the NINDS Intramural Research Program.

Table of Contents

List of Tables

List of Figures

List of Abbreviations

α-Btx: alpha-bungarotoxin
Ach: acetylcholine
AEL: after egg laying
AMPA: α-amino-3-hydroxy-5-methyl-4-isoxazolepropionic acid
BLAT: BLAST-like alignment tool
BN: Bolwig organ
BO: Bolwig nerve
CNS: central nervous system
CCP: complement control protein
D*α*1: *Drosophila* Alpha1
D*α*6: *Drosophila* Alpha6
DD: dark:dark (or constant darkness)
DE: differentially expressed
DLM: dorsolongitudinal muscle
DLMmn: DLM motoneuron
ECM: extracellular matrix
EPSC: excitatory postsynaptic current
FACS: fluorescence-activated cell sorting
GF: giant fiber
GPCR: G protein-coupled receptor
iGluR: ionotropic glutamate receptor
KC: Kenyon cell
LBD: ligand-binding domain
LD: light:dark (or 12hr light:12hr dark)
LL: light:light (or constant light)
LNv: ventral lateral neuron
lOLP: larval optic lobe pioneer
LON: larval optic neuropil
LPTC: lobula plate tangential cell
LTP: long-term potentiation
mAchR: muscarinic acetylcholine receptor
MB: mushroom body
MBON: MB output neuron
mEPSC: mini EPSC
MiMIC: Minos-mediated integration cassette
nAchR: nicotinic acetylcholine receptor
NMDA: n-methyl-d-aspartate
NMJ: neuromuscular junction
NBRE: NGFI-B Response Element
PDF: pigment-dispersing factor
PDFR: PDF receptor
PDZ: **P**SD95, **D**lgA, **Z**o-1

PN: projection neuron
PNS: peripheral nervous system
PSD: postsynaptic density
PSI: peripherally synapsing interneuron
qFISH: quantitative fluorescent in situ hybridization
RPKM: reads per kilobase per million
RT: room temperature
S2: *Drosophila* Schneider cells
scRNAseq: single-cell RNA sequencing
TF: transcription factor
TM: transmembrane
TSS: transcription start site
VGSC: voltage-gated sodium channel
VNC: ventral nerve cord
VTA: ventral tegmental area

Chapter 1: Identification of the Principle nAchR Subunits Regulating LNv Dendrite Morphogenesis and Neurophysiology

Abstract

The synapse is a fundamental unit of the nervous system and is constructed, maintained and modified through a wide array of genetic and protein-protein interactions. The molecular components and cellular features of postsynaptic development have been well characterized using the vertebrate cholinergic neuromuscular junction (NMJ) in the periphery and the dense glutamatergic neuron-neuron synapses of the brain as primary models. However, this has left other synapse types understudied, including the central nicotinic-type cholinergic synapse. In many animal models, such as *Drosophila* and *C. elegans*, acetylcholine (Ach) is the primary conductor of central nervous system (CNS) excitatory neurotransmission. Additionally, nicotinic synapses in the vertebrate brain are often studied with respect to how they modulate other excitatory or inhibitory circuits and consequently less is known about their own development. To address this, we have investigated the central cholinergic synapse using the ventral lateral neurons (LNv) of larval *Drosophila*, which receive cholinergic presynaptic input *via* nicotinic acetylcholine receptors (nAchR). Inspection of cell-specific RNAseq datasets and RNAi-based screening enabled the identification of two nAchR subunits, *Drosophila* Alpha1 ($D\alpha1$) and *Drosophila* Alpha6 ($D\alpha6$), as those principally participating in LNv postsynaptic development. Later morphological and live-imaging assays revealed a functional distinction between

the two: both subunits have a role in mediating neurotransmission in the LNv but only *Dα6* is needed for dendrite morphogenesis. These findings broaden what is known about the complexity of nAchR identity and subunit composition in *Drosophila* and exemplify how individual neurons can rely on a subset of neurotransmitter receptor genes from their complete genomic repertoire to carry out certain functions at their postsynaptic compartment.

Introduction

Historical model systems of synapse development

The field of neurotransmitters and their receptors began with the discovery of Ach over 100 years ago (2). Early model systems included frog skeletal muscle and specialized electric organs from several species of eels and rays, chosen for their relative ease of accessibility and sheer amount of raw synaptic material available to study (3-6). More detailed investigations at the cellular and molecular level uncovered the complexity of protein-protein interactions that are necessary for the induction, maturation and maintenance of the NMJ as well as the stereotypical phases observed during differentiation and refinement of the muscle cell (i.e. myotube) postsynaptic membrane and its associated motoneuron axon terminal(s) (reviewed by (7-10)).

The process of NMJ differentiation in the peripheral nervous system (PNS) begins when the approaching axonal bouton innervates the membrane of the myotube and releases several factors. Among them are Agrin, which binds to the Lrp4-MuSK coreceptor complex leading to nAchR recruitment and clustering at

the myotube midline (11-19). This aggregation of nAchRs relies on the trafficking protein Rapsyn (20-23). Interestingly, receptor clustering has been shown to occur independently of Agrin itself, although in some species mature and fully-functional NMJs will typically only develop following Agrin exposure or will occur outside the normal midline region in the absence of Agrin (24-28). There is a concurrent release of presynaptic neuregulin which, following ErbB receptor binding on the myotube surface, stimulates nAchR subunit transcription in specialized subsynaptic nuclei just below the membrane surface (29-33). Finally, stimulation of mature nAchRs by presynaptically-released Ach is also used to repress nAchR expression and clustering at extrasynaptic regions (34-40).

During NMJ maturation, there are visible changes to synapse anatomy, postsynaptic nAchR distribution and synapse size (41, 42). What begins as a more-or-less flat surface invaginates during the encroachment of the axon terminal, creating sunken "gutters", after which steep secondary invaginations, or "junctional folds", form (43, 44). One group of proteins, including the nAchRs themselves as well as laminins connecting the membrane to the ECM, occupy the primary sunken membrane whereas a separate class, including the voltage-gated sodium channels (VGSC), are situated in the deeper gutters (45-47). These cytological events and others, such as the removal of superfluous axon terminals, gradually enhance synaptic transmission at the NMJ, which can be seen in the gradual rise in the amplitude of action potentials (48-50). Importantly, there is also a critical switch in receptor composition. All nAchR pentamers at the NMJ, regardless of location in the body, invariably contain four muscle-specific subunits. During the

embryonic (or fetal) stage, they exist in the stoichiometry $\alpha 1_2\beta 1_1\gamma_1\delta_1$. In the early postnatal days, there is a rapid replacement of this subtype by the $\alpha 1_2\beta 1_1\varepsilon_1\delta_1$, which occurs by transcriptional upregulation of the ε subunit (51, 52). Disruption of this neonatal switch, such as by deletion of the ε gene locus, results in disordered postsynaptic molecular architecture and can result in impaired neuromuscular activity and even death of the animal (53, 54).

In contrast to the nAchR-rich vertebrate NMJ, neurotransmission conducted by ionotropic glutamate receptors (iGluRs) is the primary means of relaying rapid, excitatory synaptic activity in the vertebrate CNS. Due to their abundance and widespread involvement in both cognition and processing of sensorimotor information, these glutamatergic synapses have been the primary model for understanding the development and function of neuron-neuron excitatory synapses, and the dendrites on which they are found, in the mammalian brain and spinal cord (reviewed (55-57)). In this system, the postsynaptic compartment develops on dendrite spines, protrusions of the dendrite shafts (Cajal 1888, Berkley 1896 and reviewed by (58, 59)). The molecules here are organized into a dense region, the postsynaptic density (PSD), which is composed of a stunning array of proteins (reviewed by (60)).

Within the membrane itself are the actual glutamate receptors and are connected to scaffolding proteins, including PSD-95, which interact together *via* their **P**SD95, **D**lgA, **Z**o-1 (PDZ) domains (61-63). These are used to not only stabilize the receptor in the membrane but also provide a link to both the cytoskeleton as well as cell signaling molecules, such as the highly abundant

CamKII, which use intracellular pathways to modulate receptor function based on previous levels of synaptic activity. (64, 65).

Several model systems, including the optic tectal neurons of *Xenopus* tadpoles, have helped define how some of the basic developmental transitions common to central glutamatergic synapses (66-68). Here, dendrite branches that are initially highly motile and capable of rapid restructuring will stabilize, leading to a period of arbor expansion. During this time, relatively low levels of neurotransmission, mediated mainly by the n-methyl-d-aspartate (NMDA) receptor iGluR subtype, are gradually strengthened by recruitment of the α-amino-3-hydroxy-5-methyl-4-isoxazolepropionic acid (AMPA) receptor iGluR subtype, which conducts most synaptic activity in the mature synapse. This process, which is calcium- and CamKII-dependent, is similar to the mechanism responsible for long-term potentiation (LTP). LTP was discovered in pioneering early studies using anesthetized rabbits, when brief hippocampal stimulation was found to result in elevated synaptic activity shortly afterwards (69). When activated by a sufficiently large stimulus, NMDA receptors that are normally silent due to magnesium ion blockage are opened, causing the calcium influx that leads to intracellular signaling cascades regulating gene expression as well as delivery of AMPA receptors to this particular postsynaptic site ((70, 71) and reviewed by (72-74)).

Basic features of *Drosophila* nAchR subunits

The polypeptide structure of a typical *Drosophila* nAchR subunit is reminiscent of the prototypical nAchR gene product found in other species.

Although different paralogs differ in size and may possess unique secondary structures, they are all characterized by basic features, including an N-terminal extracellular domain, four transmembrane (TM) passes, two of which are connected by an extensive intracellular loop of highly variable length, and a small extracellular C-terminal segment (Figure 1.1a)(75, 76). To form a functional pentameric receptor, five subunits are coassembled during ER and Golgi processing after each one is separately translated. Although any individual vertebrate nAchR receptor may be composed of identical or non-identical subunits, our knowledge of *Drosophila* receptor composition is relatively scarce and is a topic of continued interest.

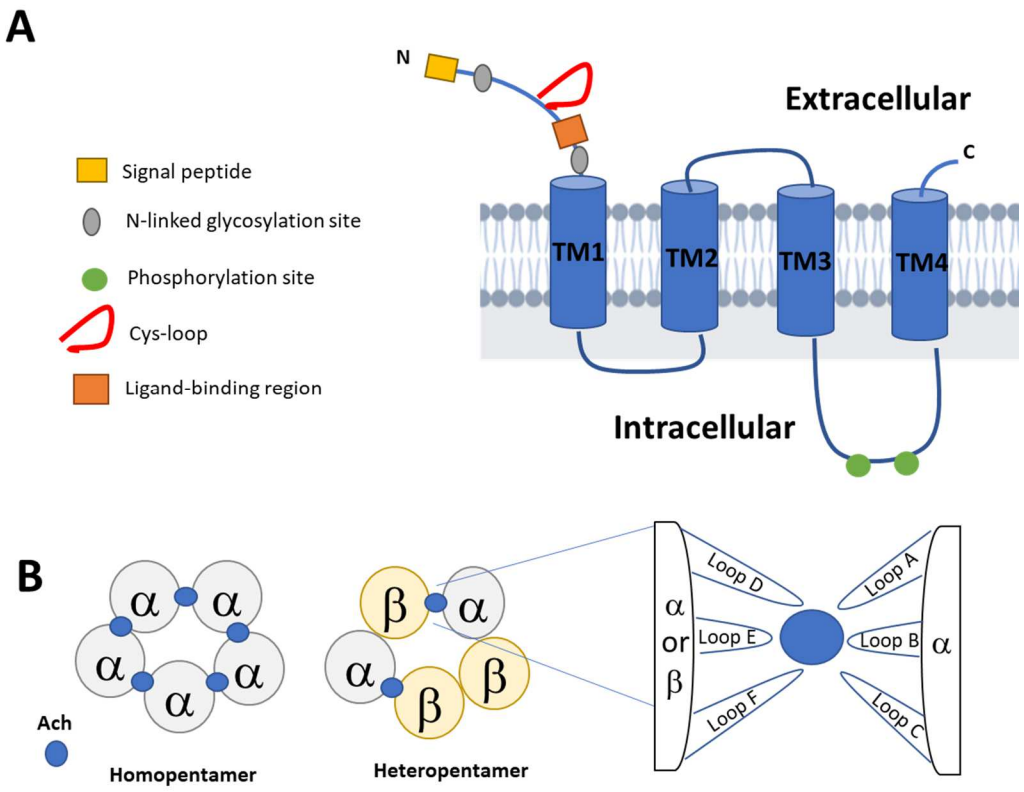

Figure 1.1: nAchR protein structure and receptor subunit composition. (a) Domain organization of a typical Drosophila nAchR subunit, including the extracellular LBD, the four TM domains and the large TM3-TM4 loop. Other features and post-translational motifs appear at approximate locations known for Dα1. (b) Comparison of the two stoichiometrically classed nAchR subtypes: homopentamers contain identical subunits whereas heteropentamers are composed of mixed subunits, though the full identity of the native nAchR(s) is still unknown. A zoom-in illustration of the ligand binding site shows the contribution of Loops A-C (α subunit only) and Loops D-F (α or β subunit).

At the N-terminus, the extracellular domain of the nAchR subunit includes N-linked glycosylation sites, some of which are found at conserved positions not only between *Drosophila* subunits but also in vertebrate nAchR genes (77-81). In addition, N-terminal signal peptide cleavage sites are common in *Drosophila* nAchR subunits and range in length from around 20 to 40 residues long, similar to their size in vertebrate orthologs (77, 78, 81-86)(UniProt). The N-terminus of each subunit also contains the functionally critical ligand-binding domain (LBD)(75, 76). Although the LBD is found in all subunits, only α subunits, which contain two adjacent extracellular cysteines (Figure 1.1b)(ex. amino acid residues 201 and 202 in *Dα1*), are capable of binding Ach or other agonists and competitive antagonists (82, 87). The non-α subunits are thought to mainly coordinate the placement of ligand within the α-subunit binding cleft. These subunits are classified as β in *Drosophila* and other insects and β, γ, δ or ε in vertebrates. Here, Ach and its analogs bind at the interface of the "principal" face of an α-subunit, comprised of Loops A-C, and the "complementary" face of either an α- or non-α subunit, composed of Loops D-F (88). However, there may be some exceptions to this simple rule. In vertebrates, the α5 subunit does not participate in ligand binding, despite having the extracellular vicinal cysteines of canonical α subunits. This is due to substitution of important nearby aromatic residues, usually Tyrosine or Tryptophan, which are also lacking in some

Drosophila "α" subunits (78, 89, 90). The α vs. β division is further complicated in the *Drosophila* system, where existing theories suggest that reversions between α- and β-subunits occurred during evolution and consequently the homolog of an α subunit for one species may in fact be a β subunit in a distantly related species (79, 91). Both scenarios could lead to a potential disconnect between the subunits' nomenclature and their true ligand binding ability.

The second key feature of the nAchR subunit is the group of TM domains, TM1-TM4. TM2 is of particular interest as it forms the pore-lining region cooperatively with the TM2 of the remaining four subunits (89). The intracellular loop between TM1 and TM2 as well as the extracellular linker between TM2 and TM3 are short and have not been the subject of intense study. Conversely, more attention has been given to the large intracellular TM3-TM4 loop, which is highly variable in length between subunits and is also involved in the assembly, and later synaptic clustering, of the pentameric channel (77, 92). Furthermore, the TM3-TM4 loop contains many predicted sites of post-translational modifications, such as phosphorylation by PKA, PKC and PKT and thus provides potential routes of regulating the receptor's activity (78, 81, 93). Finally, almost all nAchRs contain a small extracellular C-terminus following TM4. Although less studied in *Drosophila*, experiments on vertebrate nAchRs have shown this region serves as an intermediate linking the lipid bilayer environment to channel activity (94-96).

Genomics and phylogenetics of the fly nAchR gene family

There are ten nAchR subunit genes identified in the *Drosophila* genome (97). Following the mammalian nomenclature, these ten subunits are divided into

seven α-type subunits, which contain the pair of consecutive Cysteine residues, and three β-type subunits. They are located on Chromosomes X, 1 and 2. Notably, three subunits, *Dα1*, *Dα2* and *Dβ2*, are found immediately adjacent to each other at the 96A region of Chr. 3R and it is hypothesized this cluster arose from gene duplication events (98). Interestingly, not only are the orthologs of these three clustered in the mosquito *A. gambiae* genome but there is also a 3-gene nAchR subunit cluster in humans, where 15q24 contains *Chrna3, Chrna5* and *Chrnb4*, and in rodents, thus representing synteny in two phyla (99-101). Although it is not clear if these clusters were already present in the arthropod/chordate common ancestor, this clustering event is likely significant for coregulating nAchR subunit transcriptional activity because *Dα1*, *Dα2* and *Dβ3* are known to coprecipitate in fly heads. Likewise, the α3β4 receptor is a highly expressed subtype in the human autonomic ganglia (102).

Similar to other classes of neurotransmitter receptors, the nAchRs are found in many phyla of the Eumetazoa, including chordates, arthropods, nematodes, annelids and even jellyfish, suggesting a common ancestral receptor gene appeared near the origin of the animal nervous system (103). The molecular cloning and sequencing of insect nAchR genes also offered multiple pieces of evidence to support the shared ancestry between insect and vertebrate nAchRs. In particular, sequence similarities were found between *Drosophila* and vertebrate nAchRs in the region that binds the classical nicotinic antagonist α-Bungarotoxin (α-Btx) and the TM domain motifs (80, 82). Early studies revealed that the first few *Drosophila* nAchR genes sequenced (ex. *Dα1*, *Dα2* and *Dβ1*) shared a closer

relationship with the neuronal-specific subunits present only in the vertebrate CNS, as opposed to those restricted to the vertebrate NMJ. For example, the TM3-TM4 loop sequence and/or pattern of extracellular glycosylation sites of *Drosophila Dα1* and *Dα2* resemble those of the vertebrate neuronal-specific subunit *α2*, more so than vertebrate *α1*, which is confined to the muscle. Moreover, many of the intron-exon boundaries of these subunits are also shared between *Drosophila* and vertebrate neuronal subunits, such as those encoding the TM1-TM3 region (80, 82, 104-106).

Sequence similarity is even stronger for nAchR genes within the Insecta. Shortly after isolating the first genomic or cDNA clones of *Drosophila* subunits, they were used as probes and ultimately uncovered nAchR subunit genes across the insect spectrum, including the aphid, cockroach, multiple lepidopterans, honeybee as well as two additional dipterans, the housefly and bottlefly (107). In the case of *Dα1* and *Dα2*, amino acid conservation approaches 85% with other species' orthologs.

One fascinating aspect of nAchR phylogeny and conservation that appears to be very prominent in insect genomes is that multiple subunits are subject to alternative splicing and RNA A-to-I editing events. In particular, for *Dα6* and its orthologs, these sites of RNA modification are present in multiple insect orders (108). In the silkworm, there is even a developmental shift going from unedited transcripts in the larva to edited forms in the adult, although this shift does not seem to occur in *Drosophila* (108). Similar changes in *Dα4*, *Dα5* and *Dα7* also are predicted to have functional consequences as their location often corresponds

to the LBD as well as multiple TM domains and their linkers (81, 86). Some are even predicted to produce truncated polypeptides missing entire domains of the original protein. These alterations are therefore thought to vastly expand the functional diversity of the *Drosophila* nAchR gene family, which is relatively small, and is an exciting and unexplored area in the field.

LNv development in the larval *Drosophila* brain

The LNvs are second-order projection neurons which relay neuronal activity from upstream photoreceptors of the Bolwig Organ (BO) to the central brain, in part by releasing the neuropeptide Pigment Dispersing Factor (PDF) from axon terminal boutons which binds to neurons expressing PDF Receptor (PDFR) in the brain to ultimately entrain the animal's circadian rhythm with ambient light levels (109). Additionally, these neurons are also part of the larger larval visual circuit which controls other behaviors, including light avoidance and visually-guided and socially-coordinated substrate digging (110, 111).

During larval development, the LNvs are highly influenced by presynaptic activity (i.e. photoreceptor-detected light)and respond to bi-directional variations in light exposure with dramatic structural and functional modifications, representing one of the most robust instances of plasticity in the *Drosophila* CNS (112). Here, chronically-elevated light activity from a constant light (LL) environment results in a homeostatic reduction in both dendrite volume as well as magnitude in dendritic light-induced calcium transients (Figure 1.2). In contrast, larvae cultured in a constant darkness (DD) condition possess enlarged dendrite arbors and produce stronger light-induced calcium transients. Additionally,

genetic manipulation which alters neuronal excitability can simulate these alterations in light and can induce the above homeostatic adaptations independently of any modulation of light levels. Finally, this process was shown to be dependent on multiple signal transduction factors, including *NorpA* and *dnc*, which code for proteins in the G protein-coupled receptor (GPCR) signaling pathway that converts light sensation into electrical currents, as well as *shi*, a gene critical for synaptic vesicle fusion.

Recent research has elucidated the cellular basis for how light facilitates this plasticity. During early larval life, the dendrite branch terminals of the LNv are highly dynamic and undergo constant extension and retraction events (113). It is during this period of dynamic filopodia that synapse formation occurs. As this dynamic period subsides, a reduced percentage of motile branches as well decreased total distance traveled by these branches is observed; synapses stabilize and allow the arborization of the LNv dendrite. In other words, as synapse quantity and dendrite volume increase, dendrite motility decreases. This progression is drastically altered in the LL condition. Here, immature LNvs of young larvae never enter a phase of dynamic dendrite filopodia and thus produce fewer synapses and a smaller dendrite field. Moreover, the DD condition produces the opposite trend and results in even more dynamic dendrite branches. Further LNv-specific transcriptomic studies have been extremely helpful in identifying which genes are differentially expressed (DE) with elevated light input and therefore may be mediating the developmental changes associated with LD vs LL conditions. Among others isolated here were LpR1 and LpR2, lipid transport

protein receptors whose expression is thought to be upregulated by light in order to manage the increased demand of intercellular lipid shuttling in the LL condition (114, 115).

In conclusion, the fact that this nAchR-expressing neuron is well characterized and undergoes robust, experience-dependent plastic responses qualifies its use as a prime model for understanding development and plasticity of central cholinergic synapses.

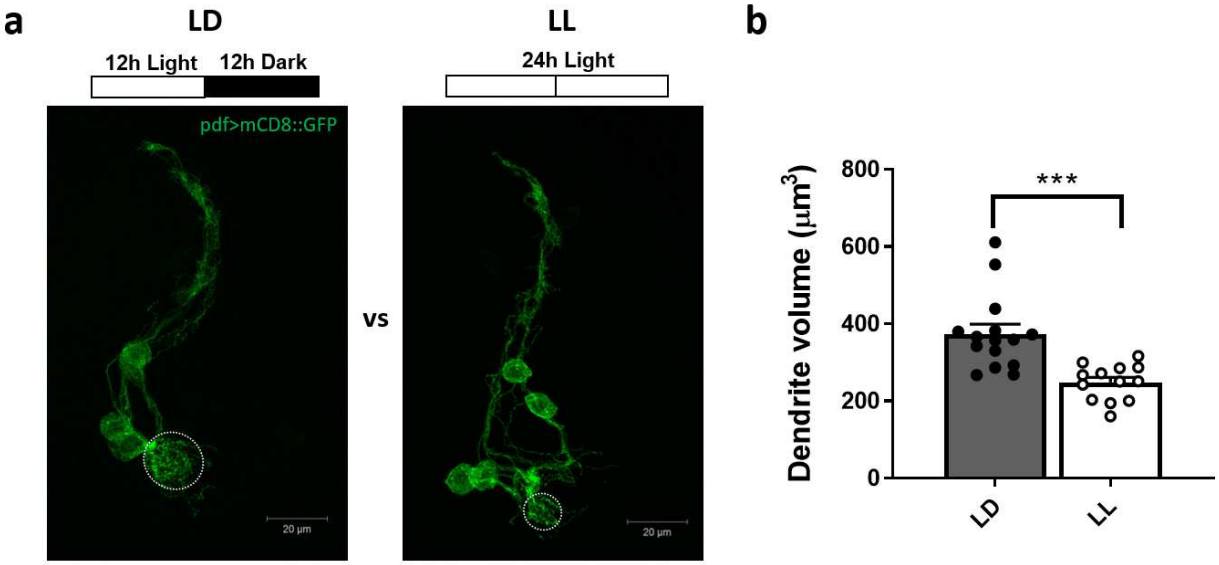

Figure 1.2: Activity-dependent plasticity of the LNv dendrite. (a) Projected confocal images of larval LNvs demonstrating the structural adaptive response between animals raised in the alternating light:dark (LD) or constant light (LL) condition. LNvs are labeled using the Pdf-Gal4 enhancer line to drive membrane-bound mCD8::GFP (green). (b) Quantification of dendrite volumes in (a). n=13-15

Methods

Sequence alignment

The phylogenetic tree was generated by including all 16 known human nAchR subunit genes and all ten *Drosophila* nAchR subunit genes. For human orthologs, the amino acid sequence used in the alignment was chosen from the primary isoform listed on the UniProt database. For *Drosophila* orthologs, polypeptide sequences were taken from the FlyBase database. In the event that multiple coding isoforms exist or are predicted, the isoform which contributes the verified polypeptide species or the predominant isoform expressed in the LNv, was selected. Phylogenetic comparisons and tree reconstructions were made by the MABL online phylogeny tool using "One click" mode (116).

Fly culturing

All flies were maintained in standard cornmeal medium, supplemented with yeast paste, and in controlled incubators set at 25°C and 60% humidity. Animals subjected to the light: dark (LD) condition were reared at alternating 12hour light-12hour dark cycles and those subjected to the LL condition received 24 hours of light. All larvae used for experiments were collected at the wandering 3rd instar stage. Brain dissections for fixation as well as live imaging were performed on samples collected between two and six hours after "lights-on" (Zeitgeber2-6).

Statistical analysis

For calcium imaging experiments, the data analyses and graphing (i.e. traces and peak $\Delta F/F$ values) were performed using a custom written MATLAB script to reduce human bias. The quantifications of dendrite volume and protein intensity were performed blindly. Raw values in all experiments were imported to Graphpad

Prism and analyzed using one-way ANOVA followed by Tukey's multiple comparisons *post-hoc* test, comparing all means against each other, with the exception of those from Figures 1.11b and 1.18 which use unpaired Students t-tests. All figures including statistical comparisons depict data in bar plots. Levels of significance were established at *: $p<.05$, **: $p<0.01$, ***: $p<0.001$. Error bars represent standard errors of the mean.

Drosophila stocks

The knockdown experiments, including the preliminary screen, and RNAi validation were performed with *Pdf-Gal4, UAS-mCD8::GFP; UAS-Dicer* (Bloomington ID: 6899, 5137 and 24650) and *Dα1-Dα7* and *Dβ1-Dβ3* RNAi stocks (Bloomington ID: 28688, 27493, 27674, 31985, 25943, 25835, 27251, 31883, 28038, and 25927). The Trojan-Gal4 studies used $D\alpha1^{MI00453\text{-}TG4.0}$ and $D\alpha6^{MI01466\text{-}TG4.1}$ (Bloomington ID: 66780 and 76137). The mutant morphology studies were performed with $D\alpha6^{DAS1}$ (Bloomington ID: 9685), *Pdf>mCD8::GFP* (made in lab) and the Minos-mediated integration cassette (MiMIC) lines $D\alpha1^{MI11851}$ and $D\alpha1^{MI00453}$ (Bloomington ID: 56462 and 42295). The mutant physiology studies used the stocks *Pdf-LexA* (112) driving *LexAop-GCaMP6s* (Bloomington ID: 44590) the MiMIC mutant line $D\alpha6^{MI01785}$ (Bloomington ID: 37925) and other mutant lines listed above. The *Dα3*, *Dα5*, *Dα6* and *Dβ2* T2A-Gal4 experiments were performed with lines from the BDSC (Bloomington ID: 84664, 84415, 84665 and 84666).

Confocal imaging and quantitative analysis of dendrite volumes

For all experiments, larval brains were dissected in 1x PBS, fixed in 4% PFA (paraformaldehyde in 1x PBST) for 40 minutes at room temperature (RT), washed three times with PBST (0.3% Triton X-100 in 1x PBS), equilibrated for 15 minutes and mounted in antifade medium (SlowFade^{TM} Antifade Kit, Thermo Scientific S2828). LNvs were imaged with a Zeiss 700 confocal microscope with a 40x oil objective and Z-stacks were obtained by taking serial sections at ~0.5µm thickness, with a typical x-y-z resolution of .09µm x .09µm x .49µm. For volumetric analysis, confocal Z-stacks of GFP-labeled dendrites were imported to the software Imaris (Bitplane) and reconstructed using the surface module. All individual volumes were generated using a predetermined threshold and then summed to create a final dendrite volume (Figure 1.3). All experiments generating dendrite volume data were blinded, by concealing the identity of each group, before the image processing step to avoid subjective bias during quantification.

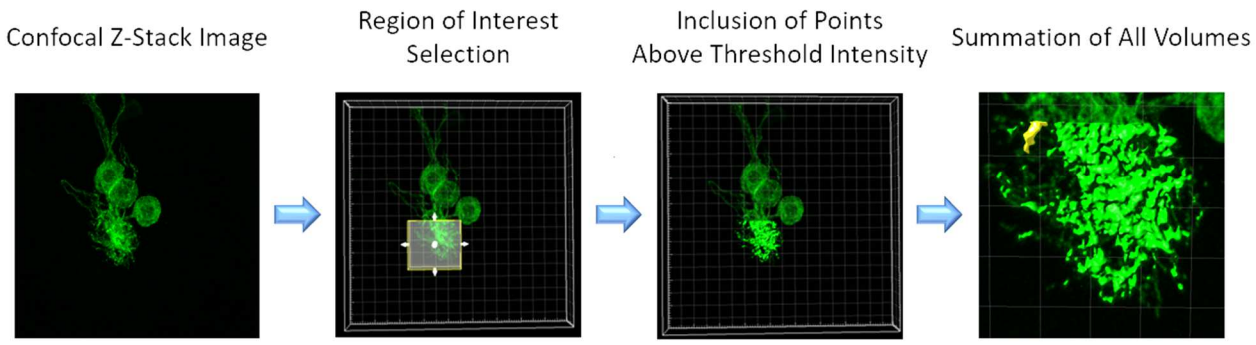

Figure 1.3: Process of dendrite surface reconstruction and volume quantification. Left/Mid-left: LNvs, expressing a membrane-bound GFP, are imaged by confocal microscopy and a region(s) of interest that both maximizes dendrite volume and minimizes cell body and axon volume is selected. Mid-right/Right: All continuous voxels above an automatic threshold are counted towards individual volumes. For this LNv, in the far-right image the yellow object is an example of a single surface whereas the remaining 34 surfaces are green (total of 35 volumes).

Immunohistochemistry

After fixation and washing as described directly above, whole mount brain tissues were incubated with primary antibodies, including mouse anti-Pdf (1:10 DSHB, Iowa City, Iowa) and Rabbit anti-Dα6 (1;1000, Chihiro Hama, Kyoto Sangyo University, Kyoto City, Japan), in 5% normal donkey serum (NDS) and 1x PBST at 4℃ overnight. Samples were then washed three times with 1x PBST for 30 minutes at RT, blocked with NDS for 1 hour at RT incubated in secondary antibody, including Alexa 647 Goat anti-mouse, A555^{+} Goat anti-rabbit and Alexa488^{+} Goat anti-mouse (1:500 Thermo Fisher, Waltham, Massachusetts), for 2 hours at RT or at 4℃ overnight. Brains were then washed again three times with 1x PBST for 30 minutes at RT and finally mounted and imaged.

RT-qPCR

For all samples analyzed, RNA was extracted and purified from third instar larval whole CNS tissue (Quick RNA MiniPrep Kit, Zymo Research, Irvine, California) and was converted to cDNA using Superscript III Reverse Transcriptase (Thermo Fisher, Waltham, Massachusetts). The *Dα1* region targeted was based upon pre-designed RT-PCR primers from FlyPrimerBank (Harvard Medical School). ID PP34653 F: 5' ATATGGCTACC GGATATTGTGCT 3' and R: 5' ACTTTGCCCGTGTGATGAAGA 3', which amplify an mRNA product connecting the 3rd and 4th coding exons. qPCR was carried out with the BioRad CFX96 Real Time System model (Biorad Laboratories, Hercules, California) and the SsoAdvanced Universal SYBR Green Supermix dye (Qiagen, Valencia, California).

Generation of transgenic *Dα6*-overexpression line

The coding sequence of the *Drosophila Dα6*-RE, the isoform most highly expressed in the larval LNv determined by the RNA-seq analysis (115), was amplified using the forward primer 5'-ACAGATCTTGCGGCCG CATGGACTCCCCGCTGCCAGCGTCG-3' and the reverse primer 5' ACAAA GATCCTCTAGATTATTGCACGATTATGTGCGGAGCG 3'. The resulting fragment was digested with NotI and XbaI and cloned into the vector pUAST. After verifying the *Dα6* sequence by sequencing and restriction digestion, plasmids were injected by Rainbow Transgenic Flies (Camarillo, CA) and transformed by random P-element insertion, followed by standard screening and balancing.

Calcium imaging analyses

The protocol used here is adapted from previous publications (112, 113). Eye-brain explants, including the intact BO, optic tract, eye disks and brain lobes, were taken from wandering 3rd instar larvae expressing *Pdf-LexA* driving *LexAop-GCaMP6s* or *Pdf-Gal4* driving *UAS-GCaMP6s*. After dissection in 1x PBS, samples were directly mounted in an external saline buffer (120mM NaCl, 4mM MgCl2, 3mM KCl, 10mM NaHCO3, 10mM Glucose, 10mM Sucrose, 5mM TES, 10mM HEPES, 2mM Ca^{2+}, PH 7.2) for live *ex-vivo* imaging. Imaging was performed using a Zeiss LSM 780 confocal microscope in combination with a Coherent Vision II two-photon laser tuned to 920nm for GCaMP excitation. Samples were recorded with a 40x water objective lens and 3x optical zoom. The frame rate was set to 100ms for a total of 1000 frames over a 100s recording session. GCaMP signals in the LNv (at the axon terminal unless otherwise stated) were recorded with a 256x90 pixel resolution. Each recording session included two 100ms 561nm light pulse stimulations separated by 40s to allow for complete measurement of calcium response and return to baseline fluorescence. Fluorescence change following each stimulation was calculated by $\Delta F/F_0$, where ΔF represents the change in fluorescence from baseline levels and F_0 represents the average fluorescence from the 20 frames immediately preceding stimulation (Figure 1.4). Only one recording was used per sample. Traces and values in figures are derived from the data obtained from the second stimulation but are comparable to that of the first stimulation.

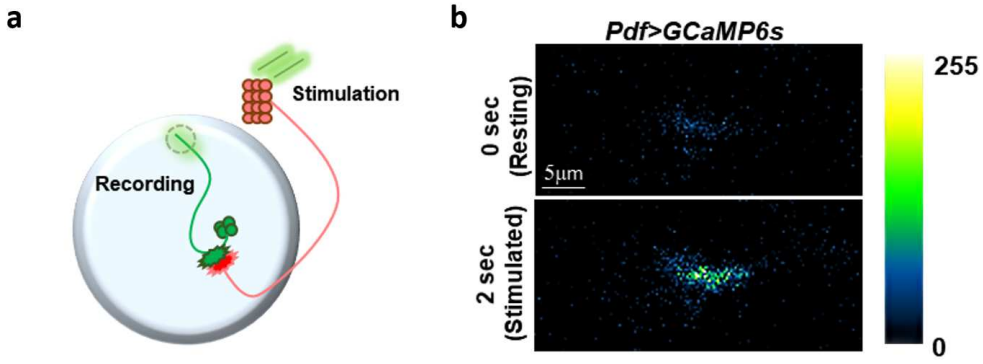

Figure 1.4: Process of inducing and recording light-evoked calcium transients in the LNv. (a) A schematic diagram illustrating the calcium imaging experiment in LNvs. A laser pulse activates the photoreceptors leading to depolarization of the downstream LNv, which is measured at its axonal terminal (dashed circle). (B) Pseudo-colored frames of GCaMP6s signal intensity before and after photoreceptor stimulation.

Results

Phylogenetic analysis of the *Drosophila* nAchR gene family

As covered in the introduction, the genome of *Drosophila melanogaster* contains 10 nAchR subunit-encoding genes. This is fewer than the 16 found in humans and at least 27 in *C. elegans,* but similar or equivalent to the gene family size in other insects (89, 117). Site-directed mutagenesis studies have demonstrated the functional significance of individual amino acid residues and therefore a preliminary, but informative, step of this project was to identify the relatedness among all ten *Drosophila* subunits (reviewed in (89, 118)).

We found that subunits *Dα5-Dα7* clustered with the human nAchRα7 (*CHRNA7)*, which is known for its ability to form homomeric pentamers and its

relatively high ratio of Ca:Na ion conductance ((119, 120) and reviewed in (121)). *Dα1-Dα4* and *Dβ2* cluster together as well but their relationship to a particular human ortholog are not as clear in this case since there seems to be a general species divergence between this group and its sister group (*CHRNA1-CHRNA6 and CHRNB3)*. Finally, the *Dβ3* subunit has the lowest homology with other nAchR subunits, both fly and human. Interestingly, several other insect species possess one or more nAchR subunit gene which are very dissimilar to all other paralogs within that species (117).

Although this analysis was completed independently, evolutionary relationships between fly, human and other insect nAchR subunits has been analyzed in the past, for instance by M Grauso et al. in 2002. Our alignment was nearly identical with that of Grauso and others with one exception: *Dβ1* is less related to the human muscle-specific subunits (i.e. β1, γ, δ and ε)(Figure 1.5. All other phylogenetic relationships produced from this homology alignment were essentially the same as those calculated by Grauso *et al.* 2002.

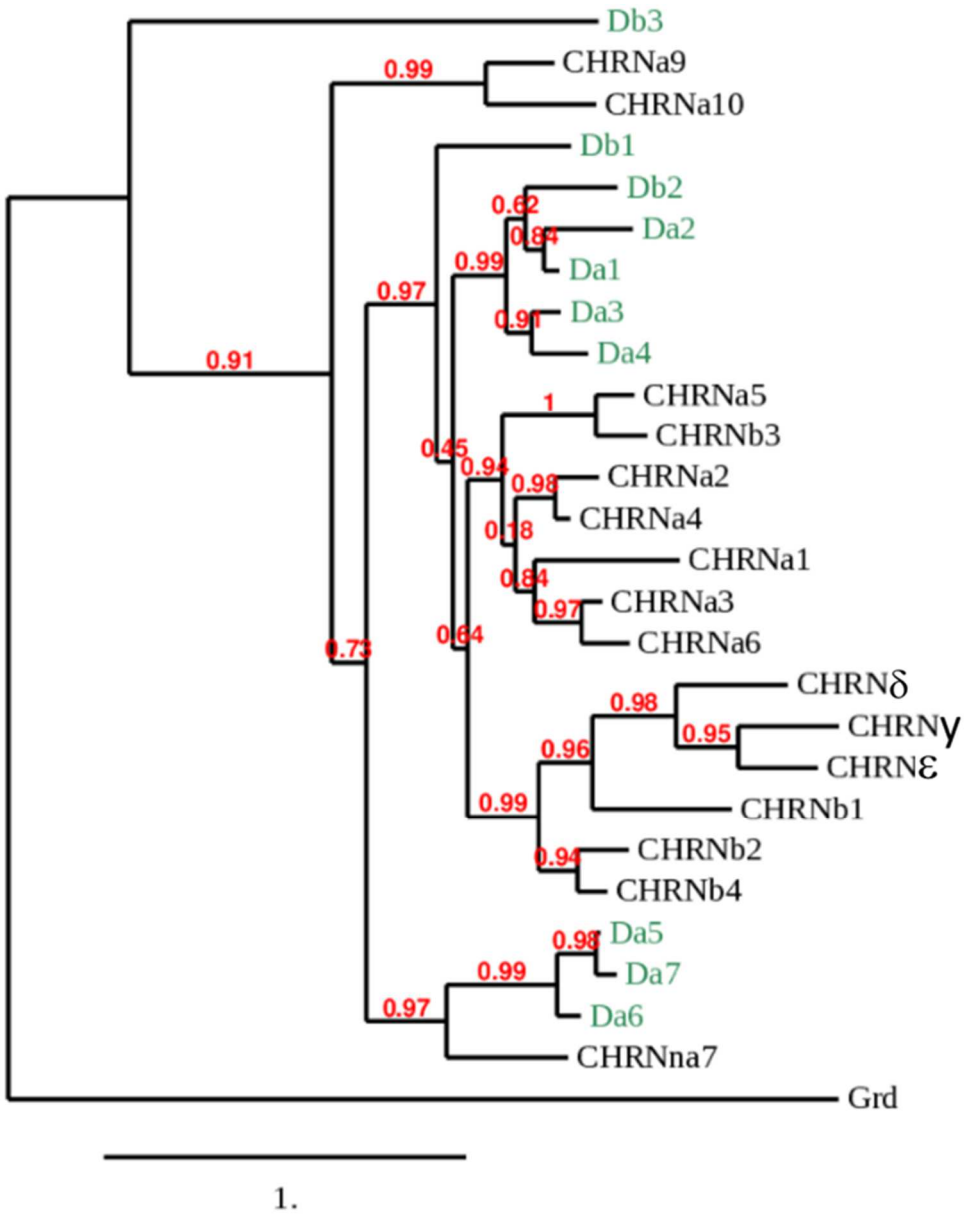

Figure 1.5: Evolutionary relatedness of fly nAchR genes. Phylogenetic tree depicting relationships of fly nAchR subunit genes both within the D. melanogaster genome (green) and with their human nAchR orthologs (black). The majority of fly nAchR genes form two distinct clusters: the vertebrate "α7-like" and the mixed "α-β". The outgroup Grd is the Drosophila glycine/GABA dual receptor gene (also a member of the Cys-loop ligand-gated ion channel superfamily). *Bootstrap values (red) appear prior to branching.*

Transcriptomics reveals AchR gene expression variation in the larval LNv

nAchR expression in the *Drosophila* CNS is nearly ubiquitous but few studies have reported on expression profiles of individual cell types. We therefore took two non-biased approaches to investigate all potential nAchR subunits in the LNv. The first was done by extracting published transcriptomic data from a previous RNA sequencing study (115). Here, the brain lobes of wandering third instar larvae expressing the *Pdf-Gal4* and *UAS-mCD8::GFP* transgenes were dissociated and sorted by FACS (fluorescence-activated cell sorting), using the GFP channel to isolate the Pdf^{+} neurons. In the larval brain, there are only four *PDF*-expressing neurons per brain hemisphere, which are the LNvs, that allows for high confidence sorting. Normalization of total nAchR subunit reads created a clear picture of the relative abundance for all subunit transcripts (Figure 1.6).

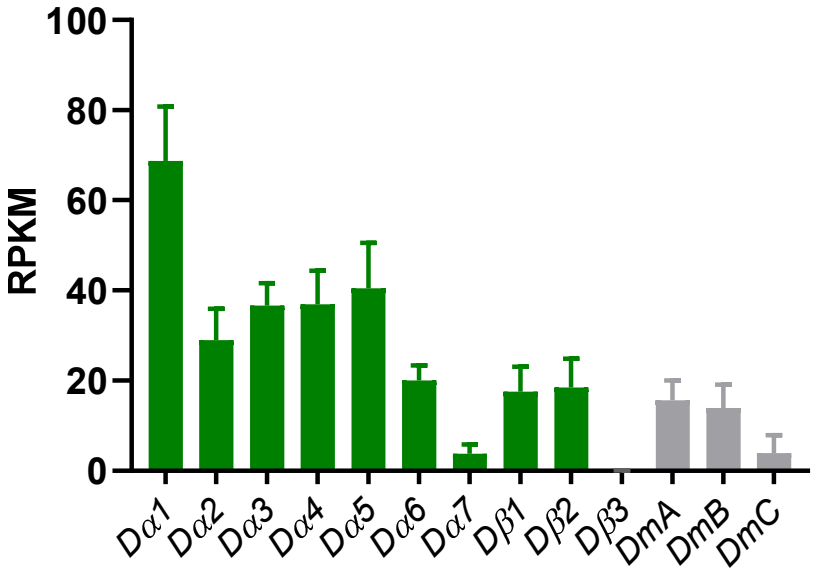

Figure 1.6: Cell-specific RNA-seq results reveal diverse AchR gene expression. Relative expression levels of nicotinic (Dα1-7, Dβ1-3) and muscarinic (DmA, B, C) AchR subunits in LNvs from larvae raised in light:dark (LD) conditions. RPKM: Reads per kilobase per million.

It appeared that although most subunits were detected, levels varied along a continuum. At one end of the spectrum was *Dα1*, clearly the most abundant gene at a level nearly twice as high as the next highest subunit. At the opposite end, *Dα7* is extremely low and *Dβ3* is essentially absent. The paucity of *Dα7* is a departure from other studies where it has been shown to be a central component in the adult olfactory circuit, visual system and giant fiber (GF) escape-reflex pathway (122-124). There also did not seem to be a correlation between sequence-based relatedness, from Figure 1.4, and mRNA presence. For example, the highly similar *Dα5*, *Dα6* and *Dα7* range from second-highest to minimally expressed. Finally, transcripts for the three known *Drosophila* muscarinic acetylcholine receptors (mAchR) genes were present at substantial quantities,

though the relevance of this remains to be determined as previous work using dissociated LNvs demonstrated negligible sensitivity to both muscarinic agonist and antagonist action (125).

Multiple *Drosophila* nAchR subunits are quite widespread in both the larval and adult CNS, based on *in situ* RNA and immunohistochemical analyses, and high-throughput RNAseq data from several sources indicate the majority of nAchR genes are at least moderately expressed in third instar larval neural tissue, albeit lower than that of pupae or adults (126, 127). We therefore compared the LNv-specific dataset to an *elav>GFP*-sorted population to ask whether any particular subunits are unusually high in the LNvs, as compared to a typical CNS neuron. Here, we found that several subunits, including $D\alpha l$, are enriched in the LNv at least two-fold compared to the $elav^{+}$ group (Figure 1.7).

Lastly, to provide a foundation for studying the transcriptional basis of light-dependent plasticity in the LNv, we compared this standard LD dataset to one generated with an altered level of synaptic input. As mentioned earlier, using larvae cultured with chronically elevated light activity (LL) provides an excellent reference point for this purpose. Interestingly, a statistical comparison revealed that transcript levels of nearly all subunits do not significantly differ between the baseline LD condition versus the high-stimulation LL condition (Figure 1.8). Only $D\alpha l$, is significantly altered. Specifically, constant light reduces $D\alpha l$ roughly 3.5 fold relative to the LD condition. Because $D\alpha l$ is both the most abundant subunit in the LNv and the only subunit whose expression is modified

by light activity, this subunit likley plays a major role during the events accompanying larval LNv postsynaptic development.

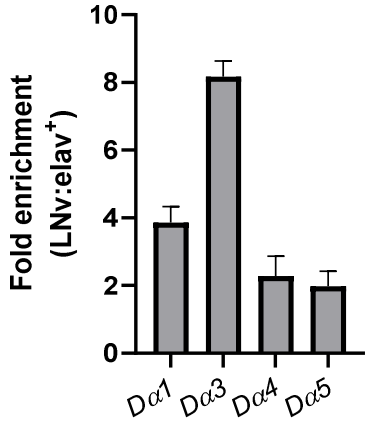

Figure 1.7: Enrichment of nAchR genes in the LNv. Transcripts of four nAchR subunits are detected at twice the level, or higher, in the LNv when compared to the average elav-positive neuron in the CNS.

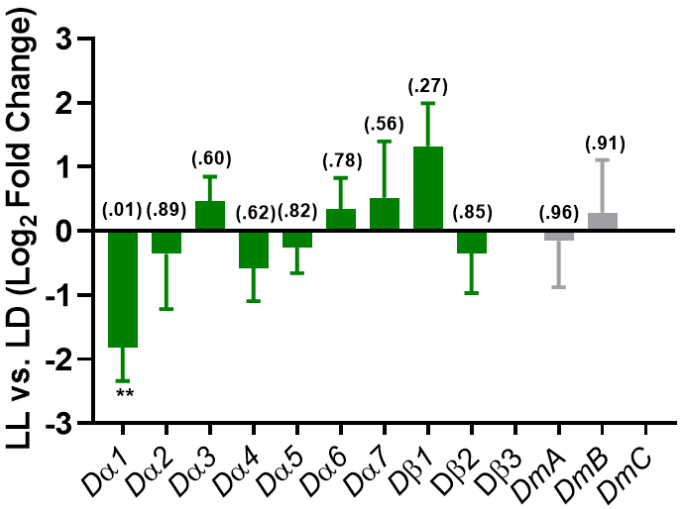

Figure 1.8: Comparison of RNA-seq datasets reveals the influence of light on nAchR subunit expression. Chronically elevated activity in the LL condition significantly reduces Dα1 expression in the LNv. No other subunits display activity-dependent transcriptional modulation. p-values analyzed by DESeq2 are denoted above the bar.

$D\alpha1$ and $D\alpha6$ are expressed in the larval LNvs but only $D\alpha6$ functions in dendrite morphogenesis

To complement the above transcriptomic approach for identifying the relevant nAchR subunits, we performed a small-scale morphological screen in parallel for all ten *Drosophila* subunit genes. By crossing the stock containing the *Pdf-Gal4>mCD8::GFP* marker, which labels the LNv membrane, with different *UAS-dsRNA* lines targeting single nAchR subunits we could quickly, albeit subjectively, isolate which subunits are potentially needed for a wildtype LNv dendrite. Here, RNAi-mediated knockdown of only $D\alpha6$ resulted in reduced LNv dendrite volume (Figure 1.9a). Surprisingly, RNAi lines targeting all other subunits, including $D\alpha1$, failed to produce an abnormally large or small dendritic arbor.

To uncover any relationship between the homeostatic plasticity of the LNv and $D\alpha6$ function, we also performed the identical screen with constant light. However, $D\alpha6$ knockdown did not appear to influence the dendritic field in the LL condition (data not shown). And, as in the LD condition above, RNAi targeting the remaining subunits in the LL condition also showed no difference. Finally, the resulting morphologies were quantitatively assessed for $D\alpha1$ and $D\alpha6$ in a follow-up experiment by reconstruction of the dendritic arbor, which confirmed the absence of a $D\alpha1$ phenotype and the LD-specific $D\alpha6$ reduction phenotype. Moreover, statistical comparisons in $D\alpha6$ RNAi animals revealed that the robust LD vs. LL volumetric plasticity invariably seen in wildtype animals is abolished in $D\alpha6$-deficient larvae (Figure 1.9b,c). Thus, $D\alpha6$ may play a role in

general LNv dendrite morphogenesis as well as experience-dependent structural plasticity.

The transcriptomic and screening data above was our first indication that *Dα1* and *Dα6* were among the ten subunits critical for LNv form and function. However, we performed several additional experiments to confirm this was indeed the case. Firstly, to validate the RNAseq data and confirm that *Dα1* and *Dα6* are expressed in the larval LNvs, we examined the endogenous expression pattern of *Dα1* and *Dα6* using two Gene-trap Gal4 lines, $D\alpha1^{MI00453\text{-}TG4.0}$ (*Dα1-TG4*) and $D\alpha6^{MI01466\text{-}TG4.1}$ (*Dα6-TG4*), both of which contain a Gal4 element inserted in the intronic region of the receptor subunit gene such that it is under the control of the native promoter (128, 129). By crossing these lines with a membrane-targeted *mCD8::GFP* and a nuclear marker, *redStinger*, these enhancer Gal4 lines demarcate the neuropil and cell bodies expressing the subunits (Figure 1.10). In addition to observing a wide distribution of both subunits throughout the larval brain, labeling of the LNvs through anti-PDF antibody staining indicated that while *Dα1* expression is fairly high in most cells of each hemispherical cluster, *Dα6* is quite low. In fact, *RedStinger* signal for this subunit typically appeared

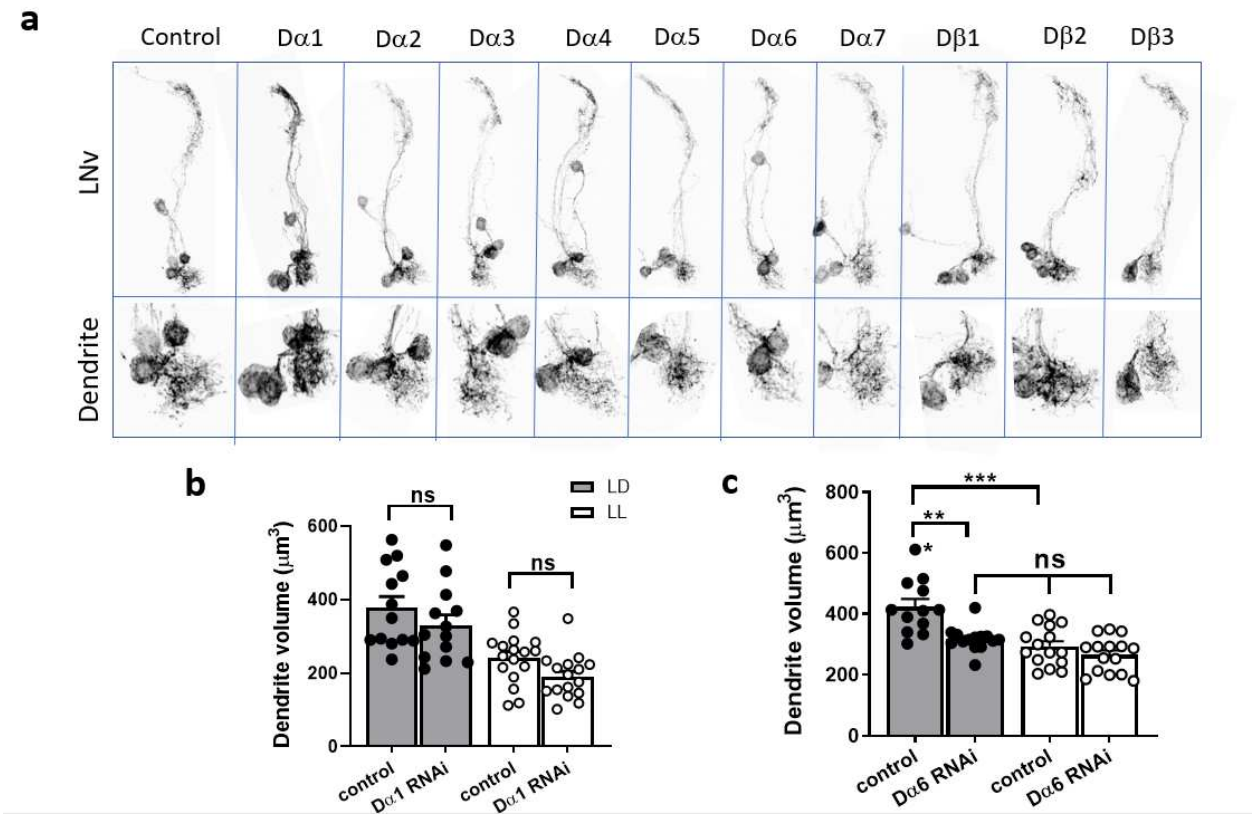

Figure 1.9: Morphological screen identifies Dα6 as a candidate gene influencing LNv morphogenesis. (a) Tissue-specific RNAi-based screen targeting all nAchR subunits implicates only Dα6 in LNv morphology. Top: Whole LNv; Bottom: Magnified view of dendrite arbor. (b and c) Quantitative analysis of separate trials to assess the role of Dα1 and Dα6 in determining dendrite volume. (b) Knockdown of Dα1 has no statistical effect on dendrite volume in either the LD or LL condition. (c) Knockdown of Dα6 results in a significantly smaller dendrite arbor in the LD condition and eliminates the LL-induced decrease. No effect is seen in constant light. Sample size n represents the number of larvae tested, n=12-17. Error bars represent mean ± SEM.

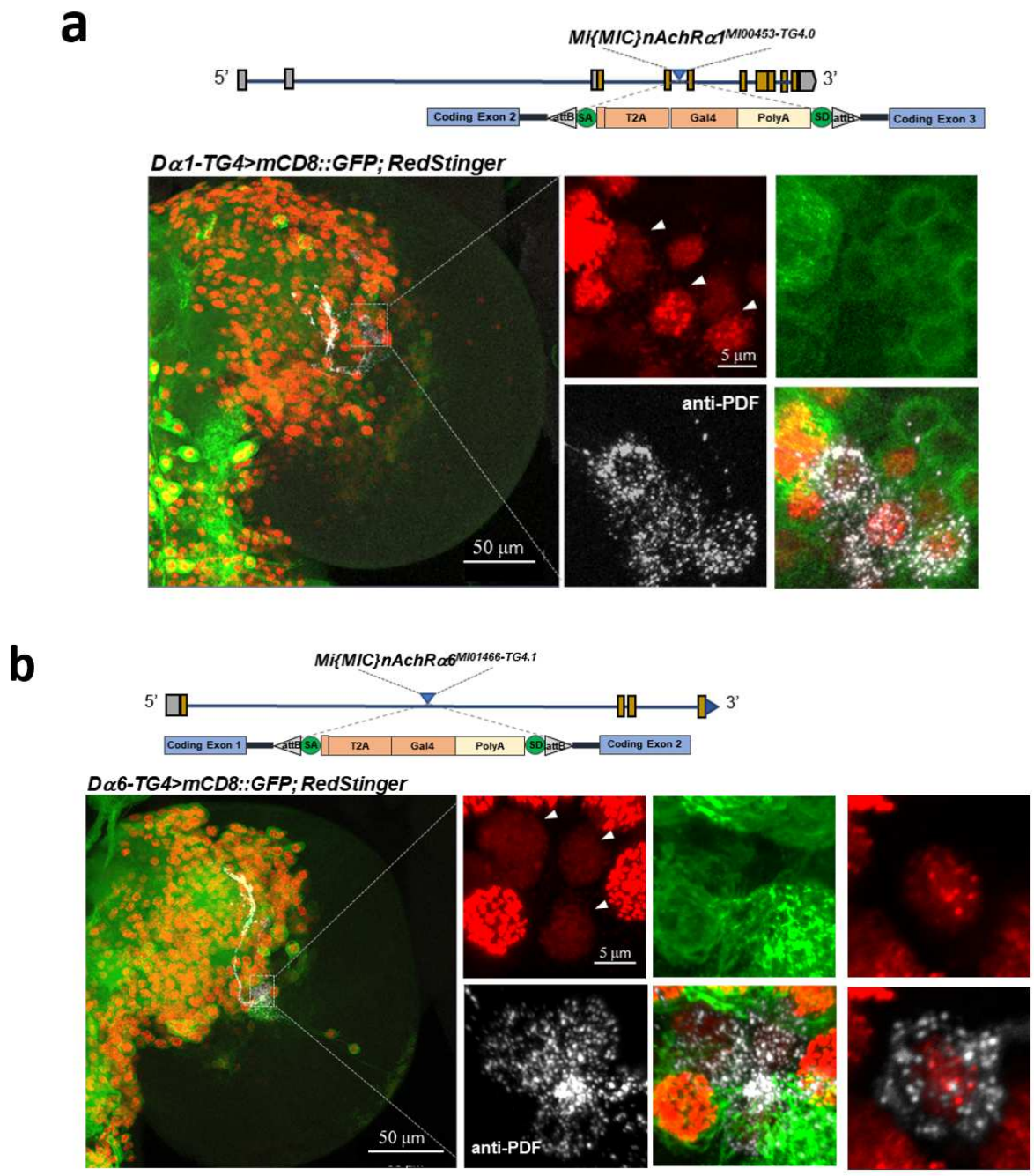

Figure 1.10: The expression of Dα1 and Dα6 in the larval LNvs is confirmed using Gene-trap Gal4 lines. Top (a and b): Schematics of the Trojan-Gal4 constructs and the insertion sites within the Dα1 (a) and Dα6 (b) genomic loci. Bottom (a and b): Representative projected confocal images displaying the broad distribution pattern of Dα1 (a) and Dα6 (b) in the larval brain lobe (left) and in the LNvs (right). The Trojan-Gal4-driven expression of the nuclear marker RedStinger (red) and the membrane marker mCD8::GFP (green) are shown. LNvs (arrowheads indicated in red channel) are stained using anti-PDF antibody (white).

in only one or two cells per cluster. Although this doesn't necessarily discount the expression of *Dα6* in the LNvs detected from our RNAseq data, it does raise questions about the homogeneity within the four-neuron cluster. Also notable is the *Dα6* reporter signal coming from the larval optic lobe pioneer neurons (lOLP) neurons, the interneurons which indirectly link the Rh6 photoreceptor neurons with the LNvs (Figure 1.11)(130)

Secondly, due to intrinsic variation in the efficiency between different RNAi constructs, as well as the driver being used and cell type(s) they are expressed in, we measured the efficacy of the *Dα1* and *Dα6* dsRNA lines. When expressed through the *actin-Gal4* driver, the *Dα1* dsRNA construct removes decreases levels by roughly 60 percent of total *Dα1* RNA in the larval CNS, as measured by RT-qPCR (Figure 1.12a). The *Dα6* dsRNA construct, assayed by anti-Dα6 antibody staining, appeared to be less effective as Dα6 protein levels in the LNv soma were only reduced by around 35 percent (Figure 1.12b).

Although not surprising, the incomplete elimination of nAchR subunit RNA *via* RNAi prompted us to validate the morphological screening data with mutant alleles. Here, using the same reconstruction technique above, we tested a *Dα1* loss-of-function mutant using a trans-heterozygote consisting of two MiMIC alleles inserted in either a coding intron ($D\alpha1^{MI00453}$) or exon ($D\alpha1^{MI11851}$), which only express *Dα1* RNA in the larval CNS at 3% of wildtype levels as measured by RT-qPCR (Figure 1.13) (131) (Venken, Schulze et al. 2011) (Venken, Schulze et al. 2011) (Venken, Schulze et al. 2011) (Venken, Schulze et al. 2011) (Venken, Schulze et al. 2011). Consistent with the knock-

down experiments, there were no significant changes in LNv dendrite volume in the *Dα1* mutant under LD and LL conditions as compared to the control group (Figure 1.14).

The contribution of *Dα6* to LNv morphogenesis was examined by mutant analysis using the null allele $D\alpha6^{DAS1}$, which contains a G to A substitution that eliminates the first splicing event and produces a truncated polypeptide (132). Similar to the RNAi knockdown approach, *Dα6* deficiency led to a significant reduction in the LNv dendrite volume and a loss of LL-induced dendrite plasticity (Figure 1.15). It was, however, unexpected that overexpressing *Dα6* in the LNv could not rescue the LD-specific phenotype. Further, the LD-LL volumetric difference was only partially restored. A likely reason for this is due to the non-autonomous source of *Dα6* coming from one or both lOLP neurons, which play an intimate role in conducting neural activity downstream of the photoreceptors (Figure 1.11).

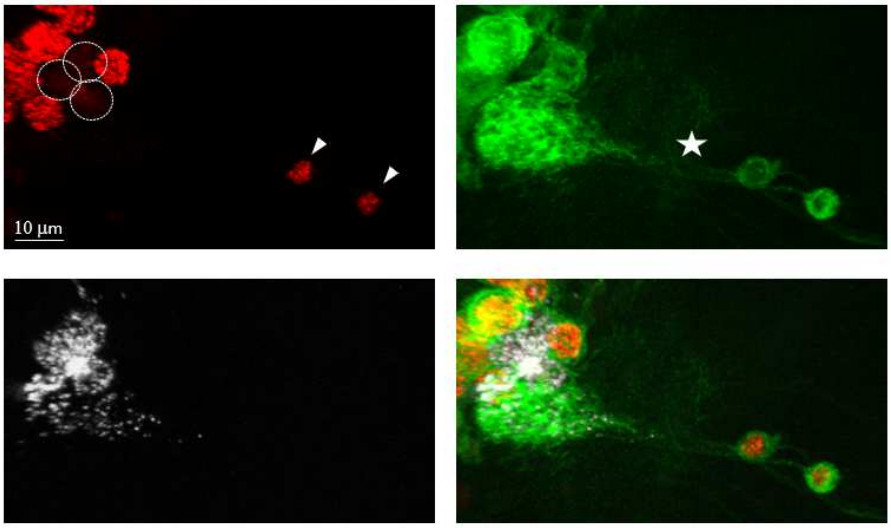

Figure 1.11: Dα6 expression in the larval OLP neurons. Two of the three lOLP neurons, whose neuropil projections form part of the LON, are positive for nuclear RedStinger (red) and mCD8::GFP (green). Cell bodies and neurites indicated by arrowheads and star, respectively.

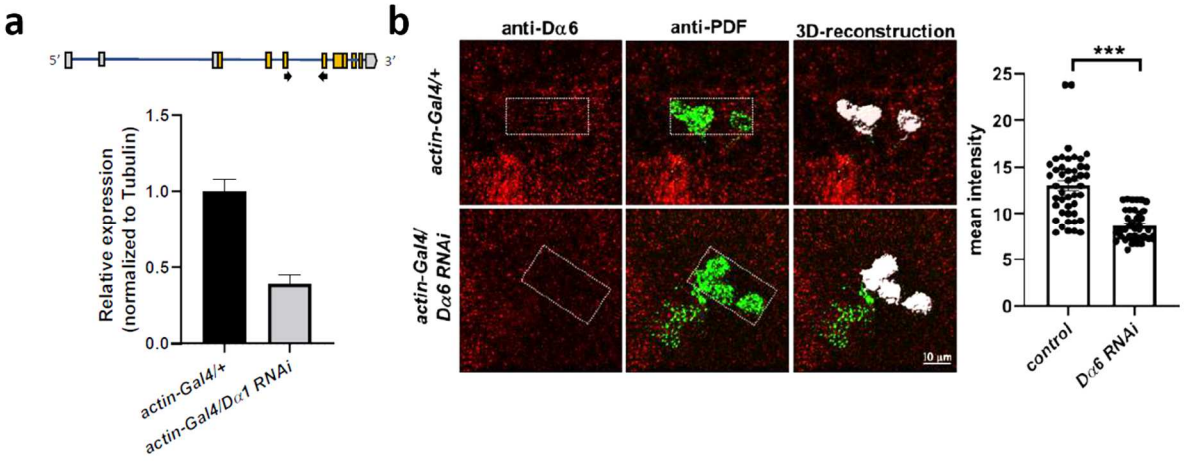

Figure 1.12. Efficiency of Dα1 and Dα6 RNAi transgenes. (a) Driving the Dα1 dsRNA transgene with the actin-Gal4 enhancer reduces CNS-wide Dα1 RNA levels below 50% of wildtype values. (b) The Dα6 dsRNA transgene driven by the Pdf-Gal4 enhancer significantly reduces Dα6 protein (red) in reconstructed soma (grey) of mCD8::GFP labeled LNvs (green). Sample size n represents the number of LNv soma quantified, n>30. Error bars represent mean ± SEM.

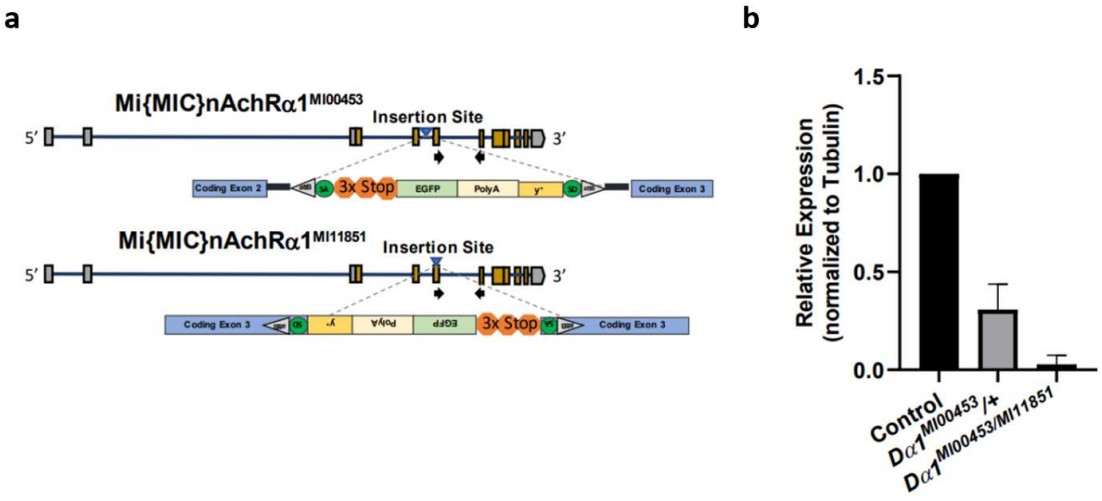

Figure 1.13. Strength of Dα1 MiMIC alleles. (a) Schematic of Dα1 gene structure showing placement of MiMIC insertions as well as RT-qPCR primer location (black arrows), which is downstream of both insertions. (b) The Dα1^{MI00453} allele strongly reduces Dα1 mRNA in the larval CNS in the heterozygous condition and, when in-trans with the frameshifting Dα1^{MI11851} allele, reduces the large majority of Dα1 RNA. Error bars represent mean ± SEM.

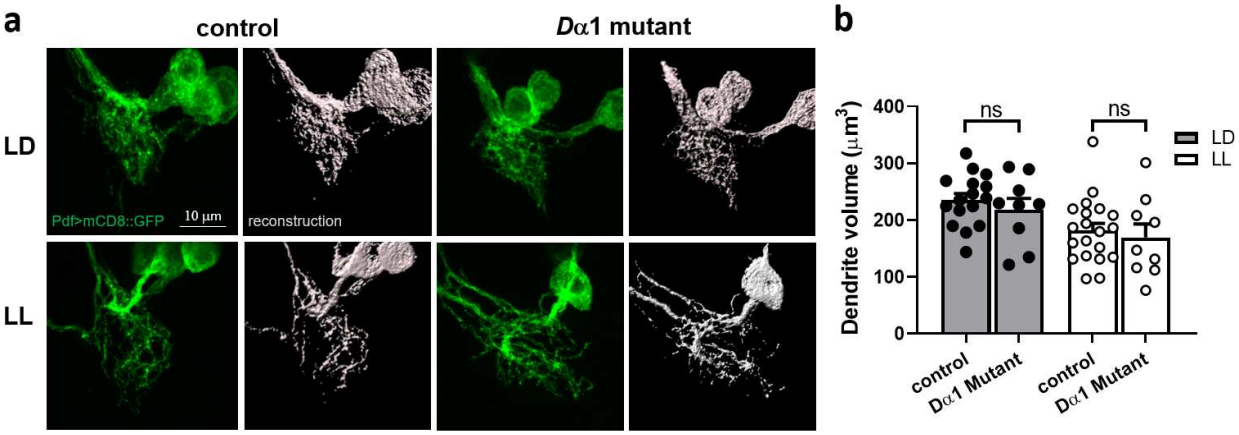

Figure 1.14. Effect of a strong transheterozygous Dα1 mutant on LNv dendrite volume. (a) Representative projected confocal images of LNv dendrites labeled by mCD8::GFP (left, green) and their 3D reconstructions (right, grey) are shown. (b) Quantification of data in (a). The loss-of-function mutant of Dα1 does not have observable defects in LNv dendrite volume. Sample size n represents the number of larvae tested, n=9-19. Error bars represent mean ± SEM.

Finally, to investigate whether *Dα1* deficiency modifies the morphological defect seen in *Dα6* mutants, we generated *Dα1*/*Dα6* double mutants by combining the mutant alleles described above. There was no significant difference in dendrite volume between the *Dα1*/*Dα6* double mutant and the *Dα6* mutant (Figure 1.16), indicating that the *Dα1* deficiency neither enhances nor suppresses the dendrite phenotype exhibited by the *Dα6* mutants.

The evidence thus far enabled us to narrow our scope of investigation and focus nearly all future efforts on two subunits with seemingly distinct and unexpected activities in the LNv: *Dα1*, which is enriched in this cell type and undergoes activity-dependent transcriptional regulation but is not critical for dendrite morphogenesis, and *Dα6*, which may contribute to dendrite growth but is not particularly abundant and whose expression at the RNA level is unaffected by light input.

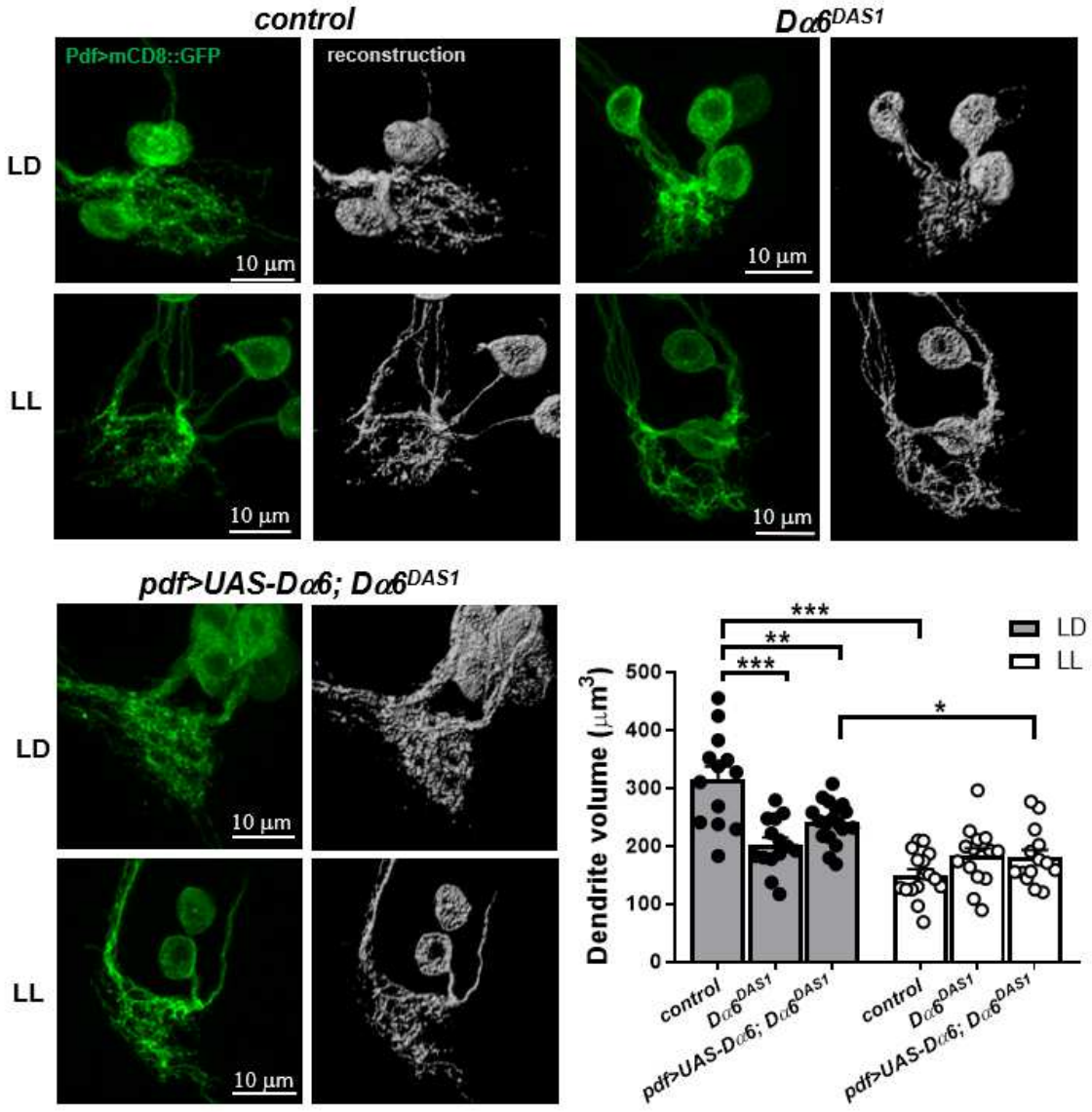

Figure 1.15. Dα6 is required for proper dendritogenesis in the larval LNv. (a) Representative projected confocal images of LNv dendrites labeled by mCD8::GFP (left, green) and their 3D reconstructions (right, grey) are shown for both the LD and LL conditions. (b) Quantification of data in (a). Null mutants and cell-specific rescue animals are compared to wildtype controls. Dα6^{DAS1} mutants have severe impairments to LNv anatomy and plasticity, which cannot be rescued by driving Dα6 overexpression in the LNs alone. Sample size n represents the number of larvae tested, n=13-18. Error bars represent mean ± SEM.

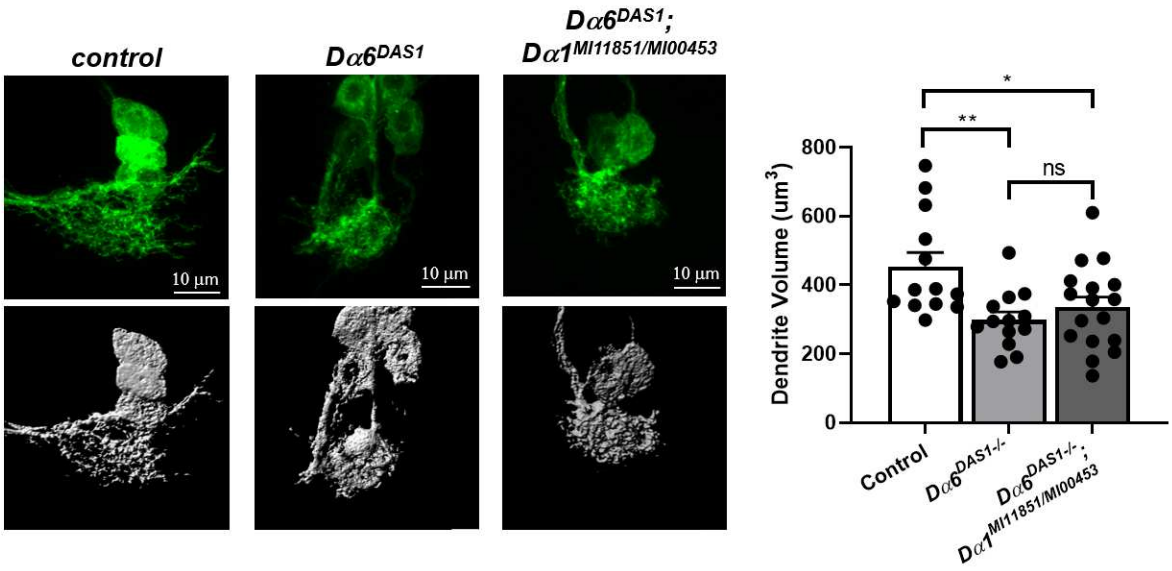

Figure 1.16. Dα1 co-deficiency does not enhance or mitigate the dendrite phenotype in Dα6 mutant LNvs. (a) Representative projected confocal images of LNv dendrites labeled by mCD8::GFP (left, green) and their 3D reconstructions (right, grey) are shown for the LD condition. (b) Quantification of data in (a). There is no statistical difference between Dα6 single mutant and Dα1/Dα6 double mutant dendrite volumes. Sample size n represents the number of larvae tested, n=13-17. Error bars represent mean ± SEM.

Both *Dα1* and *Dα6* contribute to LNv synaptic transmission

In the vertebrate CNS literature, there are reports of how glutamate receptors are vital for multiple neurophysiological properties but are apparently dispensable for the morphological traits in the same cell (133). It seemed plausible that this functional partition might be occurring in our system and could explain why *Dα1* has no robust influence on dendrite volume. Therefore, we went on to examine the involvement of *Dα1* and *Dα6* in synaptic transmission using physiological studies. LNvs receive direct and indirect synaptic input from the larval photoreceptors, and thus can be activated when the animal's intact visual circuit is subjected to light stimuli (Figure 1.4). Depolarization events in

the LNv are recorded and quantified using the transgenically-expressed, fluorescent calcium reporter GCamp. Due to the strong influx of calcium at the presynaptic terminals, the axon boutons were selected as the most suitable location for recordings.

We performed calcium imaging experiments in loss-of-function mutants for both subunits: $D\alpha1^{MI11851}/D\alpha1^{MI00453}$ or $D\alpha6^{DAS1}/D\alpha6^{MI01785}$ trans-heterozygotes. Remarkably, the light-elicited calcium responses in both *Dα1* and *Dα6* mutants were significantly reduced as compared to the control flies. Response amplitudes, represented by the peak level of ΔF/F, were about 30% of control for the *Dα1* mutant and 40% of control for the *Dα6* mutant, although there was no statistical difference between the two mutant groups (Figure 1.17a,b).

We supplemented this data with that from LL-cultured larvae as well. Previously, it has been shown that LNvs of larvae raised in constant light undergo not only a reduction in dendrite volume, but also have a dampened light-evoked calcium response (112). This was replicated here with the control group showing a 40% reduction in the response amplitude in the LL condition as compared to the LD condition (Figure 1.17c,d). Interestingly, neither *Dα1* nor *Dα6* mutants show this dampened response in the LL environment. And this inability for the LL condition to further reduce light-evoked responses in the mutants suggests that the LL-induced homeostatic response and the genetic deficits generated by *Dα1* and *Dα6* mutations in the LD condition manifest due to a common pathway(s), such as alterations in the number and/or strength of the synapses.

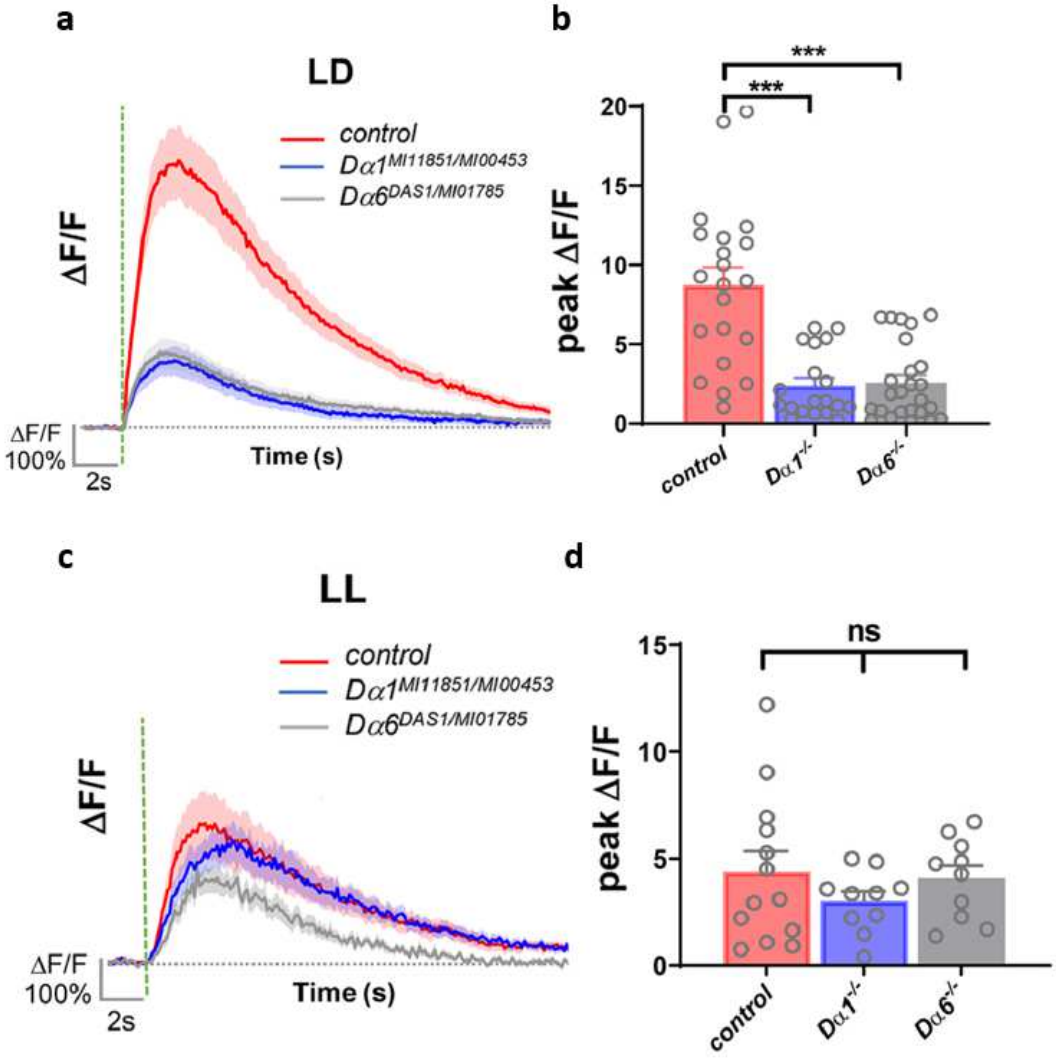

Figure 1.17. Light-elicited calcium responses in LNvs are severely affected in Dα1 and Dα6 loss-of-function mutants only in the LD condition. (a and c) Traces of average GCamp intensity change following photoreceptor stimulation (dashed green line) in the LD (a) and LL (c) conditions. Control and both mutants' curves are superimposed. The shaded area represents SEM. (b and d) Quantification of data in (a and c). In the LD condition (b), peak GCamp6s amplitude following light stimulation is significantly reduced in both Dα1 and Dα6 mutants. In the LL condition (d), no difference is observed between control animals and either mutant Sample size n represents the number of larvae tested, n=10-25. Error bars represent mean ± SEM.

Although calcium responses are generally stronger and more consistent at the axon terminal, we also pursued recordings at the dendrite region. Compared to

the axonal calcium responses, those collected from the dendrite had a much smaller amplitude, possibly due to different calcium channel densities between compartments and/or preferential influx of sodium ions at the dendrite. Nonetheless, the calcium transients collected at the postsynaptic site still showed a significantly dampened light response in the *Dα6* mutants, validating the phenotype we observed in the mutants (Figure 1.18). Importantly, this also implies that the aberrant axonal terminal recordings in the mutant are at least partly due to abnormal activity at the postsynaptic compartment, the predicted site of the nAchRs, and do not simply result from non-specific effects such as defective signal propagation along the axon.

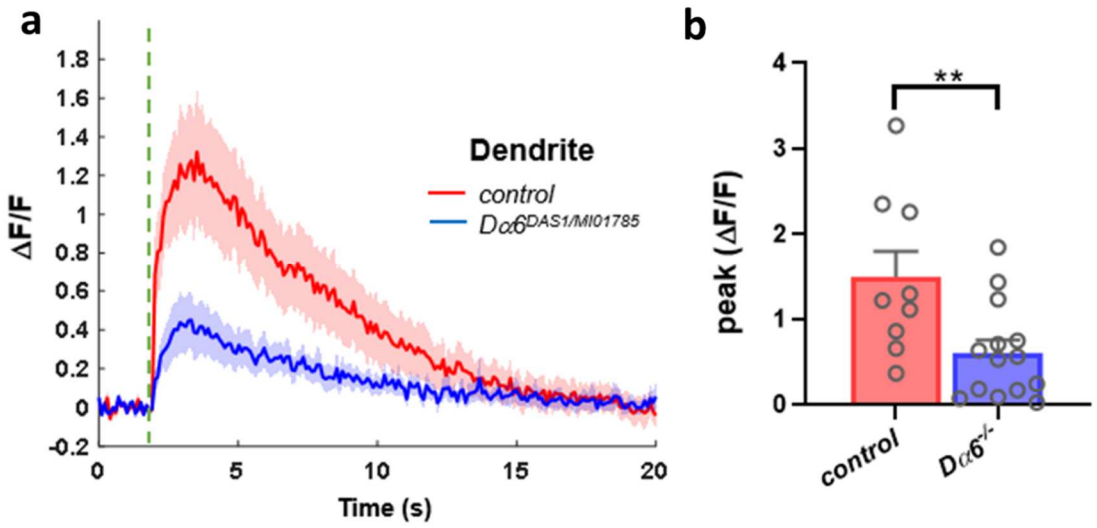

Figure 1.18. Physiological defects in Dα6 mutants can be detected in the LNv dendritic region. (a) Traces of average GCamp intensity change in the dendrite following photoreceptor stimulation (green line). The shaded area represents SEM. (b) Quantification of data in (a). Although baseline wildtype amplitude is smaller at the dendrite, calcium responses recorded in the LNv dendritic field are significantly dampened in Dα6 mutants in the LD condition. Sample size n represents the number of larvae tested, n=9-14. Error bars represent mean ± SEM.

To measure the cell-autonomous contribution of the two subunits in mediating synaptic transmissions in LNvs, we also performed LNv-specific knock-

down experiments using transgenic RNAi lines targeting either *Dα1* or *Dα6*, driven by LNv-specific Pdf-Gal4. Knocking down either subunit produced significant reductions in the light-evoked calcium responses, similar in magnitude to those of the mutant, indicating autonomous contributions to the LNv's light response from both subunits (though not ruling out non-autonomous subunit activity such as in the lOLP neurons)(Figure 1.19).

Lastly, we used the double knock-down experiments to evaluate whether there are synergistic effects generated by a deficiency in both subunits. Similar to the lack of enhancement we observed in the morphological study, there was no significant difference between the single vs. double knock-down groups in the light-evoked calcium responses (Figure 1.19).

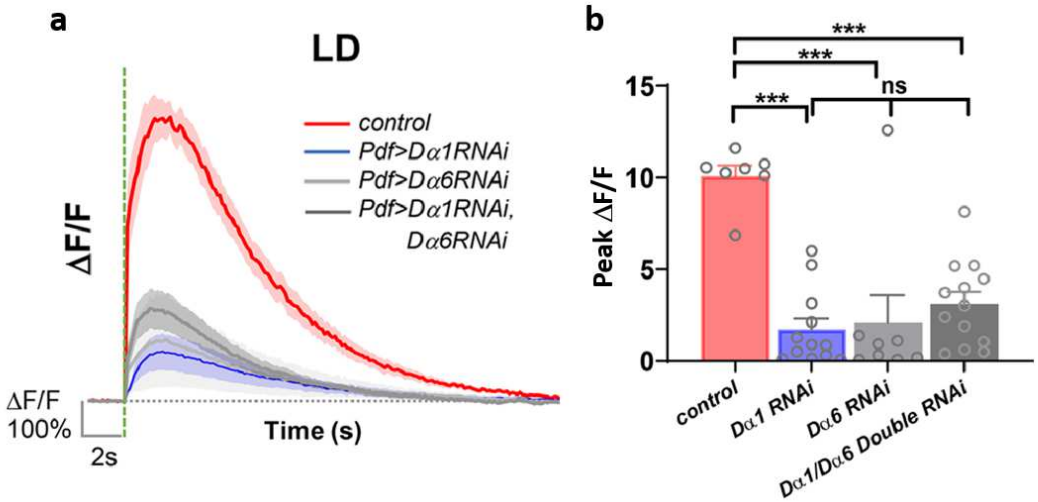

Figure 1.19. Dα1 and Dα6 have a cell-autonomous function in mediating synaptic transmission in the LNv. (a) Traces of average GCamp intensity change, measured at the axon terminal, following photoreceptor stimulation (green line). The shaded area represents SEM. (b) Quantification of data in (a). (b) LNv-specific knockdown of either Dα1 or Dα6 produces significant reductions in light-induced calcium responses. Additionally, Dα1-Dα6 double knockdown does not produce a significant change from the single knockdown phenotype. Sample size n represents the number of larvae tested. n=7-13. Error bars represent mean ± SEM.

This result suggests that *Dα1* and *Dα6* contribute to the neurotransmission in LNvs through a common pathway, such as co-assembling into common pentameric receptors that localize at the postsynaptic apparatus or regulating membrane

conductance cooperatively within the same synapse but in distinct receptor subtypes. The remaining 30% of neurotransmission in the *Dα1/Dα6* double knock-down animals could be attributed to the incomplete elimination of either subunit by the transgenic RNAi lines. However, based on the potential expression of other subunits in LNvs and the phenotypes of strong mutant combinations, another plausible explanation would be that other nAchR subunits also contribute to the process.

Endogenous nAchR expression profiles suggest additional subunits are active in the larval LNvs

Our phenotypic analyses have been focused on *Dα1* and *Dα6* so far. However, the RNA-seq analysis detected transcripts of all but one subunit in the LNv transcriptome. In addition, our calcium imaging experiments revealed that a light-evoked calcium response in the LNvs still persists with *Dα1/Dα6* double knock-down. These observations suggested the potential expression and function of additional nAchR subunits in larval LNvs. To test this possibility, we examined several nAchR subunit protein trap lines generated by CRISPR/Cas9-mediated genome editing. In these lines, Gal4 or LexA is translated as a separate protein near the stop codon of the nAchR subunit through T2A-mediated translation initiation, potentially reflecting the endogenous expression pattern of the individual subunits(134). Reporters driven by *Dα3-T2A-Gal4, Dβ2-T2A-Gal4, Dα6-T2A-Gal4* and *Dα5-T2A-LexA* indicated that, besides *Dα1* and *Dα6*, *Dα3* and *Dα5* likely also express in LNvs, while *Dβ2* expression was not detected in LNvs by this approach (Figure 1.20).

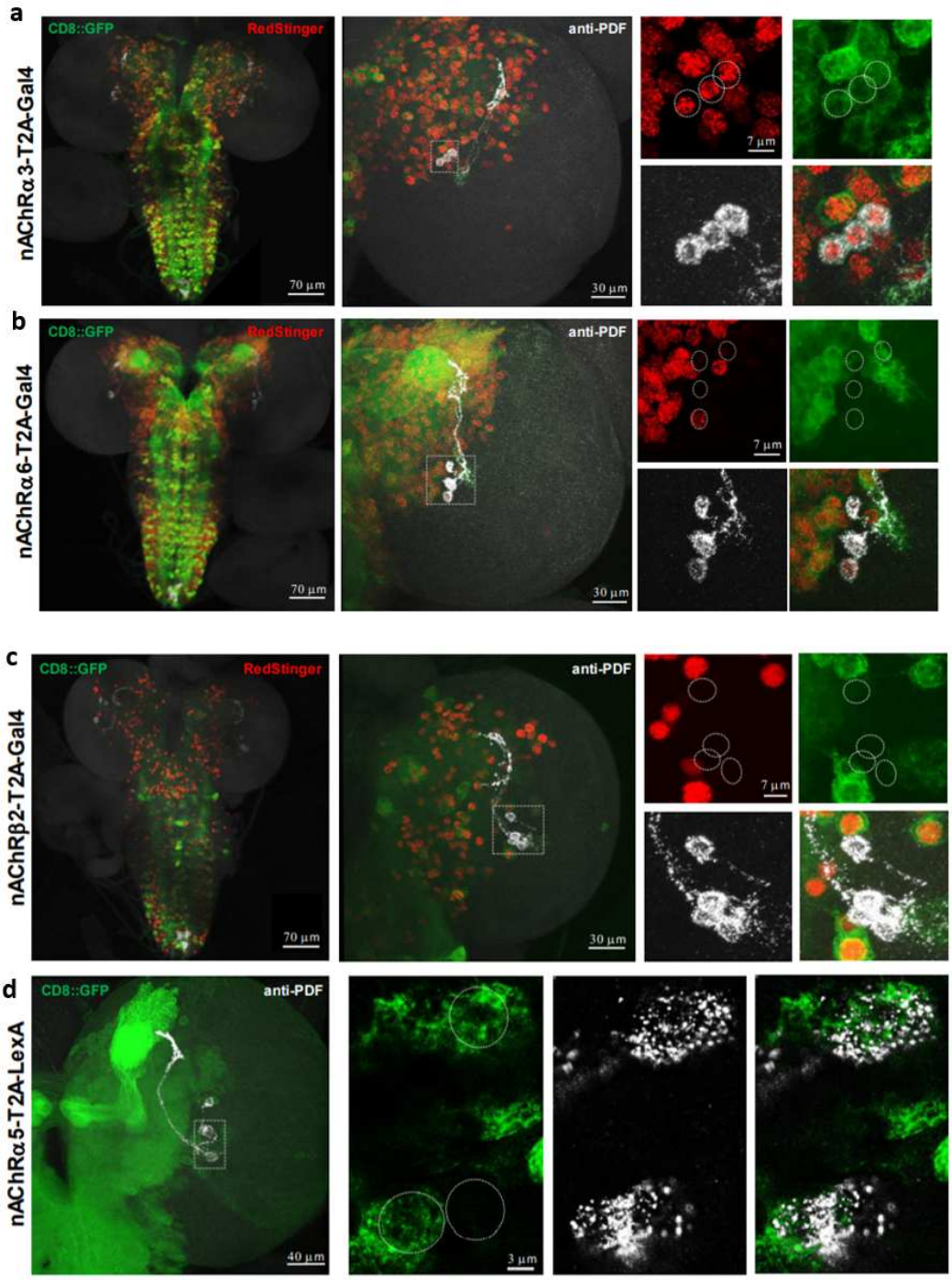

Figure 1.20. Evaluation of nAchR subunit knock-in Gal4 lines reveals the expression of Dα3 and Dα5 in the larval LNvs. (a-c) Left: Representative confocal images of the brain-wide expression patterns for select nAchR subunit genes. The knock-in Gal4 lines drive the expression of mCD8::GFP (green) and the nuclear marker RedStinger (red). LNvs are labeled using anti-PDF antibody (white). Right: Higher magnification images of LNv soma (outlined by dotted white circle) reveal the expression of Dα3 (a) in all, and Dα6 (b) in a subset of, LNvs, while Dβ2 (c) expression is not detected. (d) Left: Representative confocal images illustrating the expression pattern of Dα5-LexA driving mCD8::GFP (green) where LNvs are labeled by PDF staining (white) Right: A single optical section displaying three of the of four cells of the hemispherical cluster indicates that Dα5 is expressed within some, but not all, LNv neurons.

Discussion

Chapter 1 of this research has identified two nAchR genes, *Dα1* and *Dα6*, which are needed for postsynaptic form and function of the developing larval LNv. These two, which are quite divergent with respect to their amino acid sequence, were uncovered among the ten nAchR subunits of the *Drosophila* genome. Preliminary RNAseq datasets and morphological screening were utilized for the isolation step and immunohistochemistry and mutant analysis subsequently confirmed the subunits' significance. *Dα1*, the highly enriched subunit whose expression is sensitive to light activity, participates in LNv neurotransmission but contributes minimally to dendrite arborization. Conversely, *Dα6* is not particularly abundant in the LNv but has a strong influence on structure and physiology at the LNv dendrite. Beyond the basic functions of *Dα1* and *Dα6* delineated here, several additional points concerning subunit compensation, inter-LNv comparisons and the adaptive plasticity response are also discussed below.

nAchR subunit compensation and functional redundancy

One puzzling aspect of this work concerns the necessity of the remaining eight nAchR subunits. Individually, they were not isolated from the RNAi morphology-based screen. Additionally, a small-scale *post hoc* calcium imaging screen was conducted to determine how knocking down other subunits individually affects the LNv's light-induced calcium response. Similar to the morphological screen, none of the RNAi lines significantly altered peak

amplitude compared to wildtype. In contrast, the RNAseq and T2A-Gal4 line expression data do suggest that several others are expressed in the LNvs of late larvae, and even enriched in the case of *Dα3*.

One possible explanation for this is receptor subunit compensation. Firstly, the large size of the nAchR gene family in animals greatly increases the potential for subunit compensation, which may even play some evolutionary role in fully wildtype animals (89). Secondly, there are several examples in the literature where various phenotypes of nAchR-deficient animals only appear when subunit genes are missing in combination. In mice, multi-organ autonomic dysfunction is observed in β2/β4 double knockout mice, whereas individually animals have mostly normal physiology. In flies, abnormal levels of the synaptic protein Hig in the MB calyx is only observed if *Dα6* and *Dα7* are missing simultaneously (135, 136). This phenomenon is also probably responsible for the preservation of normal synaptic activity in lobulate plate tangential cells (LPTC) neurons of *Dα7* mutants despite strong *Dα7* immunoreactivity at the LPTC dendritic field (137). These instances strongly suggest that one subunit may substitute in the absence of another, provided they are similar enough at the molecular level to permit functional redundancy. It may also explain why, upon quantifying data from the original RNAi morphology screen, knockdown of other subunits slightly modifies dendrite volume but not to a significant degree (Figure 1.21). This imperfect compensatory response should not be surprising considering no two subunits will be completely identical at the molecular level.

In the case compensation is occurring, the phylogenetic relatedness could permit *Dα3*, for example, to substitute for *Dα1*. We also can rule out *Dα1* compensation for *Dα6*, since single mutants of the latter have severe and consistent phenotypes already. Although *Dα1*/*Dα3* substitution above is speculation, true compensation events wherever they occur are a vital resource which can be used to understand the molecular properties between the nAchR subunit genes in the *Drosophila* system.

Transcriptional diversity between LNvs

Currently, there is no decisive way of distinguishing each of the four LNv neurons within a single cluster, as the activity of their *Pdf* loci are all fairly similar. However, if the Stinger intensities of the *Dα1-Gal4* and *Dα6-Gal4* reporters are quantitatively accurate to some degree (shown to be the case for *Dα1* later in Chapter 3), there are likely substantial differences in *Dα1* and *Dα6* expression within the cluster.

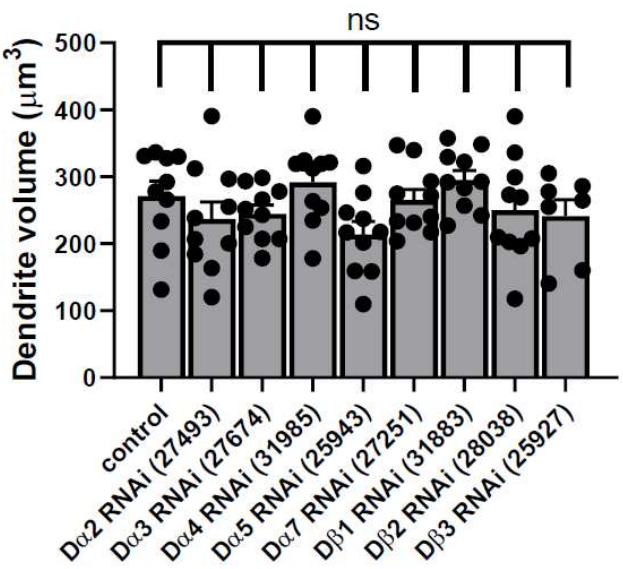

Figure 1.21. Quantification of all knockdown groups in transgenic RNAi screen. Knockdown of multiple nAchR subunit genes results in a noticeable, albeit non-significant, change in LNv dendrite volume that may indicate subtle contributions to morphogenesis. Sample size n represents the number of larvae tested, n=7-10.

Therefore, although the morphological and physiological phenotypes seen for each nAchR subunit mutant are taken as a sum of all four neurons, it is not yet possible to conclude whether or not each individual LNv contributes equally to these summed phenotypes. In the future, techniques such as stochastic and single-cell labeling as well as single-cell RNAseq (scRNAseq) may be able to help classify the four neurons into transcriptionally distinct categories and possibly reveal other genes with varying expression.

Correlation between phenotype and light input

Although *Dα1* and *Dα6* mutants display different phenotypes, these defects interestingly only occur in the LD condition. Specifically, dendrite volume and light-evoked calcium transients are both unaffected by subunit deficiencies in the

LL condition and suggests that the requirement of *Dα1* and *Dα6* is minimized in the constant light condition. Previous work has shown that ambient light significantly changes the developmental trajectory of LNvs by altering crucial synaptic properties (113). Thus, it is possible that the LD vs. LL differences in synapse number, dendrite size and/or dendrite branch motility arise from differential usage of *Dα1* and *Dα6* in different light environments. We explore this next in Chapter 2.

Chapter 2: Deconstructing the mechanism by which *Dα1* and *Dα6* support distinct aspects of LNv development

Abstract

The nAchR-containing postsynaptic specializations of the fly brain contribute to diverse aspects of *Drosophila* neurobiology, not surprising given their predominance in the insect CNS. Here, they not only mediate synaptic transmission and thus influence a multitude of simple behaviors and reflexes, but also drive cellular plasticity, adaptive behaviors and cognition, processes which may also incorporate coincident activity of other neurotransmitters or neuromodulators. Additionally, early studies had revealed a trend in nAchR regulation whereby many subunits have heightened expression during periods that correlate with intense synaptogenesis. However, because insect nAchRs have traditionally been studied in the context of insecticide function, the details of excitatory cholinergic synapse formation and regulation are only recently becoming clear. Furthermore, functional differences between individual nAchR subunits is clearly demonstrated in flies but the underlying reasons for this have not been explained. By continuing our investigation of the nAchR subunits *Dα1* and *Dα6* identified in Chapter One we reveal that both subunits are regulated under distinct transcriptional controls, including light activity and time of development. Our temporal profiling assays, as well as additional morphological and functional assessments, indicate that young immature LNvs rely on *Dα6* to specify synapse number and dendrite volume. Later, *Dα1* is exploited to promote

synaptic maturation at the LNv dendrite and ensure the enhanced level of neurotransmission at the end of larval development. Overall, this sequential usage of functionally distinct receptor subunits is very similar to that which occurs during development and maturation of glutamatergic synapses in the vertebrate CNS and points to temporal transitions in postsynaptic receptor subtypes as a general mechanism underlying development and maturation of synapses.

Introduction

nAchR gene expression and localization in the fly nervous system

Functionally, nAchR receptors in the insect CNS are analogous to ionotropic glutamate receptors (iGluR) in the vertebrate brain and spinal cord. Both are responsible for receiving and propagating fast excitatory neurotransmission (reviewed by (60, 76)). nAchRs are found in many substructures of the *Drosophila* brain and ventral ganglia (138, 139). Early *in situ* hybridization studies on embryos revealed that transcripts of multiple subunits, such as *Dβ1* and *Dα2,* are distributed broadly in the brain and ventral nerve cord (VNC) (140, 141). Interestingly, transcripts for both *Dβ1* and *Dα2* were absent from the lamina, reflecting tissue-specific expression of individual nAchR subunit genes. Enhancer reporter lines, which used the nAchR gene 5' UTR and/or several kb of regulatory elements upstream of the transcription start site, validated the conclusions drawn from the above *in situ* assays, with the exception that reporter was generally detected in the neuropil rather than the soma layer. For instance, various cis-regulatory elements upstream *Dα2* and *Dβ1* both drove

expression of the *lacZ* reporter in nearly all brain regions surveyed, but signal was again peculiarly absent from the lamina (141, 142). Additionally, it appeared that different portions of the cis-regulatory region were responsible for endowing either spatial information or the level of transcriptional activity (141, 142).

Subunit-specific antibodies also helped determine the spatial expression patterns of nAchR genes and in general, regions positive for nAchR subunit genes overlapped well with α-Btx binding sites and were often juxtaposed to areas labeled by presynaptic markers such as *ace* and *ChaT* (139, 143-145). For instance, the medulla, lobula and lobula plate of the optic lobe were all positive for *Dα1*, *Dα2*, *Dα3*, *Dβ1* and *Dβ2* labeling, but only *Dα3* staining was observed in the lamina, suggesting subunit specific functions in the adult visual circuit (98, 141, 143, 145). Immunostaining also detected multiple subunits in protocerebral structures, including the ellipsoid body, ventral bodies, mushroom body (MB) β lobes, as well as the subesophageal, thoracic and abdominal ganglia. More recently, using antibody staining and GFP-tagged subunits, the expression and localization of nAchRs was revealed at the single-cell level. For instance, *Dα7* was visualized as discrete postsynaptic puncta on the dendrites of LPTCs, as well as those of the GF neuron. These findings are consistent with the ones generated by recent tissue-specific transcriptome analysis, which reveals the expression of *Dα7* in L2 and L4 of the lamina, as well as Tm2 of the medulla (122, 124, 137, 146).

One additional tool that helped characterize and isolate different nAchR subunits is affinity purification. Here, head or whole fly extract is filtered through

an agarose column conjugated to nicotinic agonists or antagonists, primarily α-Btx or imidacloprid and its derivatives, and then eluted with a separate nicotinic ligand, thereby concentrating nAchR protein several orders of magnitude. In both *Drosophila* and *M. domestica* samples, this affinity purification approach resulted in three distinct protein bands that range from 61-69kDa (138). A related technique known as photoaffinity labeling has also been used to purify nAchRs and was able to repeatedly isolate a 66kDa-sized protein from *Drosophila* head membranes (138, 147). Both of these methods were also instrumental in the early stages of characterizing *Dα3* and *Dα5* (143, 148). For instance, assays on affinity-purified nAchRs uncovered discrepancies between predicted molecular weight and actual protein band size, providing evidence of predicted post-translational processing, such as the glycosylation events on the *Dα3* polypeptide (98).

Physiological studies of nAchRs in the *Drosophila* CNS

Unlike nAchRs of the vertebrate CNS, which are mostly neuromodulatory and localize perisynaptically or extrasynaptically, fly nAchRs are likely primarily postsynaptic (118), colocalizing with postsynaptic proteins such as DLG and CamKII , while juxtaposing presynaptic active zone molecules such as DSyd-1 (149, 150). When a *Dα7::GFP* transgene was overexpressed in Kenyon Cells (KC) of the MB, GFP puncta were observed within the dendritic claw-like ring surrounding Projection Neuron (PN) axon terminals marked by Brp^{short}::Cherry (151). Notably, fly nAchRs also coexist at the dendrite with other neurotransmitter receptors, such as the $GABA_A$ receptor *Rdl* in MN5

motoneurons, although there appears to be a spatial segregation between the two (152).

Evidence for nAchR activity in the fly brain, and insects as a whole, emerged in the 1970s and has since been demonstrated directly by physiological studies (153, 154). *In vitro* cultured embryonic $ChAT^+$ neurons produce fast and rapidly-decaying inward currents that are readily detected as both miniature excitatory postsynaptic currents (mEPSC) and action potential-evoked excitatory postsynaptic currents (EPSC), and can be reversibly silenced by application of the nAchR-specific antagonist curare, but not GABA receptor or iGluR antagonists. Notably, EPSC amplitudes are non-uniform, and several days in culture is needed to obtain maximum EPSC frequency. Simple forms of calcium-dependent plasticity are also observed as mEPSC frequency increases following multiple rounds of KCl-induced depolarization (155). In a related study, nAchR-mediated cholinergic transmission was demonstrated using cultured MB neurons of dissociated pupal brains, where the majority of mESPSCs are α-Btx sensitive with a broad amplitude distribution (156).

There is also an extensive list of *in vivo* studies documenting the physiological importance of nAchRs. A well-studied case is the function of *Dα7* in the GF circuit, where visual stimuli are relayed to the brain and transformed into motoneuron activity in the periphery, which together mediate the light-induced escape reflex. In *Dα7* null mutants, defective dorsolongitudinal muscle (DLM) responses were observed, resulting from faulty neurotransmission between lobula columnar neurons and the GF circuit as well as between the

peripherally synapsing interneuron (PSI) and DLM's motoneuron (DLMn)(122, 157-159). These studies also identified a highly conserved Tyrosine (Y195) that is directly involved in orchestrating agonist binding (159). At the upstream level of this circuit, *Dα7* is expressed in the VS-type and HS-type dendrites of LPTCs. However, despite multiple reports clearly showing *Dα7* puncta are visible on LPTC dendrites, whole cell recordings following visual stimulation appear largely normal in *Dα7* null animals (124, 137). This, and other unexpected phenotypes, supports the principal of functional subunit compensation within the nAchR gene family.

Besides mediating fast excitatory neurotransmission, nAchR activity has been linked to neural plasticity in several regions of the fly CNS. In cultured KCs from pupal MBs, nicotine induces calcium transients both from direct Ca^{2+} ion influx through nAchRs and release from intracellular stores and voltage-gated calcium channels. These calcium transients are significantly dampened by short conditioning pulses, indicating a strong experience-dependent component (160). In many cases, nAchR-mediated plasticity also involves the intricate and coincident action from other types of ionotropic or metabotropic receptor signaling. For instance, repeated calcium traces recorded in isolated MB neurons can be stimulated by consecutive exposure to Ach and GABA. However, the order of treatments determines the peak amplitude and decay kinetics of the calcium responses (161). Other studies have linked postsynaptic nAchR activity to presynaptic calcium flux as well as characterizing pre- and post-synaptic

homeostatic adaptations following artificial silencing of PN-to-KC nicotinic synapses in the MB calyx (123, 162).

The connection between nAchRs and dopamine, which is a major research subject in vertebrate models, has also been explored in *Drosophila*. Using a variety of techniques and approaches, it was found that MB KCs and a subset of dopaminergic neurons form reciprocal axon-axonal synapses that are critical for olfactory learning (163). In the larval VNC, stimulation of nAchRs induces dopamine release, whereas in the MB, dopaminergic input onto KC axon terminals requires simultaneous stimulation from both cholinergic PN inputs and glutamatergic neurotransmission from ascending VNC inputs(164, 165). Additional analyses have even implicated that specific subunits, *Dα5* and *Dα6* but not *Dα7*, are required for odor-evoked activity in the M4/6 Mushroom body output neurons (MBONs) required for olfactory learning and memory (166).

Finally, nAchR-mediated feedback loops also play an important role in the induction of homeostatic plasticity. Experiments using two populations of cultured cholinergic neurons have elucidated a mechanism by which the inhibition-induced homeostatic upregulation of synaptic activity is balanced by the enhancement of the hyperpolarizing K+ currents (167). Here, pharmacological blockade of *Dα7*-mediated synaptic activity upregulates *Dα7* protein synthesis, which strengthens mEPSC inward currents in the first phase lasting several hours after inhibition. The second phase is characterized by the calcium- and CamKII-dependent, potentiation of the K^+ channel *Shal*, which reverts mEPSC frequency and amplitude towards their original, pre-stimulation

values. This pathway was also replicated *in vivo* using transgenic means to downregulate cholinergic activity (168). Additionally, this subsequent study implicated the transcription factor NFAT as the primary intermediate linking increased *Dα7*-dependent synaptic transmission with *Shal* upregulation and also demonstrated that elevating *Da7* alone, by simple overexpression or maturation assistance with the nAchR-associated protein Nacho, is sufficient to induce the homeostatic response.

In summary, nAchR activity throughout the CNS of *Drosophila* is important for shaping neuronal plasticity, innate behaviors like the visually-induced jump/escape reflex as well as complex behaviors such as olfactory conditioning (163, 169, 170). In addition, these actions are performed not only through the nAchR-mediated calcium influx or neuronal activation but also involve complex interactions between cholinergic signaling and other types of neurotransmission.

Subunit-subunit interactions and mature receptor composition

Vertebrate nAchR subtypes show significant functional and pharmacological diversity and the clear identification of distinguishable subtypes is particularly conducive to their research. *Drosophila* nAchRs are also characterized by a variety of biochemical and biophysical properties. However, it is still not clear in *Drosophila* which subunits co-assemble and in what stoichiometry, and is in large part due to the lack of an effective heterologous system for *in vitro* expression (171). Currently, there is still no definitive description of a functional native pentameric nAchR receptor in the *Drosophila*

nervous system, although there are several lines of evidence that suggest certain subunits could co-assemble.

Early *in situ* hybridization and immunohistochemical studies consistently reported co-localization of specific subunits. For example, *Dα1* and *Dβ1* are both concentrated in the ventral bodies and lateral triangles of the central complex and within the same medulla and lobula layers of the optic lobe (145). Additionally, to understand native receptor compositions, co-immunoprecipitation experiments have been conducted for various *Drosophila* nAchR subunits. Dα1 and Dα2 can be reciprocally immunoprecipitated from adult head membrane extracts, as can *Dα3* together with Dβ1 (143). Serial immunoaffinity chromatography experiments have also been conducted, where Dα1-containing receptors were used as bait to isolate Dα2-containing receptors, which were then used to further bait Dβ2-containing receptors. All three subunits are detected at all three filtering steps, supporting their association *in vivo* as a ternary receptor complex (98). Interestingly, these three subunits form a cluster on Chromosome 3R.

Unfortunately, some concerns have been raised for *Drosophila* studies due to conflicting results generated by different biochemical methods as well as those studies which strictly use hybrid heterologous systems and therefore may not be an entirely accurate representation of native receptor interactions (98, 144, 172). One way to achieve greater confidence in a proposed instance of co-assembly is to look for phenotype synergism between single and double nAchR mutants. For example, the toxic effects of the insecticide Spinosad are blunted in in $D\alpha1^{-/-}$ and $D\beta2^{-/-}$ single mutant flies. However, $D\alpha1^{-/-}/D\beta2^{-/-}$ double mutants are no more

resistant to Spinosad than their single mutant counterparts(173). Although this does not unequivocally mean *Dα1* and *Dβ2* are coassembled, it is the expectation for co-assembly because a change in either one of these subunits would be sufficient to disrupt function of the entire pentamer.

Methods

The following Chapter 2 protocols were previously described in Chapter 1

Calcium imaging analyses, Confocal imaging and quantification of dendrite volume and Statistical analysis. Flies were cultured using the same conditions and dissected at the same developmental stage, with the exception of the late 1st instar, (48hr hr after egg laying (AEL)) of the qFISH (quantitative fluorescent in situ hybridization) experiments and the late 1st instar, (48hr AEL), late 2nd instar (72hr AEL) and early-mid 3rd instar (96hr AEL) of the developmental calcium imaging experiments.

Drosophila stocks

The stocks *Rh5,6>Brp::mCherry* and *hs-flp, Pdf-Gal4/CyO; UAS-FRT-mCD2stop-FRT-mCD8::GFP* were acquired from our lab's previous study (113). All other stocks used can be found above in Chapter 1 methods.

Immunohistochemistry

Anti-HA labeling was conducted using the rat anti-HA primary antibody (1:200) and the secondary antibody Cy3 Goat anti-rat (1:500). Steps in the overall protocol is identical to that found in Chapter 1 Methods.

Quantitative fluorescent *in situ* hybridization assay (qFISH)

The qFISH protocol is based on Yin et al., 2018 with slight modifications (115). Larvae were dissected in DPBS (DEPC treated 1x PBS) with the ventral nerve cord removed. The brain lobes were subsequently broken with hypodermic needles and digested in a mixture of 200µL 1x Collagenase/1x Dispase and 50µL 1x Liberase at 25°C for 20-30 minutes. Enzyme-treated brains were titrated 100 times until no substantial fragments remained. Digestion reaction was terminated by addition of 1mL SM3-FBS (Schneider's insect medium with a 100µg/mL Penicillin-Streptomycin-Kanamycin antibiotic cocktail and 5% Fetal Bovine Serum). Cells/tissue fragments were centrifuged at 950g for 5 minutes at 10°C. All but 50µL of supernatant was removed and 50µL new SM3-FBS was added, mixed and then incubated at RT in a chamber pre-treated with .25mg/mL Concanavalin-A for 15 minutes to allow for cell adherence, followed by fixation in 4% PFA. Chambers were washed with PBS three times and subjected to serial ethanol washes (50%, 70%, 100%, 70% and 50%), then washed with 1x PBS and incubated in a 1:15 Protease III solution (in 1x DPBS). Chambers were then rinsed with PBS before undergoing the hybridization portion of the protocol, which is performed using the RNAScope kit (ACD Bio, Catalog no. 320850, 820851) supplied with *Dα1* or *Dα6* mRNA hybridization probes (Catalog no. 555611, 515521). Dissociated cells were incubated with either *Dα1* or *Dα6* probes at 40°C for 2 hours. After the washing and amplification steps following the manufacturer's protocol, the dissociated cells were stained using the anti-PDF antibody and mounted with Vectashield mounting medium with DAPI for imaging.

Insect S2 cell transient transfection

Drosophila Schneider (S2) cell transfections were performed using Lipofectin (Thermo Fisher, Waltham, Massachusetts) following the standard protocol from the manufacturer. S2 cells were seeded in a 24-well plate and transfected with 6 µL of Lipofectin along with 1 µg of DNA containing both the actin-*Gal4* and either UAS-*Dα1-GFP*$_{11}$ or UAS-*Dα6-GFP*$_{11}$. Transfected cells were cultured at 27°C for two days and transferred onto a coverslip for two hours before fixation by 4% PFA and staining using anti-HA antibody.

Generation of transgenic *UAS-Dα6-GFP11-HA* and *UAS-Dα1-GFP11-HA* lines

The *GFP*$_{11}$*-HA* tag (synthesized by Integrated DNA Technologies, Inc., USA) has the sequence 5'-CGTGACCACATGGTCCTTCATGAGTATGTAAATGCTG CTGGGATTACAGGAGGCGGTTACCCATACGATGTTCCAGATTACGCT-3'. It was inserted into the receptor subunit cDNA using overlap PCR. For *Dα6*, the insertion was placed at G429, located in the 2nd intracellular loop. The position was derived from a previously generated *Dα7-GFP* fusion transgene (124). The first junction was prepared using reverse primer 5'-GACCATGTGGTCACGGCCAGATATTG-3'. The *GFP*$_{p11}$*-HA* tag was amplified using forward primer 5'- CAATATCTGGCCGTGACCACATGGTCC-3' and reverse primer 3' GGTTTGGGAAGCGTAATCTGGAACATCG-3'. The second junction was prepared using forward primer 5'-GATTACGCTTCCC AAACCGCCATT GG-3'. For *Dα1,* the *GFP*$_{p11}$*-HA* tag was placed at C420, a homologous position in the 2nd intracellular loop. The first junction was prepared

using reverse primer 5'-CATGAAGGACCATGTGGTCACGACAGT GGGCG CTAATCCCG-3'. The *GFP$_{11}$-HA* tag was amplified using forward primer 5'-GCGCCCACTGTCGTGACCACATGGTCC-3' and reverse primer 5' GGTTCTGCGAAAGCGTAATCT GGAACATCG-3'. The second junction was prepared using forward primer 5' GTTCCAGATTACGCTTTCGCAGA ACCGCCG-3'.

Endogenous tagging of nAchR subunit genes

CRISPR-mediated mutagenesis was done by WellGenetics Inc. (Taipei City, Taiwan) using modified methods of Kondo and Ueda (174). Genome editing of *Dα1* (CG5610) and *Dα6* (CG4128) was performed in parallel. The final product of each was designed to encode a subunit which is tagged, in frame, with the GFP$_{11}$ fragment followed by three HA epitopes (Figure 2.1). In *Dα1*, the tag is placed after amino acid C420, corresponding to the 2nd intracellular loop of the folded protein. In *Dα6*, the tag is placed after G429, the homologous position in this subunit. gRNA sequences for *Dα1* and *Dα6* were designed based on minimal distance from the site of editing (<50bp), minimal off-target sequences, and moderate GC content (40%-70%). The *Dα1* gRNA site: ACAGATCGTCGTCGGCGCCC[GGG], was created using the Sense oligo: 5'-CTTCGACAGATCGTCGTCGGCGCCC and the Antisense oligo 5'-AAACGGGCGCCGA CGACGATCTGTC. The PAM site of the donor plasmid was converted from GGG→GGC. The *Dα6* gRNA site: TTACGCCGACGAGCCA ATGG[CGG], was created using the Sense oligo: 5'-CTTCGTTACGCCGACGAGC CAATGG and the Antisense oligo 5'-

AAACCCATTG GCTCGTCGGCGTAAC. The PAM site of the donor plasmid was converted from CGG→CCG. Both gRNA fragments were individually cloned into the U6-promoter plasmid. The *Dα1* upstream homology arm was created using a 1012bp fragment (-2812bp through -1801bp relative to the stop codon). Forward Oligo: 5'- TAGTGGGCACATTACCAACG; Reverse Oligo: 5'-ACAGTGGGCGCTAATCCC. The *Dα1* downstream homology arm was created using a 1037bp fragment (-1800 through -764 relative to the stop codon). Forward Oligo: 5'- ATCTGTTCAGCCCGTCGG; Reverse Oligo: 5'-AGACCGATTGCCCTTCACT. The *Dα6* upstream homology arm was created using a 1032bp fragment (-1859bp through -828bp relative to the stop codon). Forward Oligo: 5'-CCGACACAGAAAACCAATGA; Reverse Oligo: 5'-GCCAGATATTGTGTGCCGG. The *Dα6* downstream homology arm was created using a 1055bp fragment (-827 through -228 relative to the stop codon). Forward Oligo: 5'-TCGCAAACGGCCATTGGCTCGTCGGC; Reverse Oligo: 5'-CAACATTTTCGTTTTGCTC. Separately, a GFP_{11}-LoxP-3xP3-RFP-LoxP-3xHA cassette was made through several restriction reactions. The GFP_{11} and 3xP3-RFP components were linked *via* BgIII and the 3xP3-RFP and 3xHA components were linked *via* NheI, with the dinucleotide CG immediately 5' to the NheI site. This cassette was fused to the *Dα1* upstream homology arm with XbaI at the GFP_{11} side and to the *Dα1* downstream homology arm with XhoI at the 3xHA side. This cassette was also separately fused to the *Dα6* upstream and downstream homology arms using identical restriction enzymes. Both products were individually cloned into the vector pUC57-Kan as a donor template for repair. The

donor plasmid and U6-promoter gRNA plasmid for each target gene, together with a third plasmid providing the Cas9 source (*hs-Cas9*), were microinjected into w^{1118} embryos. Adults were later crossed with balancer flies and F1 offspring carrying the selection marker 3xP3-RFP were retrieved and further validated by genomic PCR and sequencing. Subsequently, adults from multiple independent lines were crossed with a *hs-Cre* genetic background in order to remove the RFP marker, together with its 3xP3 promoter and a single LoxP site. Multiple independent RFP-negative lines were established by screening for RFP removal, and were then validated by genomic PCR and sequencing: *Dα1* Forward primer: 5'-agaattcgcggccgctctagaCGTGACCACATGGTCCTTCATGAGTATGT, *Dα1* Reverse primer: 5'-GGG ATCCTTCGATGGTCTTC; *Dα6* Forward primer: 5'agaattcgcggccgctctagaCGTGACC ACATGGTCCTTCATGAGTATGT, *Dα6* Reverse primer: 5'-TGGTTGAGTGCGGAT GAATA

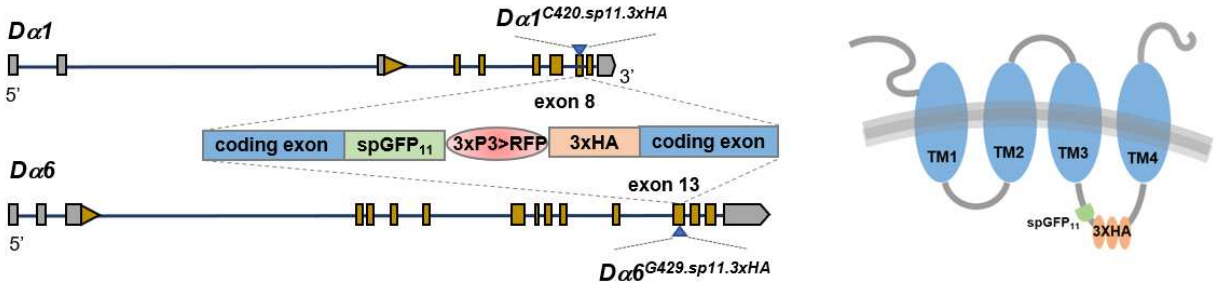

Figure 2.1. Schematic diagram illustrating the constructs used for endogenous tagging of Dα1 and Dα6 by CRISPR/Cas9-mediated genome editing. The knock-in allele initially contains an RFP selection marker (right). Following Cre-mediated excision, the targeted subunit is transcribed with the addition of the GFP_{Sp11} and 3xHA-tag inserted within the 2nd intracellular loop of the protein (right).

Super-resolution imaging and nAchR protein quantification

LNvs in Figures 2.10 and 2.11 were imaged with a Zeiss LSM 880 confocal microscope equipped with an AiryScan detector. Samples were imaged using a 63x oil objective with 4x zoom. Z-stacks were obtained by taking serial sections at 0.18µm thickness, with a typical x-y-z resolution of .04µm x .04µm x .18µm and a pixel dwell time of 0.66µs. For Dα1 and Dα6 signal quantification, confocal Z-stacks were imported to the 3D visualization software Imaris (Bitplane). LNv cell bodies were reconstructed using the surface module based on the signal generated by anti-PDF staining. Average HA signal (555nm channel) was calculated within the reconstructed surface and normalized to the average anti-PDF signal (488nm channel) within the same surface.

Quantitative analysis of putative synaptic contacts

Following dendrite surface reconstruction and volume calculation (described in Chapter 1), the Brp-mCherry puncta representing discrete presynaptic terminals were determined using the Spots module of Imaris to identify spherical volumes of 0.6µm in diameter. The intensity threshold, used in previous experiments, was determined by manual counting (113). The "Spots close to surface" Imaris extension was subsequently used to determine all puncta whose center is within 0.3µm of the reconstructed LNv dendrite surface. This effectively reveals the number of BO-LNv synapses in this region. All experiments generating dendrite volume and/or synapse number data were blinded, by concealing the identity of each group, before the image processing step to avoid subjective bias during quantification.

Dendrite dynamics analysis

Single labeling of the LNvs and time-lapse imaging of dendrite dynamics are as described (113, 175). Using heat shock-mediated flippase activity, we obtained single labeled LNvs in larval brains collected at the wandering 3rd instar larval stage (i.e. 120hr AEL). The dissection step is similar to the calcium imaging step above, using the same external buffer, confocal microscope, 40x water objective and two-photon settings. Here, entire dendritic arbors, imaged at 3.3x optic zoom, were recorded at 1-minute intervals for a total imaging time of 10 minutes. A typical x-y-z resolution was .13µm x .13µm x .25µm. The y-width and z-depth were adjusted to keep each Z-stack frame equal to 60 seconds. All samples which underwent excessive drifting, rotation, distortion or degradation were not included for image processing and quantification. 4D time-lapse data sets were processed by Hyugens Professional (Scientific Volume Imaging) for deconvolution and to correct for minor drifting. Processed images were analyzed with Imaris, where all branch terminals appearing any time during the 10-minute recording session were manually marked and tracked through all 10 time frames using the "Spots" module. All branches were classified as either static or dynamic. The criteria for the "dynamic" class was any branch which exhibited an extension or retraction event at any time during the recording session. A 0.3µm threshold for extension and retraction events was used to prevent the inclusion of very small movements, which tend to arise from incomplete drift correction or minor human error. To calculate branch terminal displacement, the 3D coordinates of all branch terminals for the

entire recording session were exported as CSV files, where a 0.3μm threshold was again used, followed by summation of all movements within the entire arbor.

3D homology modeling of nAchR subunits

The amino acid sequence of the major isoform for *Dα1* and *Dα6*, or one of the major isoforms expressed in the larval LNv, was queried into the Phyre2 protein folding server (176). This generated *Dα1* and *Dα6* 3D structures that were predicted based on the previously deposited crystal structure of human α4 (*Chrna4*) derived from the α4β2 heteropentamer. Finally, the folding information contained in the output file was visualized using PyMOL (The PyMOL Molecular Graphics System, Version 2.0 Schrödinger, LLC.)

Results

***Dα1* and *Dα6* expression is developmentally regulated and with distinct transcriptional responses to activity**

The results from Chapter 1 were a strong indication that *Dα1* and *Dα6* are requisite subunits for proper LNv biology. Although there is a functional divergence with respect to dendrite morphogenesis, both seem to contribute in similar ways tosynaptic transmission. In the vertebrate system, one of the most well characterized receptor subtype relationships is the NMDA receptor-dependent AMPA receptor expression and clustering that drives maturation of central glutamatergic synapses. This phenomenon provides a clear example for how temporal control can be a key factor during synapse formation and was therefore used to guide the next phase of this project. How are *Dα1* and *Dα6* are utilized

during LNv dendrite development to influence different features of LNv form and function?

The first objective was to determine if in fact there was a temporal component to *Dα1* and *Dα6* expression in the LNv. To quantitatively analyze any change in their transcript levels in developing LNvs we performed qFISH experiments on acutely dissociated LNvs using subunit-specific probes (115). The transcript levels of both subunits were assessed in LNvs collected during two developmental stages: 48hr AEL, the peak time for LNv synapse formation, and 120hr AEL, when the LNv reaches its mature state preceding pupation (113). Quantification of qFISH signals at both time points revealed that the expression level of *Dα1* is low in young LNvs (48hr AEL) but is significantly upregulated later in development (120hr AEL) (Figure 2.2). Specifically, the number of *Dα1* mRNA puncta (red) in the LNv (green) is roughly four times higher at the late, 120hr AEL stage compared to the young 48hr AEL stage. Moreover, we observed that the LL condition had a strong effect on eliminating the developmental upregulation of *Dα1*, shown by the lack of a significant difference between the two LL time points. In contrast, the level of *Dα6* transcript in LNvs declined significantly during larval development (Figure 2.3). The average LNv contains between two and three *Dα6* mRNA puncta by 48hr AEL. But by the 120hr AEL stage, regardless of light condition, the typical LNv is expressing one, or no, *Dα6* trancsripts. The lack of change between LD and LL conditions, at each time point, indicates that the temporal regulation of *Dα6* expression at the mRNA level is activity-independent.

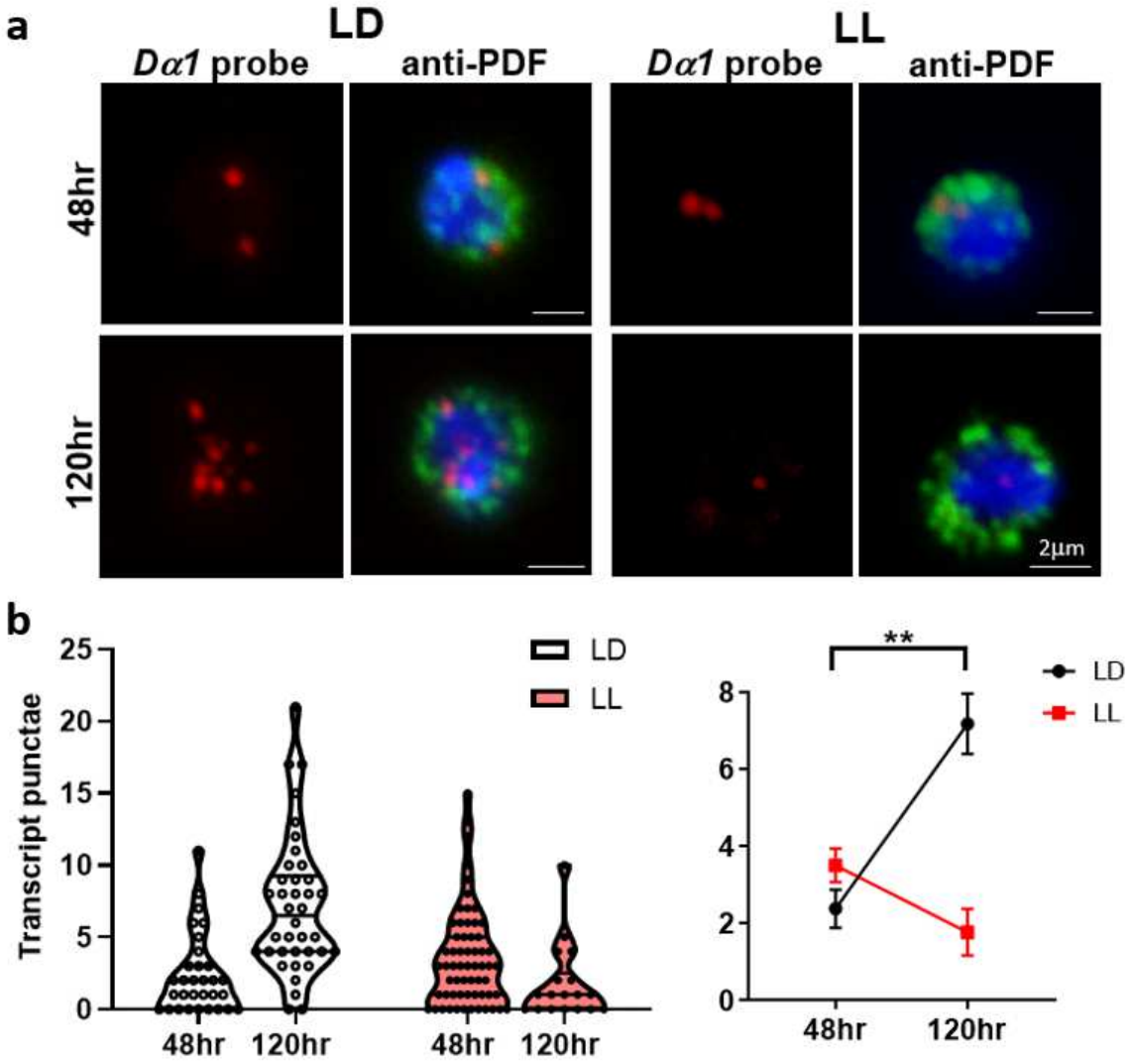

Figure 2.2 The transcript level of Dα1 in the LNvs is regulated during development and influenced by activity. (a) Representative projected confocal images of qFISH experiments labeling Dα1 mRNA transcripts (red) in acutely dissociated LNvs (green) are shown. Cell nuclei are stained with DAPI (blue). The LNvs were collected from larvae at two stages and in two conditions. (b): Quantification of the Dα1 transcript level represented by the violin plot (left) and the trend line (right) reveals a significant increase at the later developmental stage when larvae are cultured in the LD condition (black) but not the LL condition (red). n represents the number of dissociated LNvs, n=18-62. Error bars represent mean ± SEM.

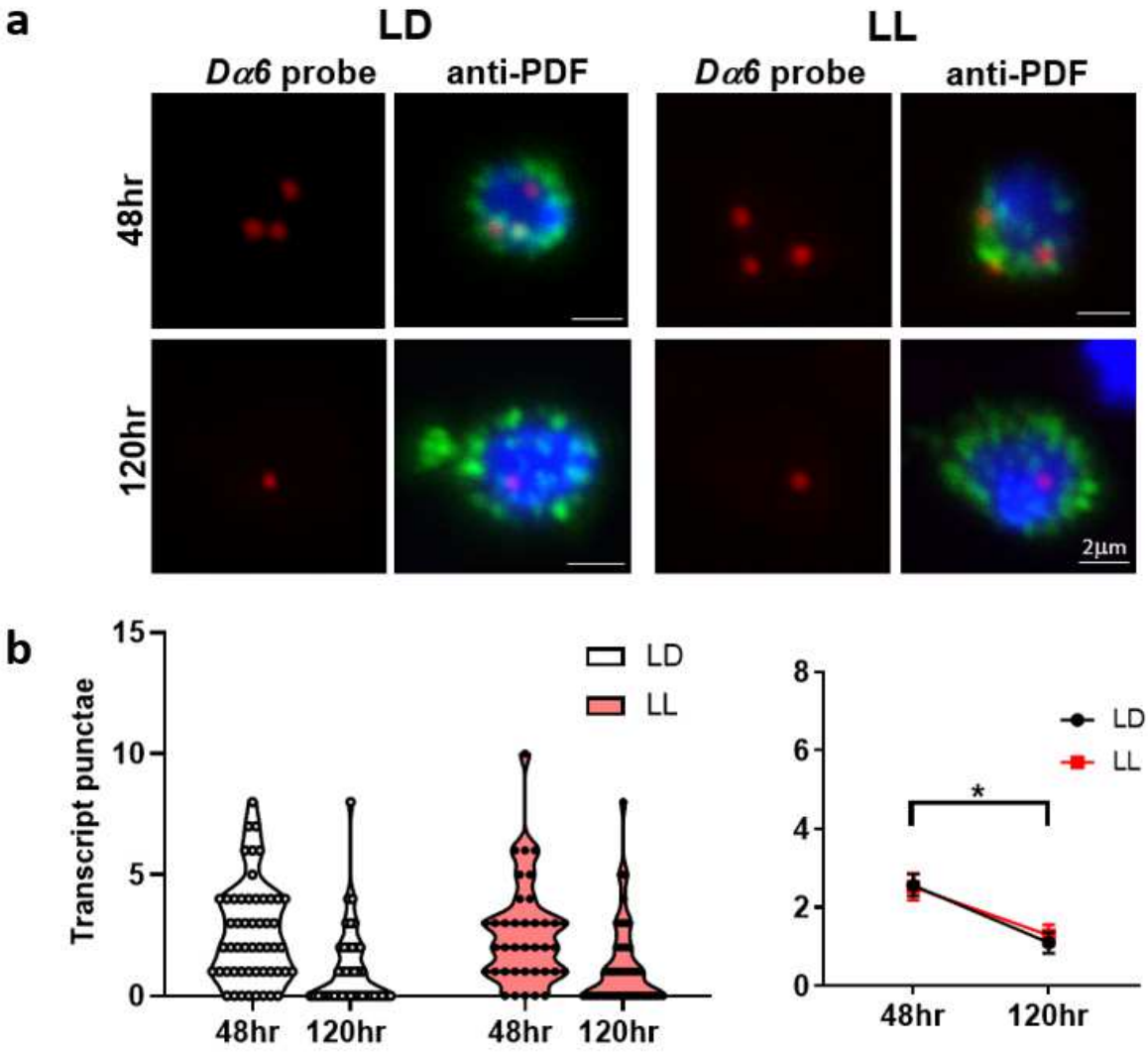

Figure 2.3. The transcript level of Dα6 in the LNvs is downregulated during larval development and is insensitive to changes in activity. (a) Representative projected confocal images of qFISH experiments labeling Dα6 mRNA transcripts (red) in acutely dissociated LNvs (green) are shown. Cell nuclei are stained with DAPI (blue). The LNvs were collected from larvae at two stages and in two conditions. (b): Quantification of the Dα6 transcript level represented by the violin plot (left) and the trend line (right) reveals a significant decrease in both the LD (black) and LL condition (red). n represents the number of dissociated LNvs, n=39-54. Error bars represent mean ± SEM.

We were able to conclude from these straightforward experiments not only that *Dα1* and *Dα6* have opposing temporal profiles in the LNv but also that the sensitivity to chronic alterations in neuronal activity induced by the LL condition

is subunit-specific. These observations are also consistent with the results obtained from the RNA-seq analyses (Figure 1.5, 1.7), which also report LD-LL differential expression for *Dα1* but not *Dα6*.

During the course of this project, transcriptomic data stemming from an independently-procured scRNA-seq study on the 1st instar larval brain (177) was published and we were interested to see if these results would corroborate our qFISH findings. This was accomplished by identifying the LNvs using the expression of its signature neuropeptide PDF. Similar to our lab's data obtained at the 3rd instar stage, the LNv transcriptome in the 1st instar stage also contains all nAchR subunits except *Dα7* and *Dβ3* (Figure 2.4). And indeed, not only was the relative abundance of the nine subunits different at the two developmental stages, but the *Dα1*:*Dα6* expression ratio was inverted. Here, *Dα6* was the second-most abundant subunit, after *Dα3*. This change in relative quantity from 48hr. AEL to 120hr. AEL thus perfectly aligned with the *Dα1* increase and *Dα6* decrease witnessed in our *in situ* experiments.

Endogenous tagging of nAchR subunits reveals the developmental regulation and localization of Dα1 and Dα6 protein

To confirm the temporal regulation of *Dα1* and *Dα6* at the protein level, we next moved on to evaluate their levels and localization in the developing LNvs. Previous studies have shown that a GFP-tagged *Dα7* transgene with the GFP inserted in the large, intracellular 3rd loop (i.e. TM3-TM4 loop) localizes specifically to the dendritic region when expressed in *Drosophila* central neurons (124).

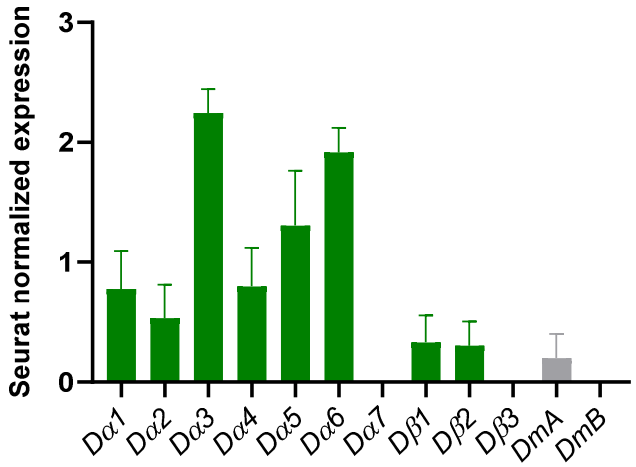

Figure 2.4. Relative abundance of AchR subunits in LNvs at the 1st instar larval stage. Analysis of a published ScRNA-seq dataset generated using first instar larval brain (Brunet Avalos) shows the relative expression level of nicotinic and muscarinic Ach receptor subunits. Similar to our LNv-specific RNA-seq data collected at the 3rd instar larval stage, transcripts of most nAchR and mAchR subunits are detected at the early stage although the relative abundance of the subunits is different at the two stages. Dα3 and Dα6 are the highest expressing subunits in the immature LNvs. Expression levels were normalized by Seurat.

However, our *Dα1-GFP* transgene with the GFP inserted in the corresponding part of the Dα1 protein appeared to form aggregates within the soma when tested *in vitro* with the S2 Cell system (Figure 2.5). Similarly, in transgenic flies expressing *UAS-Dα1-GFP* under a *Pdf-Gal4* driver, GFP fluorescence was virtually absent in the dendrites and the same aggregates were sometimes observed in the cell bodies. Both assays, which also yielded the same results for a *Dα6-GFP* transgene, suggested that these subunits were not properly delivered to the dendrite due to potential deficits in receptor assembly and/or trafficking caused by the bulky GFP tag.

To resolve this, we tried the same overexpression approach but substituted the full length GFP tag with the much smaller split GFP tag (GFP_{sp11}), followed by three copies of the HA epitope (178). This seemed to permit better expression in

the S2 cells, evidenced by GFP reconstitution signal and anti-HA antibody signal on the membrane as well as the absence of GFP aggregates (Figure 2.6). However, these constructs still failed *in vivo*. We hypothesized that this was being caused by problems associated with subunit overexpression, as nAchR proteins require additional factors for correct polypeptide folding, assembly and postsynaptic delivery and insertion. Any exogenous receptor protein may put strain on these processing proteins and ultimately lead to a breakdown in receptor assembly and transport.

To overcome these barriers, we chose to create new knock-in alleles with small tags that would both solve the issue of overexpression and minimize reporter tag interference. Using CRISPR/Cas9-mediated genome editing, we generated and validated *Drosophila* knock-in lines expressing *Dα1* and *Dα6* receptors tagged with the GFP_{11}-3xHA fragment (Figures 2.1 and 2.7 and Appendices A and B). These endogenously tagged receptors were readily detected by anti-HA antibody, which revealed wide, yet distinct, distributions of the two nAchR subunits in larval brain lobes and the VNC (Figure 2.8), while brains from the control genotype showed no clear signal (Figure 2.9).

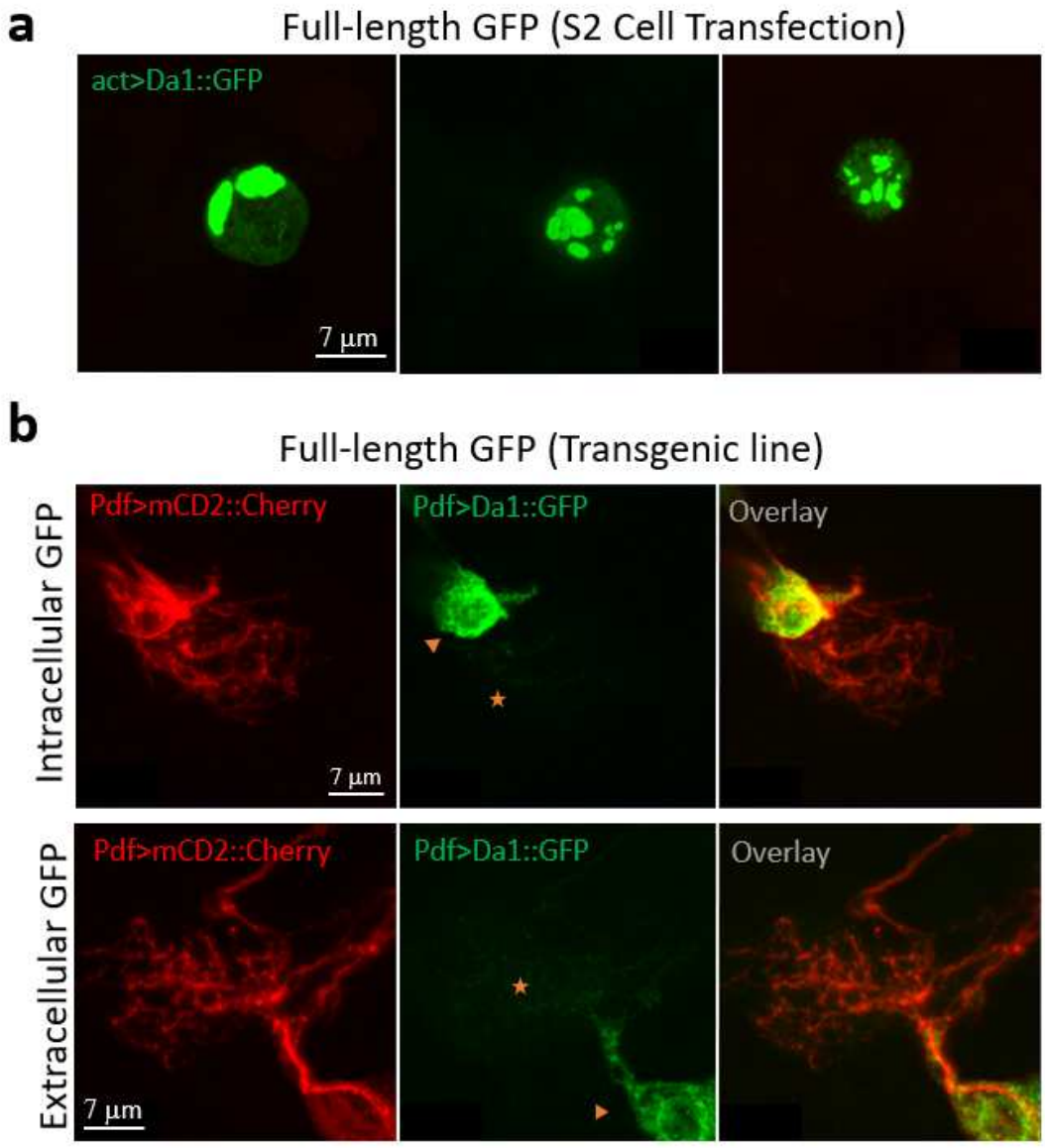

Figure 2.5. A Dα1 transgene containing a full-length intracellular GFP tag is not properly processed and trafficked. (a) Dα1::GFP$_{FL}$ (green) co-transfected with actin-Gal4 into S2 cells forms multiple, large aggregates. Examples shown are single optical sections in three separate cells (b) Top: Transgenic flies expressing Dα1-GFP$_{FL}$ (green) show poor signal distribution in the dendrite of mCherry-labeled LNvs (red). Bottom: Postsynaptic localization is improved in extracellularly-localized Dα1-GFP$_{FL}$ but still unexpectedly low.

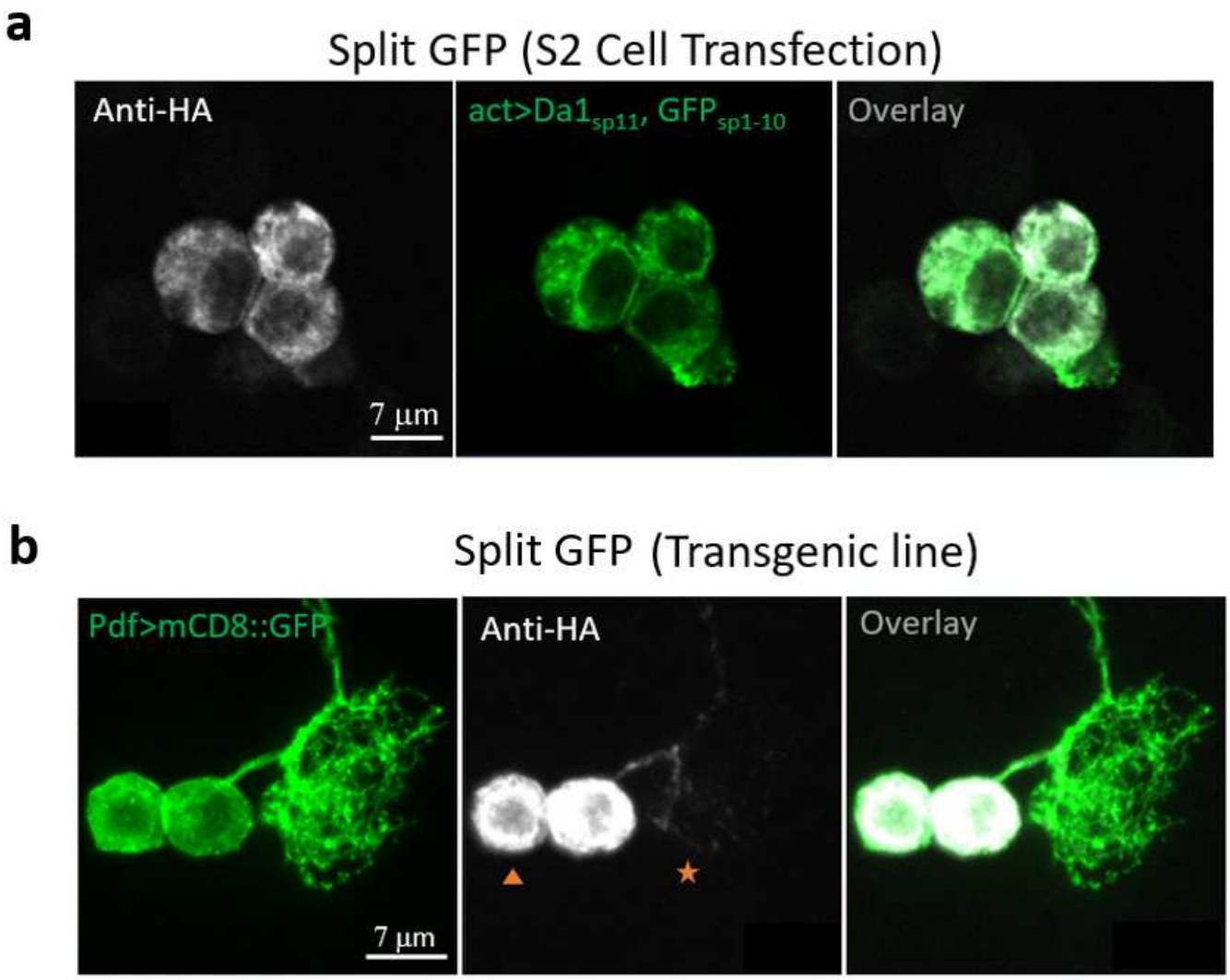

Figure 2.6. A Dα1 transgene containing a split intracellular GFP-3xHA tag resolves processing issues in vitro but not in vivo. (a) Aggregates are not observed when Dα1-GFP$_{Sp113xHA}$ (GFP: green; HA: white) is co-transfected with actin-Gal4 into S2 cells and signal is now seen at the plasma membrane. (b) HA signal (white) from the Dα1-GFP$_{Sp113xHA}$ construct expressing in transgenic flies still shows poor signal distribution in the dendrite (star) of LNvs marked with mCD8::GFP (green) and the large majority of Dα1 remains in the cell body (arrowhead). Note: green in (a) is from Dα1-GFP$_{Sp113xHA}$ and in (b) is Pdf-Gal4 driven mCD8::GFP.

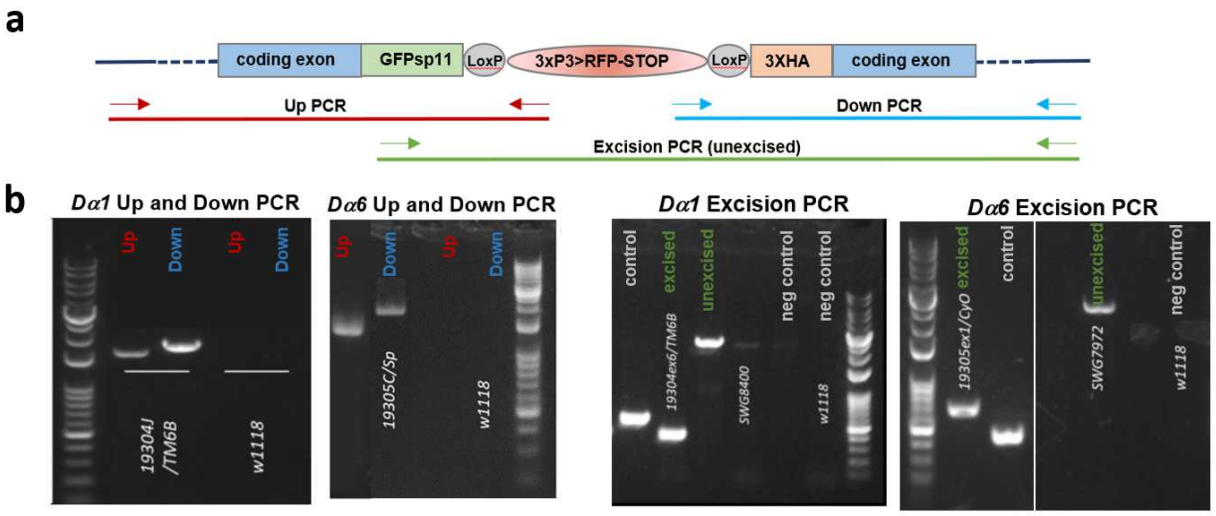

Figure 2.7. Verification of CRISPR/Cas9-mediated knock-in by genomic PCR and sequencing. (a) Schematic diagram of Dα1 and Dα6 knock-in cassette and primer designs for insertion site confirmation: Up PCR, Down PCR and Excision PCR. (b) Left: Up and Down PCR for Dα1 and Dα6 reveals correct insertion of the knock-in cassette into the genome. Genomic DNA from w^{1118} line was used as a negative control. Right: Excision PCR for Dα1 and Dα6 confirms that the 3xP3>RFP element was successfully removed by Cre Recombinase. Excised PCR products showed a size-reduced band compared to the unexcised line.

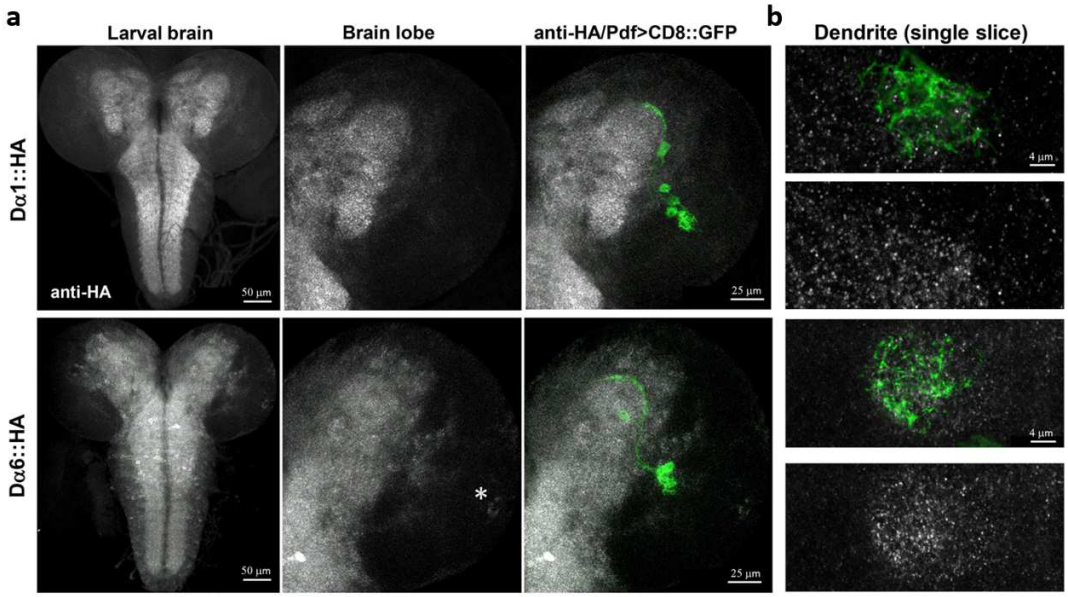

Figure 2.8. (a) CNS-wide expression pattern of Dα1-HA (top) and Dα6-HA (bottom) using anti-HA labeling (white). LNvs are labeled by Pdf-Gal4>UAS-mCD8::GFP (green). Representative projected confocal images are shown. Note the Dα6-HA signal in the lOLP neurons (white asterisk). (b): Representative single optical sections of confocal images demonstrating the localization of both Dα1-HA and Dα6-HA in the larval optic neuropil (LON).

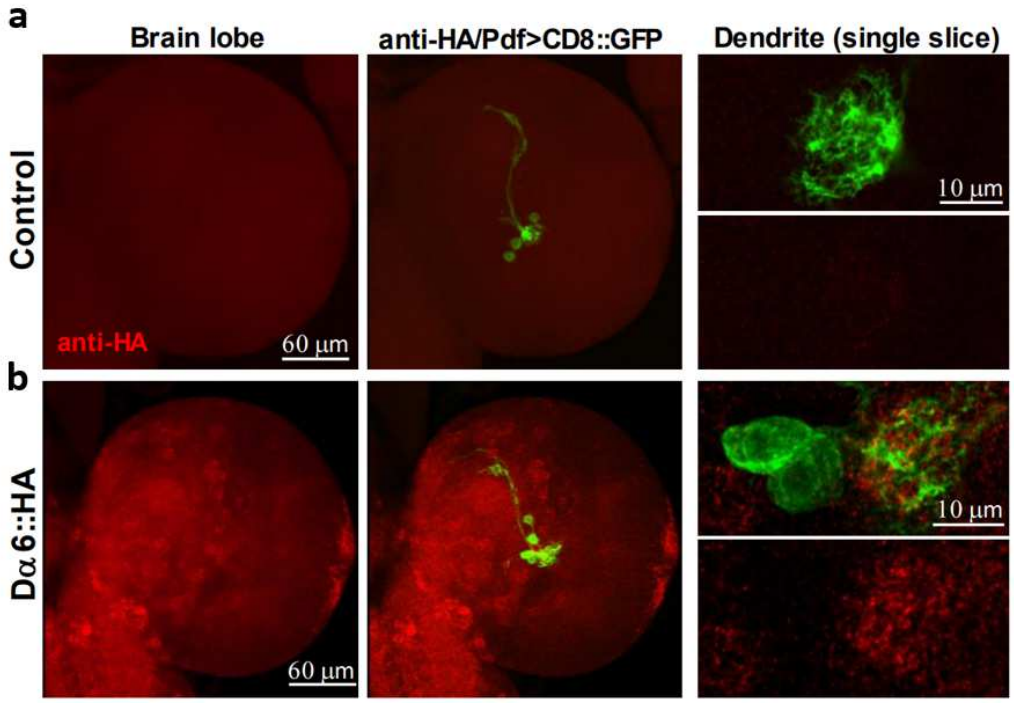

Figure 2.9. Endogenous HA tagging produces antigen-specific labeling. Left/Middle: CNS-wide staining pattern of HA-labeling (Red) in control (a) and Dα6-HA (b) samples. LNvs are labeled by Pdf-Gal4>UAS-mCD8::GFP (green). Representative projected confocal images are shown. The Dα6-HA signal is found broadly distributed in the CNS neuropil and the lateral margin of the brain lobe. No similar signals are found in the control. Right: Representative single optical sections of confocal images demonstrating the virtual lack of HA signal in the control sample (a), but the intense staining in the LNv dendritic arbor region for the Dα6-HA sample (b).

In both *Dα1* and *Dα6* knock-in lines, we observed intense signal in the synapse-rich neuropil. In the Dα6 line, a small number of cell bodies were also occasionally immunopositive. Upon closer examination using super-resolution confocal imaging, we identified numerous HA-positive puncta that were largely localized in the dendritic region and, to a lesser extent, within the soma of LNvs (Figure 2.8). To verify if Dα1 and Dα6 were localized in the postsynaptic compartment (i.e. their expected sites of action), we introduced a mCherry-tagged presynaptic active zone marker driven by the larval photoreceptor enhancer, *Rh5,6>Brp::mCherry*, into the

knock-in lines (113). HA-positive puncta for both subunits were frequently observed at the interface between these mCherry-marked, presynaptic axon terminals and *mCD8::GFP*-labeled dendritic processes, supporting the idea that Dα1 and Dα6 are incorporated into the postsynaptic apparatus in the LNvs (Figure 2.10).

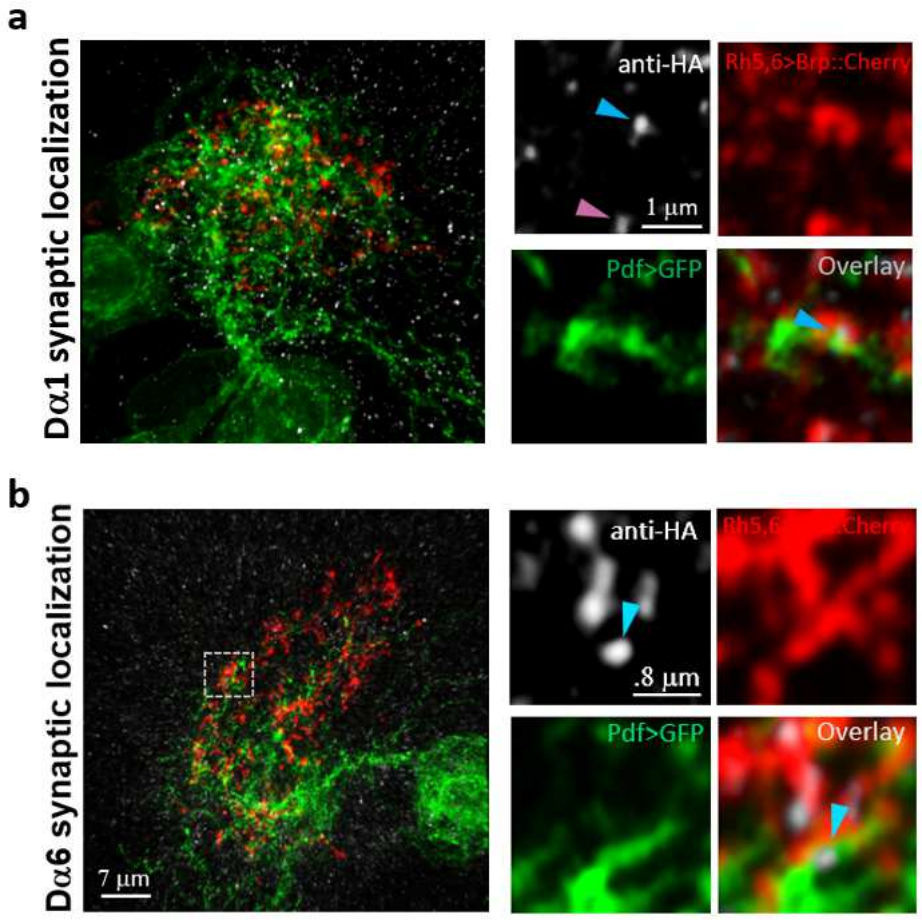

Figure 2.10. Super-resolution imaging reveals the synaptic localization of two nAchR subunit proteins. Left: Representative single optical sections of confocal images are shown. LNvs are labeled by mCD8::GFP (green) and presynaptic terminals are labeled by Rh5,6>Brp::mCherry (red). Dα1-HA (a) or Dα6-HA (b) are labeled by anti-HA antibody (white). Right: High magnification images reveal that HA positive puncta are often found at the Pdf>CD8::GFP and Rh5,6>Brp::mCherry interface (blue arrowhead) and outside this synapse as well (pink arrowhead).

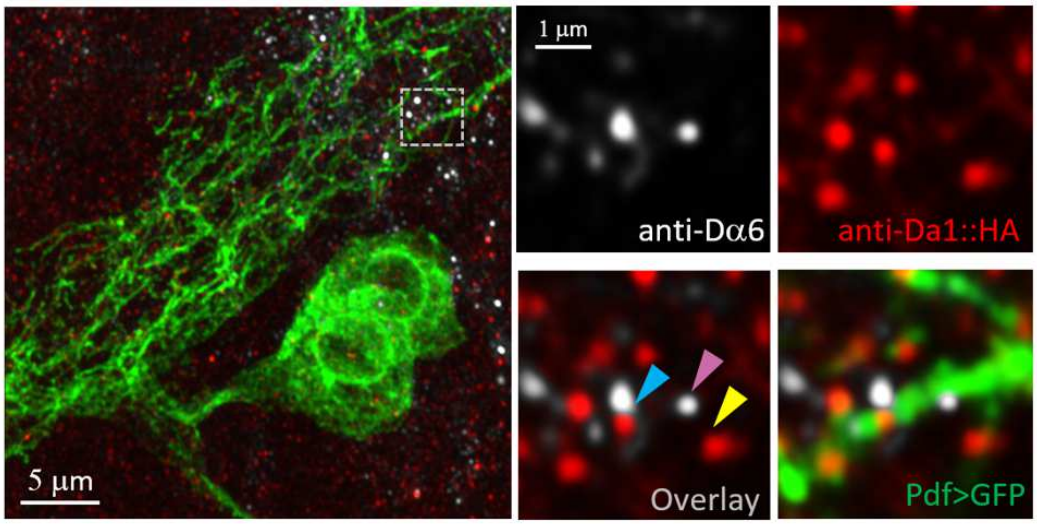

Figure 2.11. Super-resolution images demonstrate colocalization of Dα1 and Dα6. Left: Representative single optical sections of confocal images are shown. LNvs are labeled by mCD8::GFP (green). Co-labeling of Dα1-HA (red, anti-HA) and Dα6 (white, anti-Dα6) provides evidence for interactions between these two subunits within the same postsynaptic compartment (blue arrowhead). There are also examples of Dα1-HA and Dα6 appearing independently (yellow and pink arrowheads, respectively).

We also considered the possibility that both subunits may co-localize within the same synapse, which we tested by performing double immunostaining in the Dα1 knock-in line using both an anti-HA antibody and a validated anti-Dα6 antibody (179). In the late 3rd instar larval brain we found both subunits localized on the LNv dendritic arbor and in the general vicinity, presumably on non-LNv processes within the neuropil. Interestingly, although Dα1 and Dα6 signals rarely overlap, they frequently appeared to be either in close proximity or directly contacting each other (Figure 2.11). Although our immunohistochemical studies have intrinsic limitations, such as antibody efficacy and signal intensity and clarity, these results suggest that the two subunits could potentially localize and function within the same postsynaptic sites.

The HA staining signal from the tagged subunits is largely localized in the neuropil region, which contains both LNv and non-LNv neurite components that are difficult to distinguish. To resolve this issue, we relied on the GFP_{11} element in the knock-in construct to achieve tissue-specific endogenous labeling by GFP reconstitution. Although successful in the S2 cell culture system, GFP reconstitution failed in our *in vivo* experiments, when we co-expressed the GFP_{1-10} transgene in LNvs with either the *Dα1-HA* and *Dα6-HA* lines. It is possible that the reconstituted signal from the single GFP_{11} tag is too weak to be detected. Alternatively, the protein complex formed by the nAchR pentamer and its auxiliary subunits may not provide the space or a favorable nano-environment required for the reconstitution. Irrespective of the underlying cause, this inability to perform tissue-specific endogenous labeling prevented us from quantifying the level of Dα1 and Dα6 on LNv dendrites.

Therefore, to assess the developmental regulation of the two subunits we chose to examine the protein levels directly in the LNv soma. We collected knock-in animals at early vs. late developmental stages (again 48hr vs. 120hr AEL) and subjected the larval brains to anti-HA and anti-PDF staining, the latter being used to identify the LNvs and serve as an internal control to normalize the HA signal intensity (Figure 2.12). Upon 3D reconstruction of the LNv soma and quantification of both the HA and PDF intensities, we obtained the relative expression levels of Dα1 and Dα6. The results indicate that, during LNv maturation, Dα1 protein undergoes a significant upregulation, while Dα6 protein

displays a significant reduction, faithfully reflecting the different temporal dynamics in their transcript levels (Figures 2.2 and 2.3).

Together, the results we gained from studying the endogenously-tagged nAchR subunits demonstrated the temporal regulation of Dα1 and Dα6 at the protein level during larval development. In addition, observations made through super-resolution imaging support the localization of the two subunits within the postsynaptic compartment, where their relative abundance is modified *via* transcriptional regulation and could lead to changes in nAchR composition and receptor properties at the postsynaptic site.

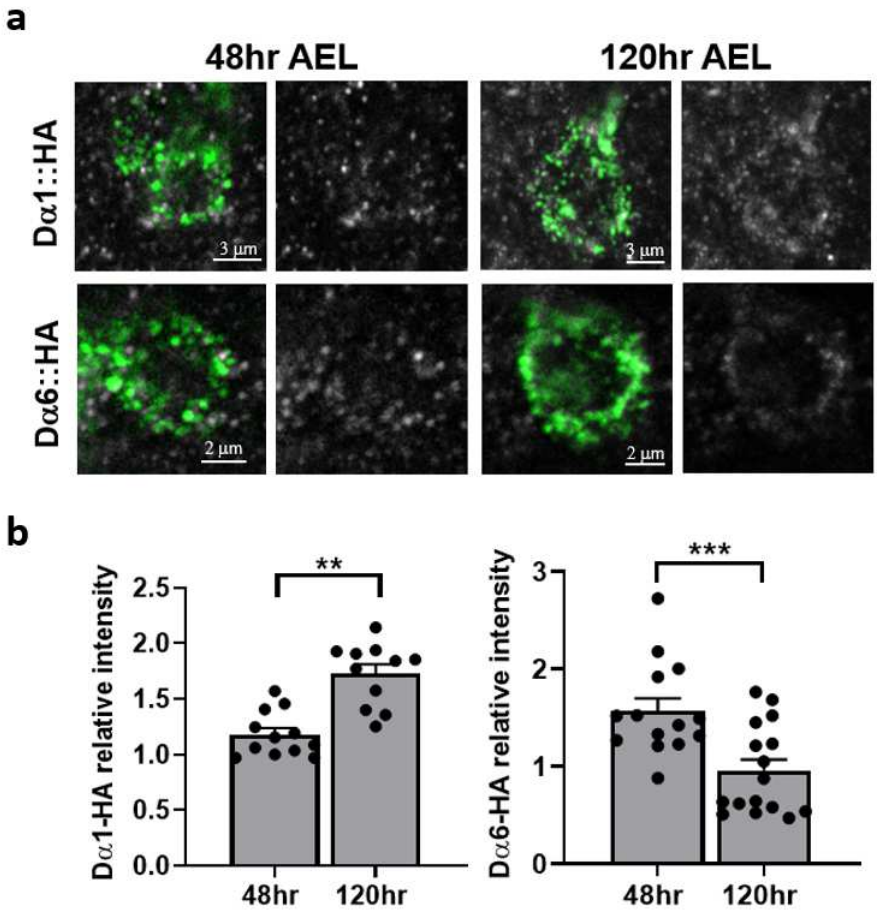

Figure 2.12. Temporal regulation of Dα1 and Dα6 protein in the LNv. (a) Dα1-HA and Dα6-HA labeled by anti-HA antibody (white) are visualized in LNv soma, labeled by anti-PDF antibody (green) at two developmental stages. (b) Quantification of HA intensity in LNv soma from (a) is shown. The protein levels of Dα1 and Dα6 change in opposite directions during development, similar to their transcript levels. Sample size n represents the number of larvae tested, n=11-16. Error bars represent mean ± SEM.

Dα6 contributes to both pre- and postsynaptic features of the LNv-BO synapse

Because *Dα6* has a specific role in supporting LNv dendrite arborization and the documented importance of synapse formation in LNv dendrite outgrowth (113), we went on to test whether *Dα6* mutants have deficits in synaptogenesis. To examine the putative synaptic contacts between the axonal projections of the Bolwig Nerve (BN) photoreceptors and the LNv dendrites, we imaged the LNv dendrites labeled by *mCD8::GFP* and the BN presynaptic terminals labeled by *Rh5,6>Brp::mCherry* (113, 180, 181). Following the 3D reconstruction of LNv dendrites and *Brp::mCherry* puncta, we calculated LNv dendrite volume and presynaptic terminal number as well as putative synapse number, which is assessed by quantifying the number of Brp::Cherry puncta in direct contact with the LNv dendrite (113). As before, $Dα6^{DAS1}$ mutants showed a significant reduction in dendrite volume (Figure 2.13). Additionally, *Dα6* deficiency had a strong impact on both the number of photoreceptor presynaptic terminals and the putative synaptic contacts between the BN and LNv. In both cases, the mutants showed a significant reduction as compared to the control group, suggesting that *Dα6* affects synaptogenesis between BN and LNvs.

As seen previously, *Dα6* overexpression solely in the LNvs was unable to rescue dendrite volume phenotype. We also observed a failure to rescue

presynaptic terminal number and synaptic contact number, which further signifies the importance of non-autonomous *Dα6* in organizing and developing this particular synapse.

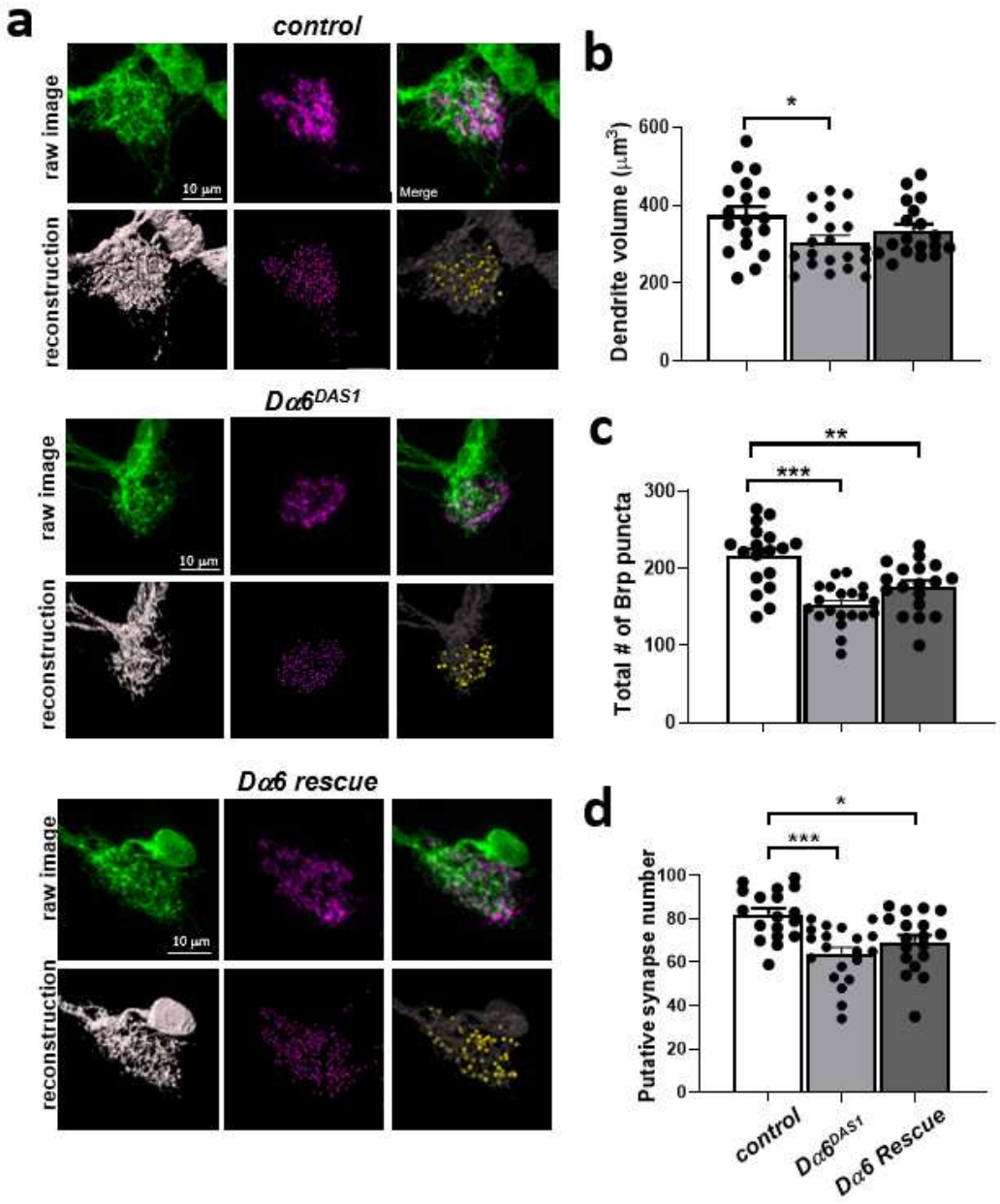

Figure 2.13. Dα6 deficiency affects synapse formation. (a) Representative projected confocal images of the LNv dendrites (green) co-labeled with Rh5,6-Brp::mCherry (magenta) are shown with 3D reconstructions of the dendrite (gray), the presynaptic terminals (purple spot) and the putative synaptic contacts (yellow spot). Dα6 deficiency significantly reduces LNv dendrite volume (b), BN presynaptic terminal number (c) and BN-LNv synaptic contacts (d), which cannot be rescued by cell-autonomous overexpression of Dα6 solely in the LNv. Sample size n represents the number of larvae tested, n=18-20. Error bars represent mean ± SEM.

Dα1 strengthens synaptic transmission during LNv maturation

The strong impact generated by *Dα1* deficiency on the LNvs' physiological properties is striking, given the lack of changes in dendrite morphology. This, combined with its transcriptional upregulation during development, led us to consider that *Dα1* mainly functions in the established, rather than nascent, synapses by enhancing synaptic transmission and contributing to synapse maturation.

To test this hypothesis, we first examined the light-evoked physiological responses in LNvs throughout larval development. At the earliest stage of testing, 48hr AEL, calcium responses in both *Dα1* and *Dα6* mutants resembled those of the wildtype (Figure 2.14a). Interestingly, *Dα6* structural deficits have also yet to appear by this stage, indicating that neither subunit may have a significant role in dendrite morphology or physiology prior to the 48hr AEL time point (Figure 2.14b). Defective transmission in each mutant becomes apparent during the ensuing larval stages, although at different paces. The calcium responses in normal, wild type controls show a clear increase between 48hr and 72hr AEL then remained relatively steady, matching the LNv maturation profiles we established previously (113) (Figure 2.15). In the *Dα6* mutant, this increase is not seen and instead there is a significant abatement in peak response amplitude by 72hr AEL. By 96hr AEL, these mutants already display the diminished response seen by 120hr AEL. In the *Dα1* mutant, however, the average calcium response gradually declines throughout time and the deficit does not fully manifest until the late-3rd instar larval stage

(120hr AEL). This supports the notion of an increasing functional requirement for *Dαl* during LNv maturation that continues through the end of larval development.

To further examine whether *Dαl* is required for strengthening cholinergic synapses during their maturation, we performed time-lapse live imaging of LNv dendrites to analyze the prevalence of dynamic dendritic filopodia. Our previous studies demonstrated that immature LNvs, between 48-72hr AEL, are characterized by highly dynamic dendritic filopodia that support synapse formation. The dendrite dynamics and the capacity for synaptogenesis decline by the mid-3rd instar stage, around 96hr AEL, marking the maturation of the LNvs.

Using a previously established protocol that allows us to track and quantify the movements of dendrite branch terminals in a single-labeled LNv, we analyzed dendrite dynamics at the wandering third instar stage (~120hr AEL), when a low prevalence of dynamic behaviors is observed in mature LNvs in the wildtype larvae. Dendrite dynamics were evaluated by two parameters, the percentage of branches exhibiting extension or retraction behaviors (% of dynamic branches) and the cumulative distance traveled by the branch terminals during the 10-minute imaging session (terminal displacement). Compared to the control group, both parameters were significantly increased when *Dαl* was knocked down (Figure 2.16). The unusually high motility of the dendrite branches seen here, which is normally associated with weaker, immature synapses, suggests *Dαl* deficiency is sufficient to compromise synaptic strength.

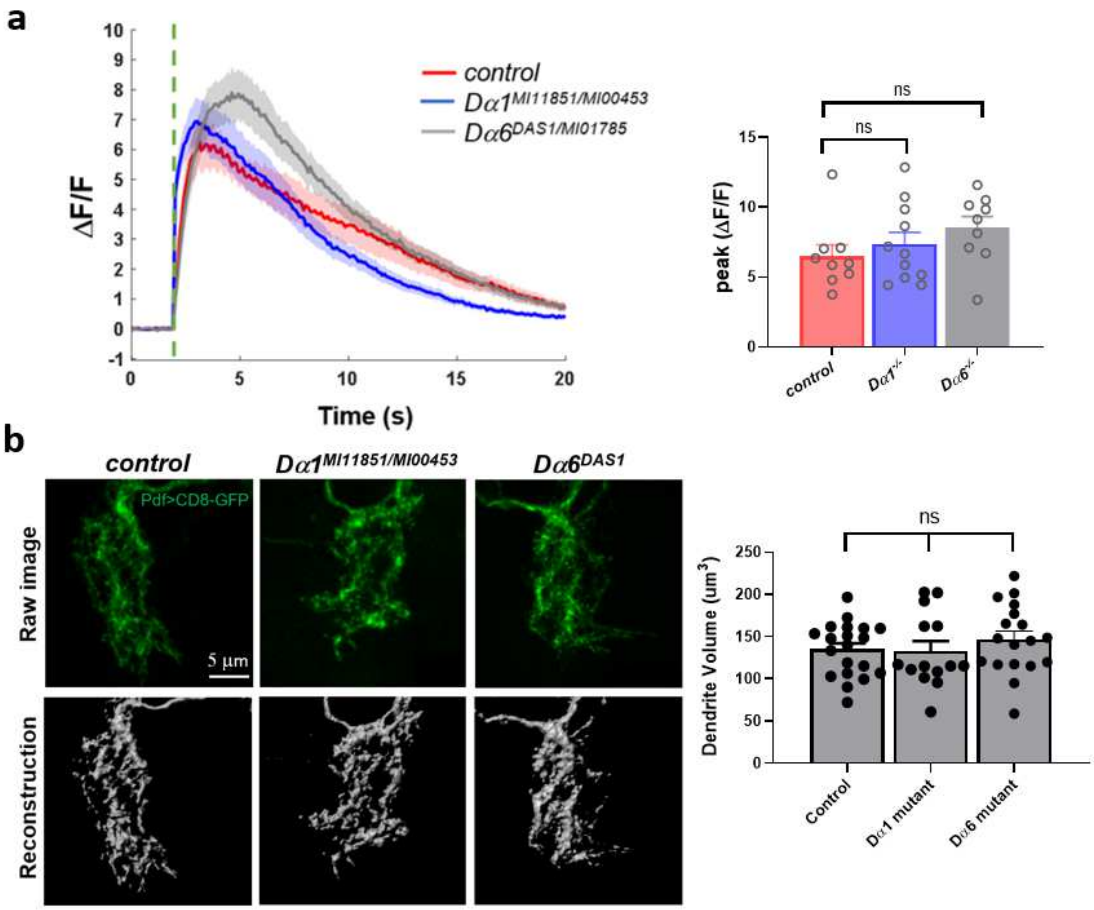

Figure 2.14. Dα1 or Dα6 deficiency has no impact on LNv morphology or physiology by the late 1st instar stage. (a) Light-induced calcium responses in LNvs taken at 48hr AEL. Left: Traces of average GCamp intensity change following photoreceptor stimulation (green line). The shaded area represents SEM. Right: Quantification of calcium trace peak amplitudes, showing no significant difference between the control and the Dα1 or Dα6 mutants. Sample size n represents the number of larvae tested, n=9-11 Error bars represent mean ± SEM. (b) Left: Representative projected confocal images of 48hr AEL LNv dendrites labeled by mCD8::GFP (top, green) and their 3D reconstructions (bottom, grey) are shown. Right: Quantification of dendrite volumes indicate no statistical difference between the Dα1 and Dα6 mutants as compared with the controls. Sample size n represents the number of larvae tested, n=14-20. Error bars represent mean ± SEM.

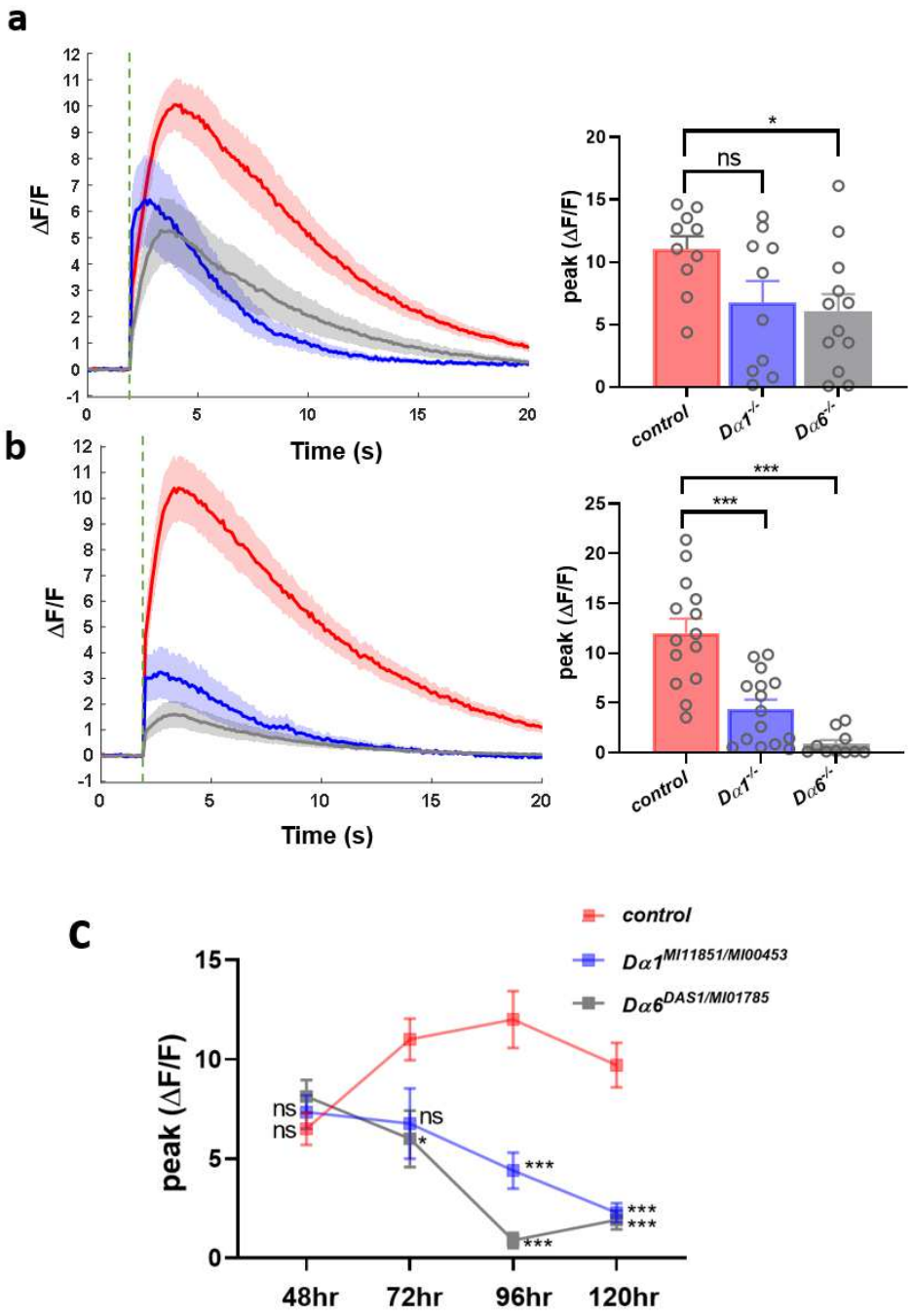

Figure 2.15 nAchR subunit deficiency leads to progressive declines in the light-evoked calcium responses during development. (a and b) Left: Calcium transients following light stimulation (green dashed line) were recorded in LNv axonal terminals at 72hr AEL (a) and 96hr AEL (b). The shaded region represents the SEM. Right: Average peak amplitude for each genotype at the two time points. At 72hr AEL, there is a significant amplitude reduction for the Dα6 mutant and by 96hr AEL both mutants have impaired neurotransmission. Sample size n represents the number of larvae tested, n=10-15. Error bars represent mean ± SEM. (c) Graph depicting the onset and the pace at which faulty synaptic transmission is observed in the LNv throughout larval development. In Dα6 mutant animals, the phenotype appears first and reaches peak deficit by 96hr AEL, whereas Dα1 mutant deficits begin at 96hr AEL and do not fully manifest until 120hr AEL. Error bars represent mean ± SEM.

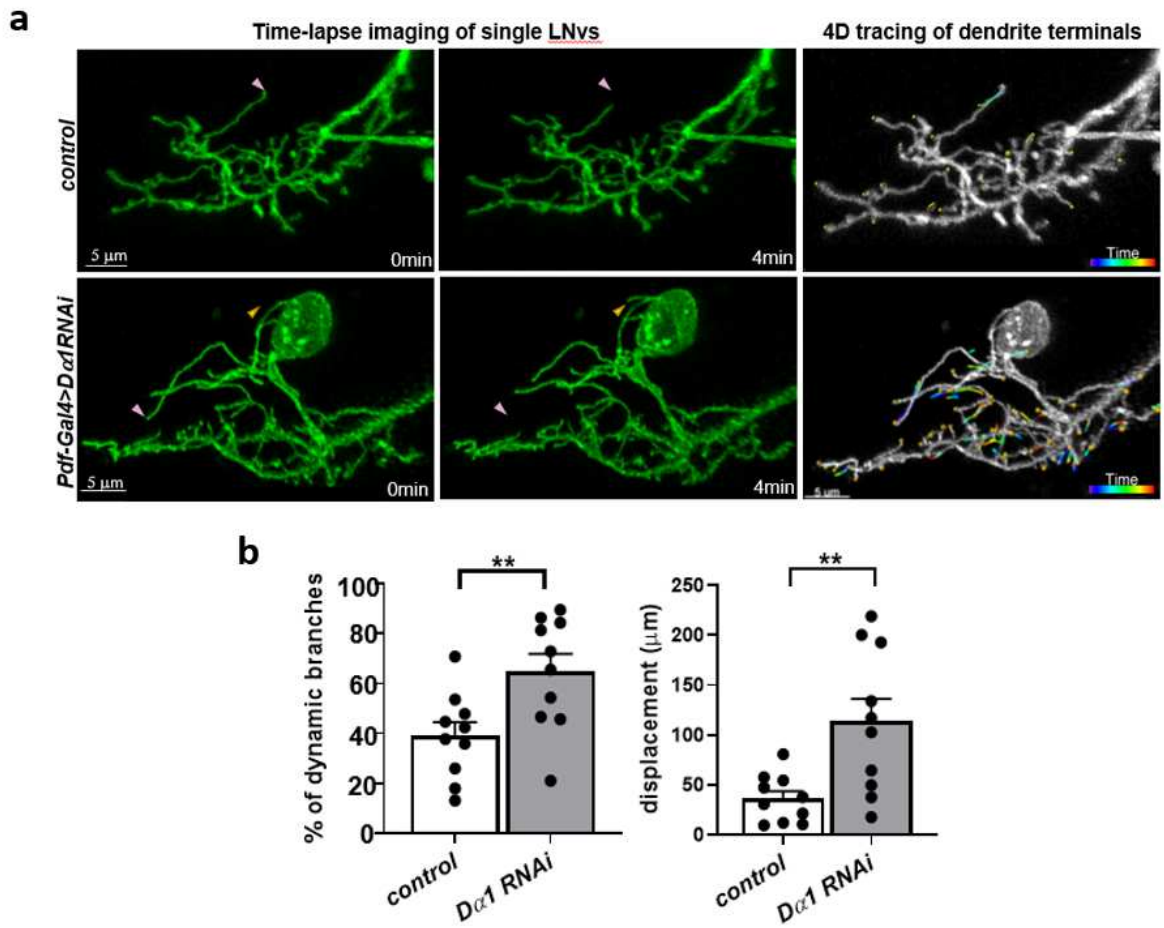

Figure 2.16. Knocking down Dα1 in LNvs leads to elevated dendrite dynamics. (a) Time-lapse imaging of LNv dendritic arbors at the wandering 3rd instar stage reveals dynamic behavior of individual branches in control (top) and Dα1 knockdown (bottom) groups. Representative maximum projected images of single-labeled LNvs are shown. Left: Two frames, collected at 0min and 4min in the imaging series, demonstrating representative extension (yellow arrowhead) and retraction (pink arrowhead) events. Right: 4D tracings of branch terminals depicting the path of dynamic filopodia over the 10 min recording session. (b) Quantification of dendrite dynamics. LNv-specific knockdown of Dα1 results in an increased percentage of dynamic branches (left) as well as increased total displacement of branches (right). Sample size n represents number of larvae. n=10 in both groups. Error bars represent mean ± SEM.

Discussion

The results obtained from Chapter 2 provide a coherent explanation for how *Dα1* and *Dα6* work in tandem to guide the morphological and physiological maturation of the LNv postsynapse. In the early larval stages, highly dynamic dendritic filopodia drive synapse formation. *Dα6* is expressed primarily during this period to facilitate

synaptogenesis, which is critical for the dendrite arbor's expansion that follows shortly. Once the synapse number reaches saturation in the early 3rd instar stage, *Dα1* becomes upregulated in an experience-dependent fashion and strengthens the established synapses by increasing neurotransmission. Although it is still unclear whether Dα1 and Dα6 co-assemble in the same nAchR pentameric channel, they appear to localize within the same postsynaptic compartment and likely contribute to the development and neurotransmission of central cholinergic synapses within the same functional complex. This topic, along with the prevalence of receptor subtype switching in synaptic maturation, is expounded below.

Composition of the native *Drosophila* nAchR

One of the biggest obstacles for our study was, and still is, the lack of knowledge on the native nAchR pentameric composition, both at the BN-LNv synapse and throughout the fly CNS at large. In the vertebrate system, the physiological and molecular properties of individual nAchR subunits, as well as the receptor subtypes they compose, have been characterized sufficiently to allow a detailed description of the conductance and kinetics of each receptor (182). Moreover, the tissue distribution and subcellular localization of mammalian nAchR subunits has been well studied in both the CNS and NMJ (89, 120, 121, 183). For example, the dopaminergic neurons of the Ventral Tegmental Area (VTA) express presynaptic α6α4β2β3 receptors, whereas α3β4 and α7 receptors are restricted to the cell body. In contrast, the same type of information is not yet available for insect nAchR receptors. To my knowledge, there is no existing model or description of a native *Drosophila* pentamer receptor in fly neurons. This is partly

due to the lack of information on the tissue and cellular distribution of the ten fly subunits, as well as the general technical difficulties of reconstituting *Drosophila* nAchR receptors *in vitro*.

There is experimental evidence hinting at a few configurations for receptor co-assembly, including *in vivo* co-immunoprecipitation studies suggesting that *Dα1*, *Dα2* and *Dβ2* could form heteropentamers, as well as *in vitro* reconstitution experiments using $5HT_{3A}$-nAchR chimeras, demonstrating that *Dα6* could either form homopentamers or co-assemble with *Dα7* (83, 88, 98). However, these results only suggest the minimal composition of a nAchR receptor and are far from an accurate representation of a functional channel in its native environment.

In chapter 1, we concluded from the double-knockdown calcium imaging experiment that Dα1 and Dα6 were either part of the same pentamer or were in separate pentamers but localize within the same synapse. Either scenario could explain why individual deficiencies don't synergize when in combination. Here, the Dα1/Dα6 colocalization experiment supports the latter. Dα1 and Dα6 puncta usually do not overlap but they frequently contact each other, supporting the idea that they are trafficked in different pentamers to shared postsynaptic compartments.

Temporal regulation of neurotransmitter receptor composition as a common feature for synapse maturation

The distinct functional roles and temporal regulation of the two nAchR subunits resemble developmental switches described for both glutamate and glycine receptors in the developing vertebrate CNS (5, 7). In the vertebrate system,

the maturation of excitatory glutamatergic synapses is regulated by the shifting ratio of AMPA/NMDA receptors (6). Electrophysiological recordings from *Xenopus* tectal neurons indicate that neurotransmission in immature neurons is predominantly mediated by NMDA receptors. As neurons mature, CaMKII-dependent trafficking of AMPA receptors leads to an increased AMPA/NMDA receptor ratio, which enhances neurotransmission and synapse strength, thereby contributing to the physiological maturation of the synapse (4-6). Additionally, the molecular mechanism responsible for LTP is also known to involve a change in glutamate receptor type and is mediated through Ca^{2+}- and NMDA receptor-dependent recruitment of AMPA receptors (2, 66, 67).

Our research provided supportive evidence for an analogous phenomenon occurring in the *Drosophila* CNS. We found several important features shared between central glutamatergic and cholinergic synapses: 1. There are changes in the relative abundance of two key receptor subunits during development, which could generate a shift in the receptor composition and potentially alter its physiological properties. 2. The two subunits have distinct roles in early vs. late developmental stages, and the upregulation of the late-expressing subunit, namely AMPA receptor or Dα1, specifically enhances neurotransmission. 3. These late-expressing subunits are targets of activity-dependent regulation, offering a tuning mechanism to adjust synapse strength based on input activity. One can also compare our findings to the molecular transition in receptor composition during vertebrate cholinergic NMJ development. Specifically, the embryonic form of nAchR containing a gamma subunit (α2βγδ) is replaced by adult-type nAchRs

containing an epsilon subunit (α2βεδ) *via* transcriptional regulation (68). However, the γ→ε subunit switch is essentially a replacement of the original subunit by the second. In our case, because Dα6 is still present at the LNv-BO synapse at the end of larval development, the transition in our model better resembles the NMDA→AMPA receptor change which does not outright remove the original NMDA receptor.

Distinct biophysical characteristics of *Dα1* and *Dα6* may explain their implementation at different phases of synaptic development

Because the morphological and physiological data clearly support disparate functions for *Dα1* and *Dα6*, an important question that arises is if there are advantages of expressing one subunit at a particular time over an alternative subunit. If true, this selective process would almost certainly be based, in part, on molecular differences between Dα1 and Dα6 protein that affect receptor charge and size. In the vertebrate nAchR, there are multiple amino acids and motifs at key sites that have demonstrable effects on ligand-binding affinity and ion selectivity and therefore it will be important in the future to pinpoint any major differences in secondary structure between Dα1 and Dα6. Although there is no *Drosophila* nAchR crystal structure, homology modeling using the X-ray crystal structure of human α4 (CHRNA4) was instead employed and was made possible due to high sequence conservation between human and flies (184). Many regions, including the Cys-loop and the TM domain a-helices, are both very similar to CHRNA4 (Figure 2.17). However, inspection of the C loop that contains the ligand-binding pocket revealed a major difference in the loop configuration. In

Dα6, like in CHRNA4, the loop is bent towards the ligand (nicotine, red) and encapsulates it. However, the C loop in Dα1 is predicted to be in the extended position, indicating an altered affinity for nicotine. If this reflects an actual biological difference, this may endow Dα6 with a higher affinity for endogenous ligand (i.e. Ach) and consequently result in ion channel influx at lower concentrations due to increased sensitivity. This is especially important during the early "Da6 receptor period" where the LNv has a heightened degree of plasticity.

In addition to ligand affinity, cation conductance may also explain preferential subunit use at different times during development. In humans, *Chrna7* is known for its relatively high permeability to calcium ions. Therefore, it could be beneficial to express the *Chrna7* homolog *Dα6* during the early stages of LNv development since the highly plastic nature of young, immature synapses is likely enhanced by calcium-dependent signaling pathways activated by nAchR-mediated calcium influx. In fact, neuronal plasticity in MB KCs of *Drosophila* pupae has already been linked to calcium-permeable nAchRs (Campusano 2007). Future studies relying on relevant *in vitro* expression systems and actual *Drosophila* nAchR crystal structures will help immensely with these hypotheses on subunit structure and ion permeability.

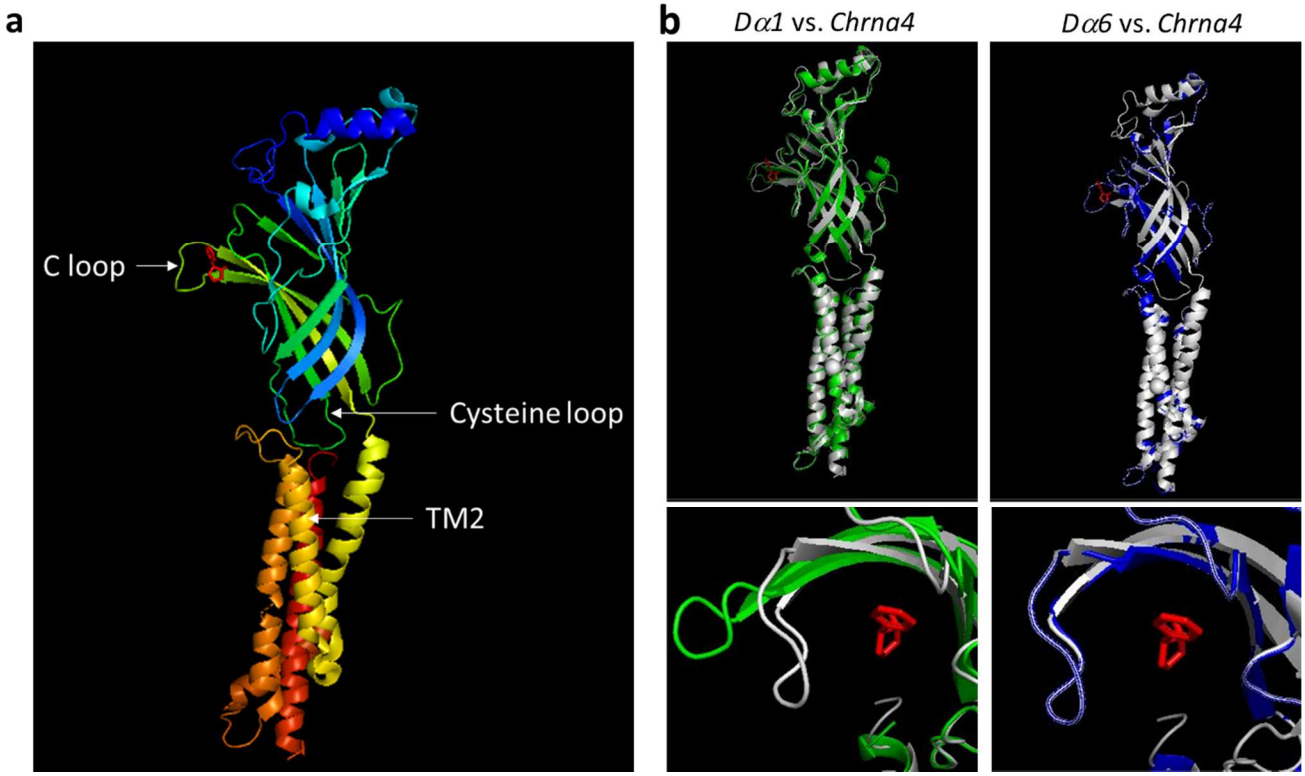

Figure 2.17. Molecular modeling predicts subunit differences in ligand-binding affinity. (a) 3D structure of Chrna4, based on α4β2 X-ray crystallography experiments. Residue position is color coded (N-terminal: blue, C-terminal: red). Select features shown are the C-loop, Cys-loop and the TM2 domain. Nicotine is the ligand (red). (b) Top: Homology modeling using Chrna4 (gray) as a template predicts the structure of Dα1 (green) and Dα6 (blue), whose secondary structures are generally similar. Bottom: Zoom-in image at the ligand-binding pocket reveals alternate configurations of the C-loop between Dα1 and Dα6.

Chapter 3: LNv dendrite development is coordinated by evolutionarily conserved transcriptional and post-translational factors

Abstract

Although neurotransmitter receptors may serve the end goal of the postsynaptic specialization, by receiving and transducing neural input, they are by no means acting in isolation during synapse development. The postsynaptic density of the cholinergic vertebrate NMJ contains a conglomerate of proteins, both cytoplasmic, transmembrane, and extracellular, that are either physically or indirectly associated with the nAchR. Postsynaptic development of the NMJ also operates under tight transcriptional controls, such as the activity-regulated production of subsynaptic nAchR subunit RNA and the temporal substitution of individual nAchR subunits. A similar situation occurs in the vertebrate brain. Hundreds of different membrane, scaffolding and cell-signaling proteins form the network necessary for glutamate receptor function. Additionally, potentiation of AMPA receptor expression is a central theme in postsynaptic maturation and long-term potentiation. Here, we further interrogate LNv development by identifying which components of this presumably expansive network are also active in our model cell. By using a combination of bioinformatic, morphological and reporter protocols, we have implicated the transcription factors Fru and Hr38, the nAchR-specific chaperone Nacho and the postsynaptic proteins Lrp4 and Hig as potential factors facilitating postsynaptic development in a central cholinergic synapse. Although additional experiments are necessary to build a complete mechanism, the work completed in this final chapter highlights how the molecular players orchestrating synapse and dendrite development share similarities not only between distantly related species but also between different synapse types in the developing animal.

Introduction

Developmental and transcriptional modulation of nAchR expression

Even during the early era of characterizing *Drosophila* nAchRs, it had become clear that the subunits and the receptors they form do not remain steady over the animal's lifespan but display stark periods of up- and down-regulation. Generally, nAchR subunits' expression is potentiated during embryogenesis, although the stage of initial detection varies by subunits (80-83, 105, 106, 140, 145, 185). For example, the major transcript of *Dα2* is already observed in 2hr old embryos whereas *Dβ1* is not detected until later embryonic stages (82). RNA transcripts probed by *in situ* hybridization show strong labeling in the SPG, SEZ and the VNC but never outside the CNS, and the end of embryogenesis usually represents the time of peak expression (79, 141). By the first instar larval stage, the transcript level tends to be greatly reduced and remains low through the duration of the larval stage. Expression typically rises again during the pupal and adult stages, but there are again noticeable differences between subunits (79, 81, 105, 106, 140). For instance, while both *Dβ1* and *Dβ2* mRNA rise sharply during pupation, *Dβ1* persists to a similar degree following eclosion whereas *Dβ2* levels drop off again in early adult heads. Antibody labeling and enhancer reporter experiments produce similar spatial and temporal patterns, with the exception that nAchR protein is concentrated in the neuropil region, rather than the cortical cell body layer where the mRNA signal is detected (141, 142, 145).

These investigations have also revealed other interesting aspects of nAchR subunit temporal regulation, such as isoform-specific expression profiles for *Dα1*

during the embryonic vs adult period (82). Moreover, for the *Dβ1* subunit, incompletely spliced transcripts were detected, and these transcripts have unique temporal expression profiles compared to the fully spliced mRNA isoforms (140). Taken together, although temporal profiles of individual subunits may vary, the general pattern of elevated nAchR mRNA and protein expression in embryos and pupae are notably in congruence with major periods of neuronal differentiation, likely enabling the increased production and delivery of the nAchR subunits that contribute to cholinergic synapse development (140).

Although the temporal regulation of nAchR subunit expression has been demonstrated for multiple subunits, the upstream transcription factors regulating expression remain unclear. Nonetheless, certain regulators have been uncovered through various screens and phenotypic analyses, including Ttk88 and Eve which specify cell fate. The *Ttk88* consensus binding site AGGG$^{C}/_{T}$GG was identified in the *Dβ2* gene, as well as several other neural-specific genes like *para* and *synapsin* (186). This observation, together with S2 cell RNAi transfection experiments, indicate that Ttk88 inhibits neuronal differentiation in non-neural lineages, in part by repressing *Dβ2* transcription. A similar phenomenon was found in aCC/RP2 motoneurons, which receive cholinergic input through nAchRs. Here, overexpression of *Eve* diminishes the strength of mEPSCs and action-potential dependent currents (187). Moreover, a transcriptomic analysis revealed an *in vivo* interaction between the *Dα1* promoter and Eve and an additional overexpression experiment showed that ectopic *Eve* is sufficient to reduce whole animal *Dα1* RNA by almost three-fold. Thus, both *Eve* and *TTk88*

function in establishing non-neuronal properties by repressing the expression of nAchR subunits.

The conditions and pathways controlling nAchR expression appear to be rather complex and diverse. For example, *Dβ1* expression is elevated in animals expressing proliferative, tumor-promoting alleles of *mali* and *efe*, but reduced in IP_3 receptor mutants (188, 189). Exposure to *Piger nigrum* extract, manipulation of JAK/STAT signaling and overexpression of TBPH (the *Drosophila* ortholog of the pathologically relevant TDP-43) also modify the expression level of *Dβ1*, although the mechanisms responsible for the changes are still uncertain (190-192). Different subunits also respond to the same stimulation with opposing changes. In the pupal MBs, ecdysone signaling activates *Dα2* transcription during early metamorphosis, whereas *Dβ1* expression is downregulated by ecdysone activity (193).

Post-translational regulation of nAchR assembly and activity by accessory proteins

There are complex processes occurring between the initial steps of nAchR subunit translation and the assembly of a fully operational pentameric channel at the synaptic site. Post-translational regulation of nAchRs involves numerous steps including protein folding and modification, receptor assembly and trafficking, as well as synaptic integration. Although it appears that at least several of the proteins regulating nAchR synthesis and processing are conserved between flies, worms and vertebrates, much remains to be discovered (92).

One of the early points of post-translational regulation occurs within the Golgi and ER complex, where critical molecular chaperones, such as *Ric-3*, are needed for nAchR subunit assembly. *Ric-3* was initially identified by genetic screens in C. elegans and found to have a conserved function in mammals as well as Drosophila (194-196). In cell culture, *Dα2* and Rat β2 transfection only produces epibatidine binding sites when co-transfected with *dRic-3* and the degree of binding varies significantly between the alternatively spliced isoforms of *dRic-3 (194)*. *Dα5-Dα6* heteromers have also been produced in follow-up studies, facilitated by either *dRic-3* or *C. elegans Ric-3* (197). Importantly, these nAchRs have α-Btx binding sites, which are only formed by fully folded, mature receptors. Furthermore, they are functional at the plasma membrane, demonstrated by the production of strong Ach-gated inward currents (194, 198). Interestingly, human *Ric-3* also facilitates the assembly of epibatidine-sensitive receptors from *Drosophila* nAchR subunits but at a much lower efficiency. Finally, coprecipitation experiments revealed that d*Ric-3* physically interacts with other α and β subunits and even the human α7 subunit, supporting the direct chaperone activity of *dRic-3* on multiple subunits (194).

After receptor assembly and trafficking, nAchRs rely on extracellular matrix (ECM) proteins to ensure a stable integration to the synaptic sites. Genetic and biochemical experiments have shown that Hasp and Hig are two such factors that sequentially regulate nAchR clustering at the postsynaptic compartment (136, 179). In the early stages of synaptogenesis, the CCP domain-containing protein Hasp is secreted in the brain and captured at cholinergic synapses. Later, the

intermediate nAchR recruiter Hig, which is also secreted from multiple neuron types as well as glia, is captured by Hasp. The MB calyx of either Hig- or Hasp-deficient animals have reduced levels of *Dα6* and *Dα7*. However, nAchR subunit deficiency can reciprocally result in reduced synaptic accumulation of Hig, whereas Hasp is unaffected due to its earlier presence at the synapse (136).

Even after the nAchR has been stably inserted into the membrane, its activity can still be altered. For instance, to dampen nAchR-mediated excitatory neurotransmission during the bouts of sleep, the GPI-anchored protein *quiver/sleepless (qvr)* is needed for the physiological downregulation of Dα3 activity (199, 200). Errant regulation of nAchR activity occurring in *qvr* mutants manifests as significant reductions in sleep, which can be rescued by application of the nAchR antagonist mecamylamine or knockdown of either *Dβ3* or *Dα3*, the latter of which also coprecipitates with Qvr *in vitro*. These results, together with the finding that *Dα3* and *Dβ3* RNA levels are unaltered *qvr* mutants, support the idea of *qvr* functioning as an activity modulator of fully assembled nAchRs.

Finally, although phosphorylation of *Drosophila* nAchRs regulated by kinases and phosphatases has not been studied in detail, multiple subunits contain predicted phosphorylation sites within their large TM3-TM4 loops, which has been linked to receptor desensitization, and nAchRs in the vertebrate system including *α4* and *α7* are known targets of PKA and PKC (201).

Methods

The following Chapter 3 protocols were previously described in Chapter 1 or 2:

Fly culturing, Confocal imaging and quantification of dendrite volume, Cell body protein quantification and Statistical analysis.

***Drosophila* stocks**

RNAi knockdown was performed with stocks targeting *hr38*, *Lrp4* and *hig* (Bloomington ID: 29376, 31105 and 28376). The *hig::GFP* overexpression stock was a gift from Chihiro Hama (Kyoto Sangyo University). The *Nacho::HA* overexpression stock was acquired from FlyORF (ID: F002996). The *fru-Gal4*$^{P1.D}$ and *Nacho-GFP* stocks were obtained from the BDSC (ID: 66696 51565). All other stocks can be found in Chapter 1 or Chapter 2 methods.

Immunohistochemistry

Photoreceptor/24B10 staining was done using mouse anti-chaoptin primary antibody (1:10 DSHB, Iowa City, Iowa). All other reagents and procedures can be found in Chapter 1 or 2 methods.

Bioinformatics analysis of the *Dα1* and *Dα6* transcriptional regulatory regions

The promoter region sequence of *Dα1* (-1841 to + 2159, relative to the transcription start site (TSS)) was pasted into the *EvoPrinter* server (NINDS/National Institutes of Health) using *D. melanogaster* as the reference genome for BLAT (BLAST-like alignment tool) alignment against 11 other *D. species*. It's *EvoPrint* profile was generated by selecting for the Relaxed output option. The promoter region

sequence of *Dα6* (-2072 to +7522, relative to the TSS) was analyzed in an identical way.

Motif comparison

Oligonucleotide sequences were entered into the TomTom Motif Comparison Tool, a part of MemeSuite (National Institutes of Health) and analyzed using the combined *Drosophila Melanogaster* databases. All resulting motifs were included in the total transcription factor binding site count.

Results

Promoter analysis of the *Dα1* and *Dα6* transcriptional regulatory regions

Chapter 2 revealed the strong, subunit-specific transcriptional controls by which each nAchR is regulated. Additionally, the introduction of Chapter 3 detailed multiple signaling pathways acting upstream of nAchR expression and some of the transcription factors acting here also have subunit-specific preferences. Therefore, our initial objective was to uncover which factors might be active in our model system.

We approached this by using several bioinformatics tools to probe putative *cis*-regulatory regions of both *Dα1* and *Dα6*. First, a region spanning several kilobases upstream and downstream of each subunit gene's TSS was selected and was analyzed using BLAT from *EvoPrinter* (Figures 3.1 and 3.2). Sequence comparisons against the analogous region from *Dα1* and *Dα6* orthologs in other *Drosophila* species identified which regions are highly conserved, and therefore likely represent the critical regulatory motifs conserved through evolution

(Appendices C and D). Following this, all major sequence stretches (generally between 10 and 30 bases) in which the majority of nucleotides are consecutive, conserved bases were queried against known transcription factor binding site motifs using the TomTom Motif comparison tool. This generated an output for both *Dα1* and *Dα6* containing consensus sites for dozens of transcription factors (Appendices E and F). As the final filtering step, this set of transcription factors was narrowed down by a comparison with those either enriched in the LNv or are differentially expressed between LD vs. LL conditions in the LNv, accomplished using values from our previous LNv-specific RNAseq dataset (Table 3.1).

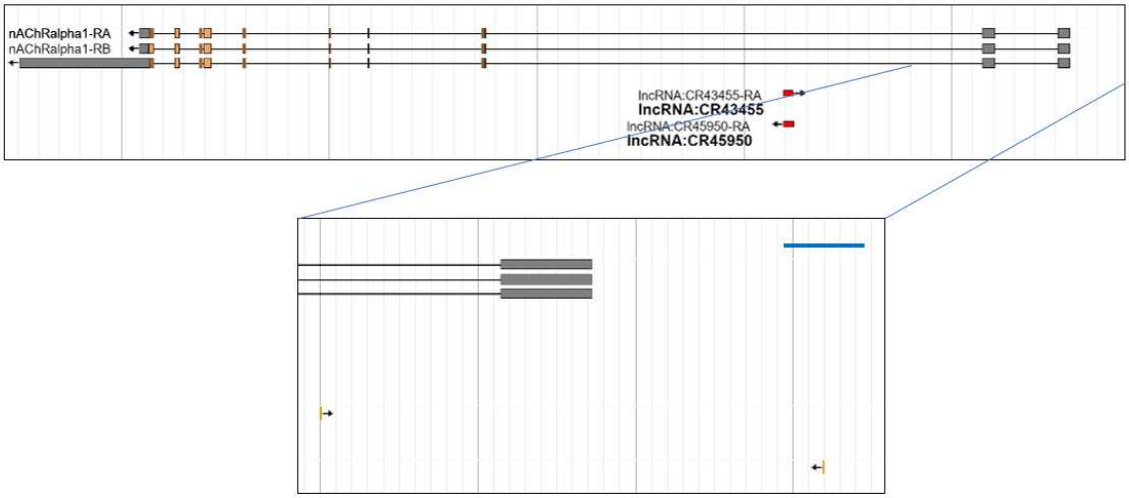

Figure 3.1. Region of Dα1 selected for promoter analysis. Top: Genomic map of the Dα1 locus. Bottom: Magnified image shows the span of promoter sequence which was analyzed by BLAT analysis (arrows). Blue scale bar represents ~1.24kb.

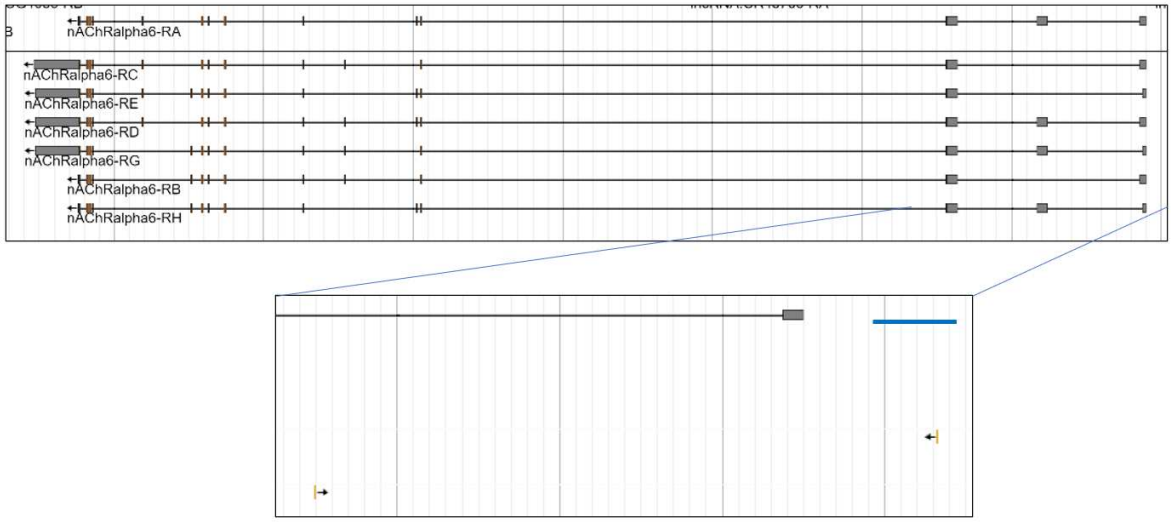

Figure 3.2. Region of Dα6 selected for promoter analysis. Top: Genomic map of the Dα6 locus. Bottom: Magnified image shows the span of promoter sequence which was analyzed by BLAT analysis (arrows). Blue scale bar represents ~1.24kb.

TF name	LNv status	Whole brain status	Increase in LL condition	Decrease in LL condition
Glut4EF	Enriched, >10x	Present	No	Yes (3.5x)
Nfl	Enriched, <10x	Present	No	Yes (2x)
Nk7.1	Enriched, <10x	Present	No	Yes (2x)
Pdp1	Enriched, >10x	Present	Yes (5x)	No
CrebA	Enriched, >10x	Present	No	Yes (3x)
CrebB	Enriched, <10x	Present	No	Yes (2.5x)
Atf3	Enriched, <10x	Present	No	Yes (4x)
Blimp-1	Not enriched	Very low	Yes (20x)	No
CG6686	Not enriched	Present	Yes (3x)	No
Dp	Not enriched	Very low	Yes (3x)	No
EcR	Not enriched	Present	Yes (3x)	No
Efa6	Not enriched	Present	No	Yes (3x)
Eip93F	Not enriched	Present	Yes (2.5x)	No
fru	Not enriched	Present	Yes (8.5x)	No
HmgZ	Not enriched	Present	Yes (2.5x)	No
Hr4	Not enriched	Present	No	Yes (5x)
l(3)neo38	Not enriched	Present	Yes(3x)	No
mamo	Not enriched	Present	Yes (4.5x)	No
psq	Not enriched	Present	Yes (2.5x)	No
schlank	Not enriched	Present	Yes (7x)	No
tou	Not enriched	Present	Yes (2.5x)	No
vri	Not enriched	Present	Yes (9x)	No
XNP	Not enriched	Present	Yes (2.5x)	No
per	Not enriched	Very low	Yes (3.5x)	No
Hr38	Enriched, >10x	Very low	No	Yes (17x)
Clk	Enriched, >10x	Very low	No	Yes (3x)
Fer2	Enriched, >10x	Very low	No	Yes (3x)
sr	Enriched, >10x	Very low	No	Yes (2x)
tim	Enriched, >10x	Very low	Yes (17x)	No

Table 3.1. Enriched or activity-dependent transcription factors in the LNv. Candidate transcription factors isolated from the LNv-specific RNAseq dataset. They are described as enriched if their LNv/elav$^+$ expression ratio > 10. Also shown is their response, if any, to constant light.

The final selection only included two genes: *fruitless (fru)* and *nk7.1*. We chose to focus on the former because its consensus site motif was detected in both the *Dα1* and *Dα6* promoter and its expression is dramatically elevated in the LL condition (Figure 3.3b and Appendices E and F). *fru* is perhaps best known as the end product in the alternative splicing cascade regulating sex-specific behaviors and brain circuits in *Drosophila* adults (202, 203). We were able to show, using the *fru-Gal4*$^{P1.D}$ gene trap driver which reports the sex-specific isoform, that the LNv is one of the few cells in the larval brain expressing this isoform (Figure 3.3a). However, it appears to have little influence in sculpting dendrite architecture of the LNv. Firstly, LNv dendrite volume does not differ between males and females. Secondly, a preliminary trial failed to show a sexually dimorphic LNv dendrite volume in *fru-Gal4*$^{P1.D}$ homozygous mutants that lack this isoform (Figure 3.4). Although the investigation of *fru* function in the LNv is in a preliminary stage, the fact that *fru* is in fact a strongly differentially expressed (DE) gene and candidate for further study provides some validation for using the BLAT-Motif Comparison method.

Site #	Gene	Genomic sequence used for comparison
1	Dα1	GGCTAATAATTTACATATAGGGCGTGGATTTTTCTCCGGC
2	Dα6	ATTTTTTCAGGTATAGTATAGAGACATTGACCAGC
3	Dα6	GTGTTGAGTGGCAAGTTGTGTACACACGCAGATTTTTCATCAATCATTT
4	Dα6	TTTTCTATTTTTCTCCTTACGCACTTTTTATTGCTCGTCCT
5	Dα6	TTGCCTTTTTTTTCG

Table 3.2. fru consensus sites in the Dα1 and Dα6 cis-regulatory regions. (a) Table showing the one and four fru-binding site motifs identified for Dα1 and Dα6, respectively.

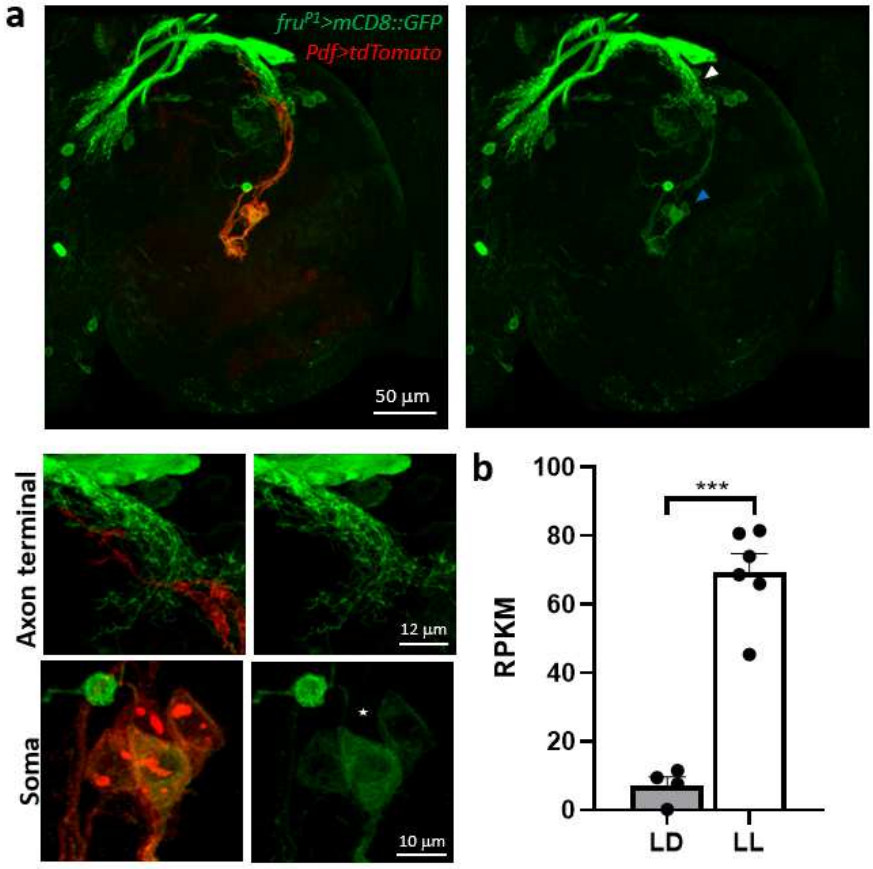

Figure 3.3. Expression of fru in the larval LNv. Shown are representative projected confocal images (a) Top: An endogenous Gal4 knock-in driving mCD8::GFP (green) supports expression of the sex-specific isoform in the LNv labeled by tdTomato (red). Axon (white arrowhead) and cell bodies (blue arrowhead) are marked. Bottom: higher magnification images of top. Note the close proximity of the LNv axon and the fru^{+} neuropil directly above. (b) Constant light strongly potentiates fru transcription in the LNv. RPKM: Reads per kilobase per million. Error bars represent mean ± SEM.

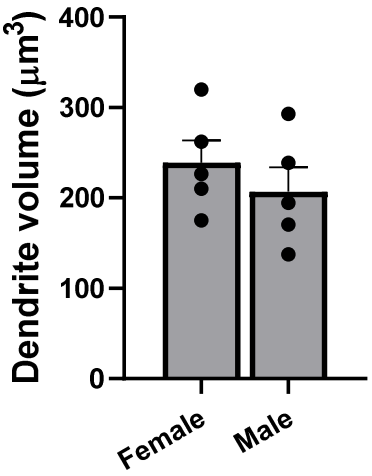

Figure 3.4 Mutation affecting the fru P1-containing isoform does not cause sex-specific differences in LNv dendrite volume. A small-scale trial indicates that male and female fru-Gal4$^{P1.D}$ homozygotes do not significantly differ in dendrite volume. Error bars represent mean ± SEM.

hr38 is a candidate activity-regulated transcription factor controlling *Dα1* expression in the LNv

In conjunction with the broad bioinformatics-guided approach, we also developed a simple system to measure *Dα1* expression, which is inversely correlated to light activity. By recombining the endogenous *Dα1-Trojan Gal4* driver with the *UAS-RedStinger* transgene we were able to create a reporter system that is sensitive enough to recapitulate the LL-induced reduction in *Dα1* transcriptional activity (Figure 3.5). Using this method, we were able to quickly screen through several transcription factors and isolated *hr38*. Hr38 functions as an immediate-early gene, or activity regulated gene, in both *Drosophila* and the silkworm *Bombyx* and undergoes a dramatic change in transcription following neuronal stimulation, thus acting in a fashion similar to mammalian C-Fos (204-

206). Using the *Dα1-Trojan Gal4* to drive *hr38* RNAi, the knockdown resulted in a significant reduction in nuclear *RedStinger* levels within the LNv soma (Figure 3.6a, b). Additionally, the *Dα1* 5' UTR contains a perfect consensus site match for the NR4A receptors (*NR4A1-NR4A3)*, the mammalian homologs of *hr38* (Figure 3.6c)(207). *hr38* also happens to appear high in the list of DE transcription factors, is enriched in the LNvs and is directly and strongly correlated with *Dα1* expression (Figure 3.6d). This warrants using the enriched or DE transcription factor (TF) list for further selection of candidate TFs.

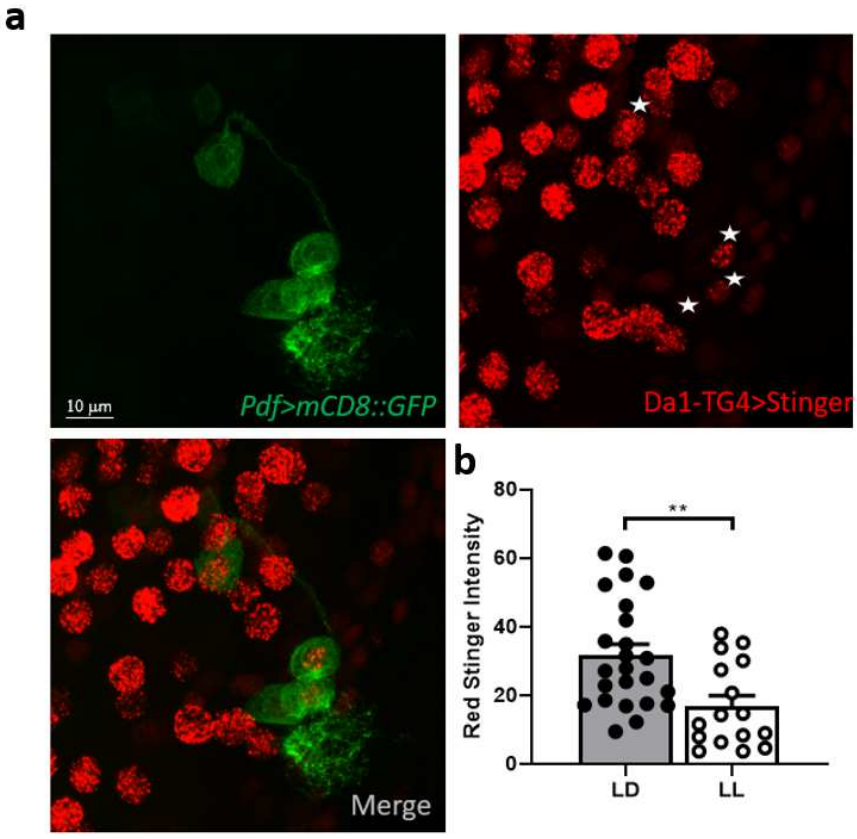

Figure 3.5. Dα1-Trojan Gal4 driven RedStinger is a reliable method of measuring Dα1 expression in the LNv. (a) A Gal4 from the endogenous Dα1 locus drives expression of Nuclear RedStinger (red) in all Dα1-expressing cells, which includes the LNvs labeled by mCD8::GFP (green). Note the RedStinger variation between the four LNvs of the same cluster (white star). (b) The Dα1>Stinger reporter system reproduces the significant reduction of Dα1 expression in LNvs induced by constant light.

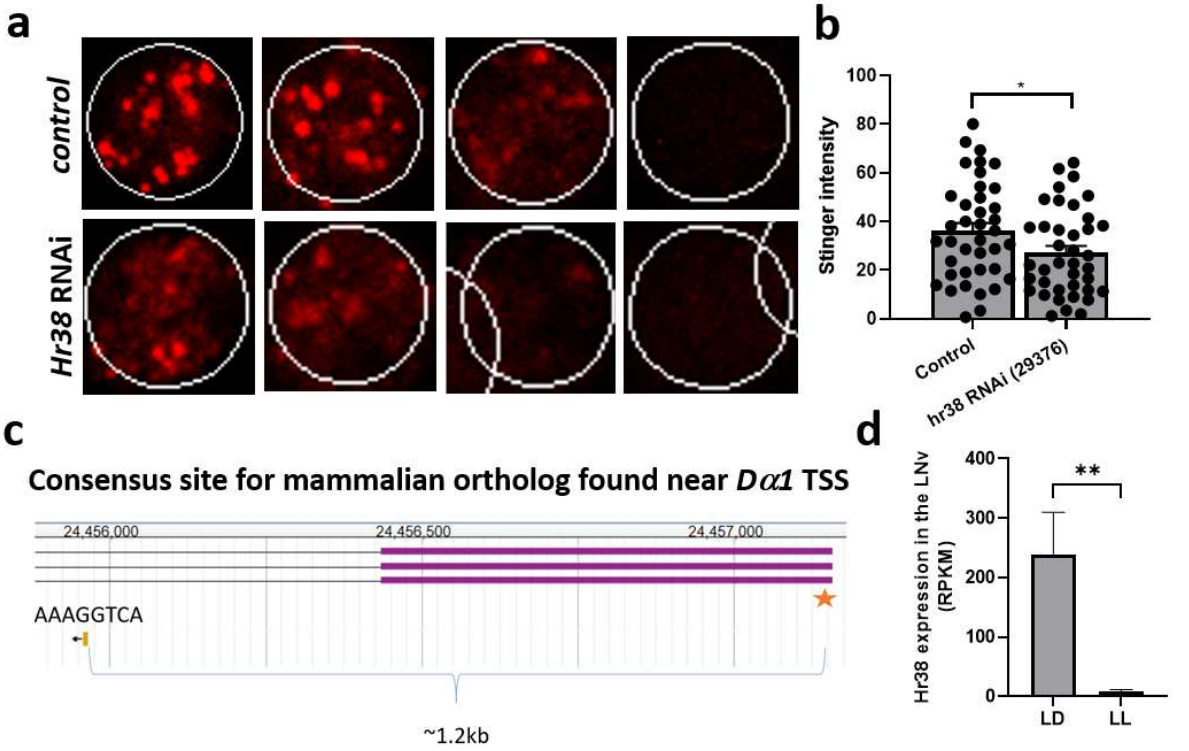

Figure 3.6. Hr38 regulates Dα1 expression in the LNv. (a) Effect of hr38 RNAi on Dα1-driven nuclear RedStinger (red) in the LNv. Shown are representative single slice optical sections of four LNv soma (white circle) from the same cluster in the wildtype (top) and knockdown (bottom) groups. (b) Quantification of data in (a). Hr38 knockdown significantly reduces Dα1 reporter signal intensity. Values are measured as arbitrary units. n represents the number of cells analyzed, n=39. Error bars represent mean ± SEM. (c) A NGFI-B Response Element (NBRE) consensus sequence binding site (AAAGGTCA, arrow) for the hr38 mammalian homolog Nr4a is found ~1kb downstream of the Da1 transcription start site (star). (d) hr38 expression in the LNv is severely repressed by elevated light input. RPKM: Reads per kilobase per million. Error bars represent mean ± SEM.

The chaperone Nacho has a potential role in nAchR assembly and maturation during LNv dendrite development

All nAchRs have complex tertiary and quaternary structures, with each individual polypeptide folded multiple times across a membrane and then assembled with four other subunits around a central axis. It is not surprising, therefore, that several molecular chaperones, such as *Ric-3*, have been identified in both vertebrate and invertebrate systems (194). Our technical difficulties in overexpressing both *Dα1* and *Dα6* in the LNv led us to believe that such auxiliary factors were also active in this neuron and that the aggregates and poor trafficking were the result of an overabundance of raw nAchR subunit protein which overwhelmed the endogenous levels of these chaperones (Figures 2.5 and 2.6).

We investigated this possibility by attempting to rescue the atypical distribution pattern seen here by simultaneously overexpressing the recently discovered Nacho. Isolated from an *in vitro* high-throughput screen for cDNA transgenes facilitating vertebrate α7 current in HEK293 cells, which is notoriously difficult, Nacho enables surface expression and functional activity specifically for nAchRs(208, 209). In animals expressing *Dα1-GFP*, as before, GFP signal is mostly restricted to the cell body and does not form the expected postsynaptic clusters in the dendrite. However, overexpression of *Drosophila Nacho (dNacho)* was able to drastically change the distribution pattern in several ways (Figure 3.7a). First, GFP signal intensity was more evenly distributed between the soma and the dendrite. Second, GFP signal was not homogenously distributed through dendrite branches but was observed within discrete puncta.

Finally, *Dα1:: GFP* often colocalizes with Nacho in the cell bodies and are both concentrated in what appear to be vesicles, an indication that the subunits and their receptors can be correctly incorporated into vesicles for soma-to-dendrite delivery rather than simply diffusing to their targets. In contrast to this stark "rescue", *Dα6-GFP* signal could not be remedied in the same way (Figure 3.7b).

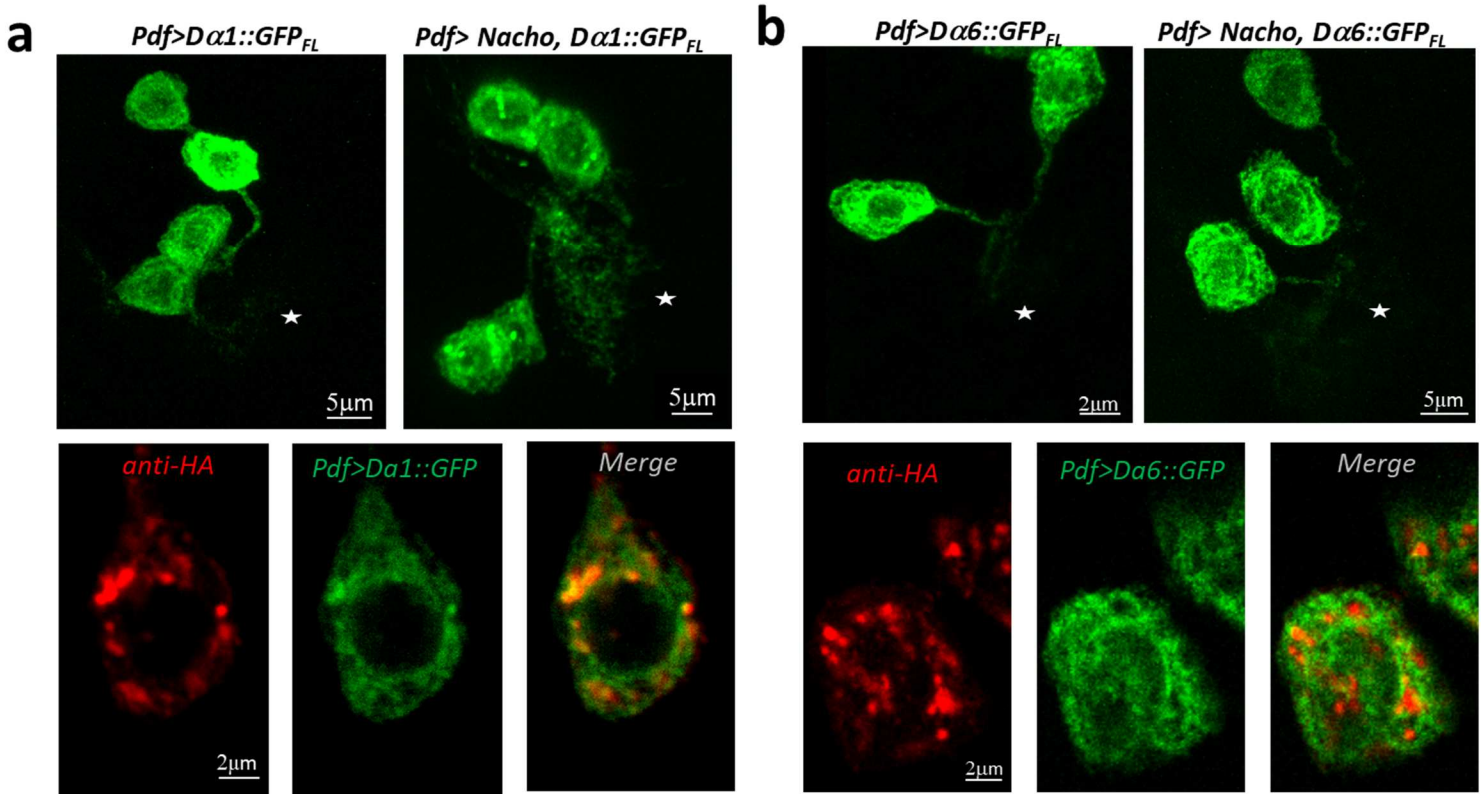

Figure 3.7: Nacho *facilitates nAchR assembly and/or trafficking in a subunit-specific fashion. (a) Top: Representative projected confocal images are shown of Pdf-Gal4 driven Dα1::GFP (green) overexpression in the LNv both without (left) and with* Nacho::HA *co-expression (right). Punctate GFP signal in the dendritic arbor (star) is distributed across a greater area in* Nacho::HA *expressing LNvs. Bottom: Separate cell body single optical sections of where LNvs express both Dα1::GFP and* Nacho *labeled by anti-HA antibody (red). Higher intensity Dα1 puncta tend to be colocalize with* Nacho *in vesicles. (b) Top: Representative projected confocal images are shown of Pdf-Gal4 driven Dα6::GFP (green) overexpression in the LNv both without (left) and with* Nacho::HA *co-expression (right). There does not appear to be a difference in the dendritic distribution (star) of Dα6 puncta between control and* Nacho*-overexpressing animals. Bottom: Separate cell body single optical sections*

The synapse-associated proteins Hig and Lrp4 contribute to LNv dendrite morphogenesis

nAchRs at the vertebrate NMJ, once delivered to the postsynaptic membrane, form complexes with transmembrane proteins, sub-membrane proteins and molecules of the extracellular matrix (ECM)(9). Therefore, we explored what components might be functional at the LNv postsynapse by performing a small-scale morphological screen using RNAi lines against likely candidates already described in the literature.

Here, we identified *hig* and *Lrp4*, which consistently caused a significant reduction in dendrite volume compared to wildtype controls (Figure 3.8). Interestingly, the severity of the reduction was nearly identical for both knockdown lines which indicated that the activity of both perhaps converge on a common downstream target, such as the *Dα6* subunit linked to dendrite structure.

Additionally, *Pdf-Gal4* driven overexpression of a *UAS-hig::GFP* construct supports an extracellular localization of Hig, consistent with previous work detailing its position within the synaptic cleft of nicotinic-type cholinergic synapses (136, 179). Here, GFP signal is found not only within the LNv but is are dispersed throughout much of the brain lobe where it appears to form distinct

clusters (Figure 3.9a). In addition to these punctate signals, there is also a strong and diffuse signal bordering the LNv axon terminal, an indication that a large percentage of Hig originating in the LNv is secreted postsynaptically and is captured at local cholinergic synapses. Furthermore, zoom-in images of the LNv dendrite reveal that Hig puncta are usually adjacent to, but do not overlap with, dendrite branches (as is expected of an ECM protein) (Figure 3.9b).

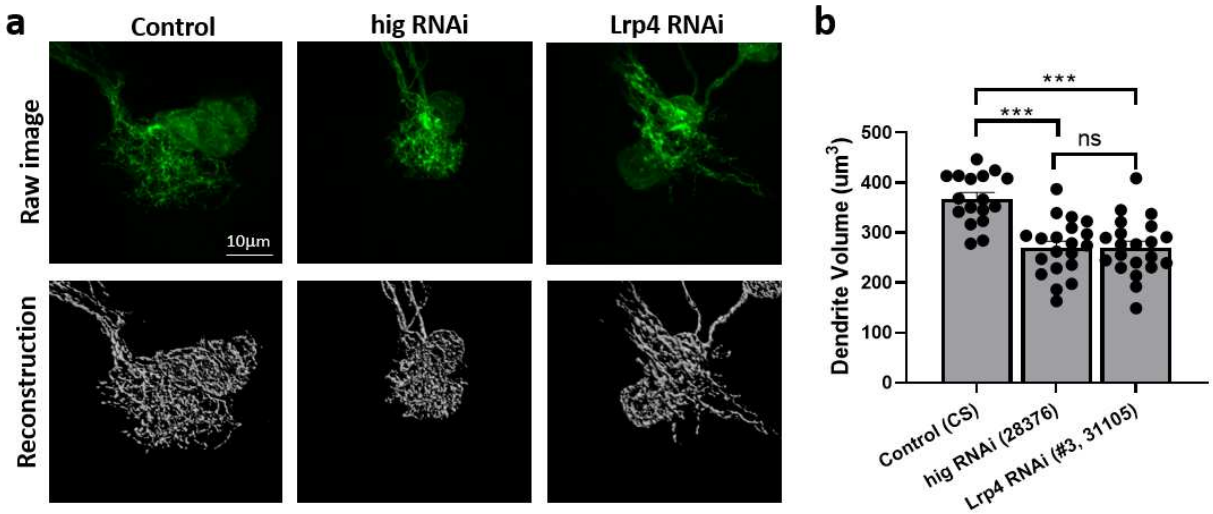

Figure 3.8. Lrp4 and hig are cell-autonomously required for proper LNv dendrite morphogenesis. (a) Representative projected confocal images of LNv dendrites labeled by mCD8::GFP (top, green) and their 3D reconstructions (bottom, grey) are shown for the LD condition. (b) Quantification of data in (a). Knockdown of both hig and Lrp4 significantly reduce LNv dendrite volume compared to wildtype controls. Sample size n represents the number of larvae tested, n=17-21. Error bars represent mean ± SEM.

Discussion

Chapter 3 vastly expanded our investigation of cholinergic synapse development in the *Drosophila* CNS. And although it is still in the early stages, the results obtained here show how nAchRs in the insect brain are tightly regulated at multiple points during their expression, starting from activity-dependent transcription

factors and ending at stable integration at the postsynaptic density *via* interactions with transmembrane and ECM proteins. This should reinforce the idea that nicotinic-type cholinergic synapses, and their development, can be faithfully modeled in the fly brain since similar mechanisms and homologous or analogous genes are functional in other well-studied synapses like the vertebrate NMJ. Below are elaborations on two of these findings and how they will direct future studies to construct a more complete model of nAchR regulation.

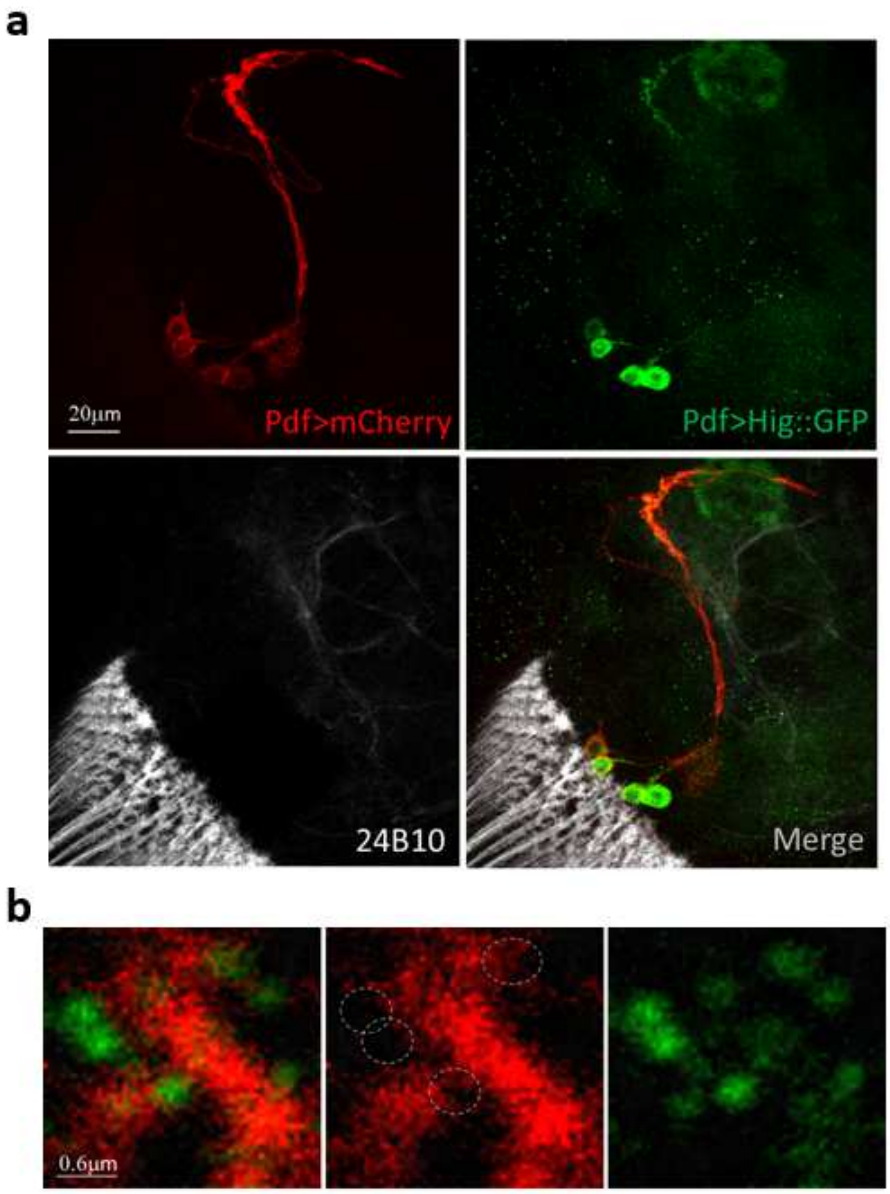

Figure 3.9. A portion of transgenic hig secreted from the LNv localizes adjacent to its own dendrite. (a) Representative projected confocal image of larval brain lobe showing the perfuse localization of hig::GFP (green) driven only in the LNv (mCherry, red) by the Pdf-Gal4 enhancer. 24B10 (white) staining demarcates the developing photoreceptors. (b) Two-channel high magnification image of the LNv dendrite showing hig::GFP puncta (green and dotted white outline) which border the dendrite branch surface.

Predicting the downstream targets of *fru* activity

The data from our previous RNAseq study was instrumental in showing the degree to which *fru* transcription is induced by chronic and excessive light input and the enhancer Gal4 labeling experiment also supported the use of the single sex-specific isoform, fru^{P1}, though other isoforms may also be expressed. Additionally, external CHIP-Seq experiments support a physical interaction between *fru* and *Dα1* or *Dα6* (210-212). The implications though are muddied somewhat by the lack of a male vs. female LNv dendrite volume differences, both in a wildtype genetic background and in fru^{P1} mutants.

There are a few explanations for these observations. Firstly, although *Dα1* and *Dα6* have FRU consensus binding sites, if *Dα1* is the only *in vivo* target then a morphological phenotype should not be expected, given the independence between *Dα1* and dendrite volume, and instead only a physiological assay would reveal any defects. Secondly, *fru* has a strong influence on the motor circuits linked to male-specific courtship behavior, which it achieves by altering axonal guidance and postsynaptic partner choice in sexually dimorphic neurons (213). Although there is little reported on presynaptic nAchRs in *Drosophila*, if a portion of *Dα1* and/or *Dα6* does in fact localize at the LNv axon then the fru^{P1} isoform expressed in the LNvs may also steer axonogenesis and synaptic connectivity and play no role in dendrite development. The strong $fru^{P1}>GFP$ neuropil near the LNv axon terminal suggests it might have postsynaptic partners which are also internally regulated by sex-specific *fru* activity. Finally, there could be other *fru* isoforms which are

the primary determinant for dendrite morphogenesis, rather than the sex-linked fru^{P1} transcript. If either of the first two possibilities is correct, it will have strong ramifications for how nAchR-mediated cholinergic neurotransmission during larval development could be under the same sex-specific regulatory program that later shapes courtship behavior in the adult animal.

Subunit-specific preferences of nAchR-associated maturation proteins

In the vertebrate CNS, there are clear differences in the physiological properties between different nAchR subunits. This is partly due to sequence divergence at critical motifs as prior experiments have identified individual amino acid changes that radically alter receptor functionality such as ion preference and desensitization kinetics (reviewed by (89)). These same sequence variations likely also contribute, in part, to the interaction between different subunits and the chaperones which modify them.

In mammalian cell culture, human and *Drosophila* Nacho are each capable of assembling mature and functional α7 receptors, which are essentially nonfunctional in its absence. Furthermore, the two coprecipitate (208, 209). The same is not true for all receptor subtypes, however, as vertebrate α4β2 and α3β4 display some functional activity at the surface. In *Drosophila*, the *Dα7* subunit (the human *α7* ortholog) has also been shown to be the target of dNacho and simply overexpressing dNacho is sufficient to heighten *Da7*-mediated synaptic activity (168). It was therefore unexpected that processing of *Dα6*, a close homolog of *Da7*, was not aided by dNacho in the same way when *Dα1*, which bears much lower homology with *Dα7*, clearly is. Thus, while the Nacho-α7

relationship appears to be conserved during evolution, its physical association with other subunits may have been enhanced or relaxed.

A simple amino acid comparison between *Dα1* and *Dα6* reveals there are extensive differences in the large intracellular loop, which is known as a key mediator for protein-protein interactions in these receptors (Figure 3.10)(reviewed by (92)). These dissimilarities may explain the outcomes of Nacho-*Dα1* and Nacho-*Dα6* rescue experiments, which were the opposite of what was predicted. Another intriguing possibility is that *dNacho* interaction with *Dα6* varies widely between isoforms. *Dα6* undergoes multiple alternative splicing events and RNA A→I editing events, several of which impact the coding region (81, 108). Finally, other genes besides *dNacho* may be required for effective *Dα6* processing, whereas dNacho alone may be sufficient for *Dα1* folding and maturation.

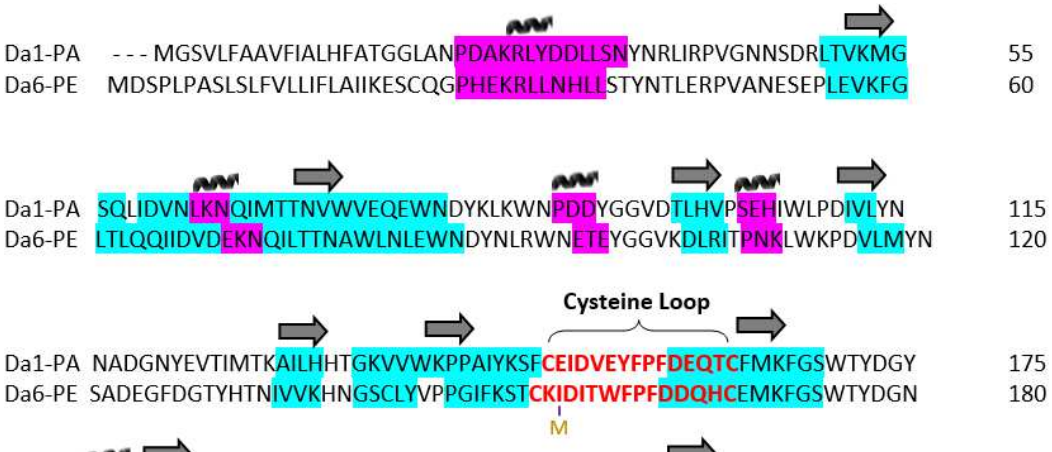

Figure 3.10. Sequence alignment of the Dα1 and Dα6 coding regions identifies similarities and differences at key structural motifs. Comparison of the Dα1 and Dα6 polypeptide sequence by Clustal Omega (1) reveals major differences, including fairly large insertion/deletion events, in the TM3-TM4 intracellular loop. Other features such as the Cys-loop and the TM domains a-helices have a much greater homology. Purple: α-helix; Blue: β-Sheet; Boxed motifs: Transmembrane domains (TM1-4); Cysteine loop and C loop vicinal cysteines are colored and highlighted in red, respectively.

Appendix A

Annotations

nnnnn: vector backbone
NNNNN: Homology Arm / Coding Region
NNNNN: Homology Arm / UTR
nnnnn: Homology Arm/ Intron
nnnnn: Homology Arm/ Intergenic Region
nnnnn: gRNA
N: Silent mutation
NNNNN: GFP11

nnnnn: loxP site
nnnnn: 3XP3-hsp70 promoter
NNNNN: RFP
nnnnn: alpha-Tub 3'UTR
NNNNN: 3xHA
nnnnnn: RE site

tcgcgcgtttcggtgatgacggtgaaaacctctgacacatgcagctcccggagacggtcacagcttgtctgtaagcggatgccgggag
cagacaagcccgtcagggcgcgtcagcgggtgttggcgggtgtcggggctggcttaactatgcggcatcagagcagattgtactgag
agtgcaccatatgcggtgtgaaataccgcacagatgcgtaaggagaaaataccgcatcaggcgccattcgccattcaggctgcgcaa
ctgttgggaagggcgatcggtgcgggcctcttcgctattacgccagctggcgaaaggggggatgtgctgcaaggcgattaagttgggta
*acgccagggttttcccagtcacgacgttgtaaaacgacggcca**gagaattc**gcggccgc**tctaga**tagtgggcacattaccaacggtgc*
atgcagcgagcgacgggaaacttgcaacttgccagtttatattccattttaaatatgcacaacaacatggaaattatatgcattcagacacac
cgctttataatgatgccgtgttcggagggcggggcgaaataatttatgacaattaacaagtgcatctgcaaggacgccggccaaaagggaaa
gttttgtccaggcattataagttctaggaaatgcctttcatgctattttgtcgccccaaactgacagcatttagatggctcattaaaatggagtca
agattaaagaagcaatttttttaataaggcgcacacttggtgtatacgtaatattgcgcatacgccgcgtggagcaataatttaagcttacggt
caaagaataaaataatttctacttcaaatggctttcgaagcgcgcgaaaatgaaagggaaatcgcaaaagaaaagacctgaaactttcaaa
tggcccagcaaaataaatggaaaacagaatgcagaaaactatttattgagtttccttattgtatccccggacctgaagtcctgcttctctgcttc
tgttgggccgccctcgaggttgagggtcctttgtctactcacttccttcggggacattgtgccaaggagcattgcgacggcgaagacaatgcag
aaaagttgcaaattgcatttacaactttatttgcctaatgctgttaatgctggcaaacactcggaaaaaagtatccacccagaattgggtccct
ggtttcggtaaaaagtaacgtaaaagcagcttacttaacaagaagctatactttctatgacacaccagtaatttcaacttcaaagaaaatgaa
ggctatgaagttaatttctgttaaaagaagtgcgttttttaaggattttaaagattttaatcagtatatttttatctttttccccagCACTACCC
GCTTCGCATCGCTTCGATTTGGCTGCGGCGGGCGGGATTAGCGCCCACTGTTCTAGACGTGACCACATGGTC
CTTCATGAGTATGTAAATGCTGCTGGGATTACAAGATCTATAACTTCGTATAATGTATGCTATACGAAGTTATggta
ccggatctaattcaattagagactaattcaattagagctaattcaattaggatccaagcttatcgatttcgaaccctcgaccgccggagtataaat
agaggcgcttcgtctacggagcgacaattcaattcaaacaagcaaagtgaacacgtcgctaagcgaaagctaagcaaataaacaagcgcag
ctgaacaagctaaacaatcgggcggccgcactagagccggtcgccaccATGAGGTCTTCCAAGAATGTTATCAAGGAGTTCAT
GAGGTTTAAGGTTCGCATGGAAGGAACGGTCAATGGGCACGAGTTTGAAATAGAAGGCGAAGGAGAGGGG
AGGCCATACGAAGGCCACAATACCGTAAAGCTTAAGGTAACCAAGGGGGGACCTTTGCCATTTGCTTGGGAT
ATTTTGTCACCACAATTTCAGTATGGAAGCAAGGTATATGTCAAGCACCCTGCCGACATACCAGACTATAAAAA
GCTGTCATTTCCTGAAGGATTTAAATGGGAAAGGGTCATGAACTTTGAAGACGGTGGCGTCGTTACTGTAACC
CAGGATTCCAGTTTGCAGGATGGCTGTTTCATCTACAAGGTCAAGTTCATTGGCGTGAACTTTCCTTCCGATG
GACCTGTTATGCAAAAGAAGACAATGGGCTGGGAAGCCAGCACTGAGCGTTTGTATCCTCGTGATGGCGTGT
TGAAAGGAGAGATTCATAAGGCTCTGAAGCTGAAAGACGGTGGTCATTACCTAGTTGAATTCAAAAGTATTTA

CATGGCAAAGAAGCCTGTGCAGCTACCAGGGTACTACTATGTTGACTCCAAACTGGATATAACAAGCCACAAC
GAAGACTATACAATCGTTGAGCAGTATGAAAGAACCGAGGGACGCCACCATCTGTTCCTTTAGcggccatcgaatt
cgagctcgcccactaagcgtcgcgccacttcaacgctcgatgggagcgtcattggtgggcggggtaaccgtcgaaatcagtgtttacgcttcca
atcgcaacaaaaaattcactgcaacactgaaaagcatacgaaaacgatgaagattgtacgagaaaccataaagtattttatccacaaagaca
cgtatagcagaaaagccaagttaactcggcgataagttgtgtacacaagaataaaatcggccagattcagtgttgtcagaaataagaaaaccc
cactatgttttttctttgccttttctttctcccagcgatcattcatttcgtggtgaaagaacggggtcattgcacggagtttcgactgcgggaaagcag
agctgccgttcacttcgtctataattagcgctttctattttccccgattcgggccgctgctgcgcttttccgcctgctgtttgtggcaagtgtagcagc
aggctgtgcacgcagtgtggcatgcacttggctttccaccgttggtatcgattctctgggacgatgagtcattcctttcggggccacagcataatc
gttgccagctcaccgaaatggtgacttcatttcttaactgccgtcaagcatgcgattgtacatacatacatatttatatatgtacatatttatgtgac
tatggtaggtcgatataatagcaatcaacgcaagcaaatgtgtcagtcctgcttacaggaacgattctatttagtaattttcgttgtataaagtaa
ttatgtatgtatgtaagccccataaatctgaaacaattaggcaaaaccatgcgaagctctgcagataacttcgtataatgtatgctatacgaagt
tatCGGCTAGCTACCCATACGATGTTCCTGACTATGCGGGCTATCCCTATGACGTCCCGGACTATGCAGGATCCTA
TCCATATGACGTTCCAGATTACGCTCTCGAGTTCGCAGAACCGCCGCTGCCCTCCTCACTGCCACTGCCGGGC
GCCGACGACGATCTGTTCAGCCCGTCGGGCCTCAACGGAGACATCAGTCCCGGCTGCTGCCCGGCCGCTGC
AGCCGCCGCTGCCGCCGATCTCAGTCCTACGTTCGAGAAGCCCTACGCCCGCGAAATGGAGAAGACCATCG
AAGGATCCCGCTTCATCGCGCAGCACGTGAAGAACAAGGATAAGTTTGAGAGTgtgagtaataactatgcagccgt
actcttttaatttctaaacttaaattgaattcgcttatttaaacctttatcataaattatatttgctaacaaagagcacattgaaaaaataaga
ttgcttttcagttaattatcataacaaacataagaacccttgcttaagaggattaaattcatggtagacagaatagtacaagtaaaaagcaatt
aacaattccagcaaatttaaaacaacttttaagccagctatgaagatttaaagtccatggcttctagtgttgctgtgtcctttcattttccattgc
aaaacaaatccttgcatttccgtttcttctcgcaatcctgattcacaattcgcattacgtccttttgcaacaccgcgatgttattaattttccatgtt
gcgaaaagaatcaaataatccgtgccacacctccgcaccacacagcattgcaaaacgggcgaaccacccgccgttggtggccaatcagccg
caatcattgtctggcactcgcagctggaacaggcagtccggactccgaatccgctgctggccagactagaaatgacctggccagcatgtctg
gtgcagtgtttatgtctgctcttgataacccgcattaggaccgtaaaaatcccccatttctgcacggccaaaacgaaccggagccggttaaatc
gcgttgctagcgtcctttctaatcaggaatcaaacgagtgggccactggcagatccttttttggatcacgttggctctgccaccgccagcagtg
ccgagtgaagggcaatcggtct***ggcgcgccaagctt***ggtgtaatcatggtcatagctgtttcctgtgtgaaattgttatccgctcacaattc
cacacaacatacgagccggaagcataaagtgtaaagcctggggtgcctaatgagtgagctaactcacattaattgcgttgcgctcact
gcccgctttccagtcgggaaacctgtcgtgccagctgcattaatgaatcggccaacgcgcggggagaggcggtttgcgtattgggcgct
cttccgcttcctcgctcactgactcgctgcgctcggtcgttcggctgcggcgagcggtatcagctcactcaaaggcggtaatacggttatcc
acagaatcaggggataacgcaggaaagaacatgtgagcaaaaggccagcaaaaggccaggaaccgtaaaaaggccgcgttgctg
gcgtttttccataggctccgccccctgacgagcatcacaaaaatcgacgctcaagtcagaggtggcgaaacccgacaggactataaa
gataccaggcgtttcccccctggaagctccctcgtgcgctctcctgttccgaccctgccgcttaccggatacctgtccgcctttctcccttcggg
aagcgtggcgctttctcatagctcacgctgtaggtatctcagttcggtgtaggtcgttcgctccaagctgggctgtgtgcacgaaccccc
gttcagcccgaccgctgcgccttatccggtaactatcgtcttgagtccaacccggtaagacacgacttatcgccactggcagcagccact
ggtaacaggattagcagagcgaggtatgtaggcggtgctacagagttcttgaagtggtggcctaactacggctacactagaagaaca
gtatttggtatctgcgctctgctgaagccagttaccttcggaaaaagagttggtagctcttgatccggcaaacaaaccaccgctggtagc

ggtggtttttttgtttgcaagcagcagattacgcgcagaaaaaaaggatctcaagaagatcctttgatcttttctacggggtctgacgctc
agtggaacgaaaactcacgttaagggattttggtcatgagattatcaaaaaggatcttcacctagatccttttaaattaaaaatgaagt
tttaaatcaagcccaatctgaataatgttacaaccaattaaccaattctgattagaaaaactcatcgagcatcaaatgaaactgcaattt
attcatatcaggattatcaataccatatttttgaaaaagccgtttctgtaatgaaggagaaaactcaccgaggcagttccataggatgg
caagatcctggtatcggtctgcgattccgactcgtccaacatcaatacaacctattaatttcccctcgtcaaaaataaggttatcaagtga
gaaatcaccatgagtgacgactgaatccggtgagaatggcaaaagtttatgcatttctttccagacttgttcaacaggccagccattac
gctcgtcatcaaaatcactcgcatcaaccaaaccgttattcattcgtgattgcgcctgagcgagacgaaatacgcgatcgctgttaaaag
gacaattacaaacaggaatcgaatgcaaccggcgcaggaacactgccagcgcatcaacaatattttcacctgaatcaggatattcttct
aatacctggaatgctgtttttccggggatcgcagtggtgagtaaccatgcatcatcaggagtacggataaaatgcttgatggtcggaa
gaggcataaattccgtcagccagtttagtctgaccatctcatctgtaacatcattggcaacgctacctttgccatgtttcagaaacaactct
ggcgcatcgggcttcccatacaagcgatagattgtcgcacctgattgcccgacattatcgcgagcccatttatacccatataaatcagca
tccatgttggaatttaatcgcggcctcgacgtttcccgttgaatatggctcataacacccttgtattactgtttatgtaagcagacagtttt
attgttcatgatgatatattttatcttgtgcaatgtaacatcagagattttgagacacgggccagagctgca

Figure A.1: Full sequence of Dα1 knock-in gene region. All elements added to the large, intracellular loop of Dα1, prior to Cre-mediated RFP removal, are shown and color coded. Sequence begins and ends with 5' and 3' ends of plasmid vector.

Appendix B

Annotations

nnnnn: vector backbone

NNNNN: Homology Arm / Coding Region

NNNNN: Homology Arm / UTR

nnnnn: Homology Arm/ Intron

nnnnn: Homology Arm/ Intergenic Region

nnnnn: gRNA

N: Silent mutation

NNNNN: GFP11

nnnnn: loxP site

nnnnn: 3XP3-hsp70 promoter

NNNNN: RFP

nnnnn: alpha-Tub 3'UTR

NNNNN: 3xHA

nnnnnn: RE site

tcgcgcgtttcggtgatgacggtgaaaacctctgacacatgcagctcccggagacggtcacagcttgtctgtaagcggatgccgggag
cagacaagcccgtcagggcgcgtcagcgggtgttggcgggtgtcggggctggcttaactatgcggcatcagagcagattgtactgag
agtgcaccatatgcggtgtgaaataccgcacagatgcgtaaggagaaaataccgcatcaggcgccattcgccattcaggctgcgcaa
ctgttgggaagggcgatcggtgcgggcctcttcgctattacgccagctggcgaaaggggggatgtgctgcaaggcgattaagttgggta
*acgccagggttttcccagtcacgacgttgtaaaacgacggcca**gagaattc**gcggccgc**tctaga**ccgacacagaaaaccaatgaacc*
ccgtccacaaaaacaagttgcttgcttttattagtgtagaatgagcagggacagtaaagtctcaaaagtaatatattgccatactatacattaa
gtattatcaataaaaagaaaaggatttaatatcaaatagaagttttgcgaaagatcgcatttcaaaataaccaatatcttacgattttactgtc
ctctgtttcgagtttgtcttcaattactaaagccatacaagccatactagcgcatgactcttaatcaaaacagtttacactaaagtgcatgcaga
gaatgaaacctaaaagtatttagtaataatccaaatgtagtggctttcactaggcattacttagtagtaacgtgcgtaacataacgtagtcaca
gcattgtaacaacacagtaattttgattacgctactttctctaatcgtaaatctaaccaaagtctttcatgaaatgaagctaaactaaagtaatg
ttgtactattttcgtaaattattatttcgagcttctgttcttagtgttttgatgattttgagagaccccggagcaccactctaatataggcattttct
ctgctctctgttcaccccacaaactgccatccgcaatccgcaaacccaaaatttcgcacctaaatccttagGCACCTACTTCAATTGCA
TCATGTTCATGGTCGCCTCGTCGGTGGTGCTGACAGTAGTGGTGCTCAACTACCACCATCGCACAGCGGAC
ATTCACGAGATGCCACCGTGGgtgagtcccccatcactttaagccactctctgttcccccgttttattgccgtacttcattcataaccag
ATCAAGTCCGTTTTCCTACAATGGCTGCCCTGGATCTTGCGAATGGGTCGACCCGGTCGCAAGATTACACGC
AAAACAATACTATTAAGCAATCGCATGAAGGAGCTGGAGCTAAAGGAGCGCTCCTCCAAATCCCTGCTGGC
CAATGTCCTCGACATCGACGACGACTTCCGGCACACAATATCTGGC**TCTAGA**CGTGACCACATGGTCCTTCAT
GAGTATGTAAATGCTGCTGGGATTACA**AGATCT**ATAACTTCGTATAATGTATGCTATACGAAGTTAT**ggtacc**ggatc
taattcaattagagactaattcaattagagctaattcaattaggatccaagcttatcgatttcgaaccctcgaccgccggagtataaatagaggc
gcttcgtctacggagcgacaattcaattcaaacaagcaaagtgaacacgtcgctaagcgaaagctaagcaaataaacaagcgcagctgaac
aagctaaacaatcgggcggccgcactagagccggtcgccaccATGAGGTCTTCCAAGAATGTTATCAAGGAGTTCATGAGG
TTTAAGGTTCGCATGGAAGGAACGGTCAATGGGCACGAGTTTGAAATAGAAGGCGAAGGAGAGGGGAGGC
CATACGAAGGCCACAATACCGTAAAGCTTAAGGTAACCAAGGGGGGACCTTTGCCATTTGCTTGGGATATTTT
GTCACCACAATTTCAGTATGGAAGCAAGGTATATGTCAAGCACCCTGCCGACATACCAGACTATAAAAAGCTGT
CATTTCCTGAAGGATTTAAATGGGAAAGGGTCATGAACTTTGAAGACGGTGGCGTCGTTACTGTAACCCAGG
ATTCCAGTTTGCAGGATGGCTGTTTCATCTACAAGGTCAAGTTCATTGGCGTGAACTTTCCTTCCGATGGACCT
GTTATGCAAAAGAAGACAATGGGCTGGGAAGCCAGCACTGAGCGTTTGTATCCTCGTGATGGCGTGTTGAAA

GGAGAGATTCATAAGGCTCTGAAGCTGAAAGACGGTGGTCATTACCTAGTTGAATTCAAAAGTATTTACATGG
CAAAGAAGCCTGTGCAGCTACCAGGGTACTACTATGTTGACTCCAAACTGGATATAACAAGCCACAACGAAGA
CTATACAATCGTTGAGCAGTATGAAAGAACCGAGGGACGCCACCATCTGTTCCTTTAGcggccatcgaattcgagctc
gcccactaagcgtcgcgccacttcaacgctcgatgggagcgtcattggtgggcggggtaaccgtcgaaatcagtgtttacgcttccaatcgcaa
caaaaaattcactgcaacactgaaaagcatacgaaaacgatgaagattgtacgagaaaccataaagtattttatccacaaagacacgtatag
cagaaaagccaagttaactcggcgataagttgtgtacacaagaataaaatcggccagattcagtgttgtcagaaataagaaaaccccactatg
ttttctttgccttttctttctcccagcgatcattcatttcgtggtgaaagaacggggtcattgcacggagtttcgactgcgggaaagcagagctgc
cgttcacttcgtctataattagcgctttctattttccccgattcgggccgctgctgcgcttttccgcctgctgtttgtggcaagtgtagcagcaggct
gtgcacgcagtgtggcatgcacttggctttccaccgttggtatcgattctctgggacgatgagtcattcctttcggggccacagcataatcgttgc
cagctcaccgaaatggtgacttcatttcttaactgccgtcaagcatgcgattgtacatacatacatatttatatatgtacatatttatgtgactatgg
taggtcgatataatagcaatcaacgcaagcaaatgtgtcagtcctgcttacaggaacgattctatttagtaattttcgttgtataaagtaattatgt
atgtatgtaagccccataaatctgaaacaattaggcaaaaccatgcgaagctctgcagataacttcgtataatgtatgctatacgaagttatCG
GCTAGCTACCCATACGATGTTCCTGACTATGCGGGCTATCCCTATGACGTCCCGGACTATGCAGGATCCTATCCA
TATGACGTTCCAGATTACGCTCTCGAGTCGCAAACGGCCATTGGCTCGTCGGCgtaagttctgctcttaatatccaaat
gttccatattcaaatgtaaattgaaatctgcagCAGCTTCGGTCGGCCCACAACGGTGGAGGAGCATCACACGGCCATC
GGCTGCAATCACAAAGATCTTCATCTAATTCTCAAAGAATTGCAATTTATTACGGCGCGGATGCGCAAAGCT
GACGACGAAGCGGAATTGATCGGCGATTGGAAGTTCGCGGCAATGGTTGTGGATAGgtaagaaagtaaaaatcc
cttgagatatttaagttcgatttgtgatacgatctaaagttaaacgaaaaacaaacatttgtcatacgagaaatattacattttggtccaaattc
tgaaagacaactgctttgtaatatttccatcactattccactattcatccgcactcaaccacacagtaatgaactttaagatatgtactcgcgaa
tgggtgtgaatttattgaaccaaaaccggcagcatttgacaggcgcctgctgtgcacgtcaaacaatatggccacacgacttccggcgggat
aaacgtacacaaacgcagtgcctcacgcacgcacgcatacaacagcatacacacacacacacacacactcacccgtgcacgtggcgcaaa
tattaaaagatggccgactgccggccgccattttgtttggcagccctgctgatttgtttgctaaaccagcgctttgcttgctcttctactccacag
ATTTTGTTTAATTGTTTTCACGCTCTTCACGATTATTGCAACGGTTACGGTGCTGCTCTCCGCTCCGCACATAA
TCGTGCAATAAGGACGCTCGAATTAGGCCATTAAGCTACGGATACGTCGGAAGCATCGGCTGACGGGAGA
TGCCTAGTTAAGTTCTTTTTCAAAAACAAAAAAACTAGCAAAGCTGCTTCAAAACAAAGCAAACAAAAACAA
ACAACAAAGAAAACTACAAAAAAAAATAATAATAAAAACAAAAAATTGTTAATTACATTTTTAAGTAAAGAC
AAAGAGCAAAACGAAAATGTTG***ggcgcgccaagctt***ggtgtaatcatggtcatagctgtttcctgtgtgaaattgttatccgctc
acaattccacacaacatacgagccggaagcataaagtgtaaagcctggggtgcctaatgagtgagctaactcacattaattgcgttgc
gctcactgcccgctttccagtcgggaaacctgtcgtgccagctgcattaatgaatcggccaacgcgcggggagaggcggtttgcgtatt
gggcgctcttccgcttcctcgctcactgactcgctgcgctcggtcgttcggctgcggcgagcggtatcagctcactcaaaggcggtaatac
ggttatccacagaatcaggggataacgcaggaaagaacatgtgagcaaaaggccagcaaaaggccaggaaccgtaaaaaggccg
cgttgctggcgttttttccataggctccgccccccctgacgagcatcacaaaaatcgacgctcaagtcagaggtggcgaaacccgacagga
ctataaagataccaggcgtttcccccctggaagctccctcgtgcgctctcctgttccgaccctgccgcttaccggatacctgtccgcctttctcc
cttcgggaagcgtggcgctttctatagctcacgctgtaggtatctcagttcggtgtaggtcgttcgctccaagctgggctgtgtgcacga
acccccccgttcagcccgaccgctgcgccttatccggtaactatcgtcttgagtccaacccggtaagacacgacttatcgccactggcagca

gccactggtaacaggattagcagagcgaggtatgtaggcggtgctacagagttcttgaagtggtggcctaactacggctacactaga
agaacagtatttggtatctgcgctctgctgaagccagttaccttcggaaaaagagttggtagctcttgatccggcaaacaaaccaccgc
tggtagcggtggttttttgtttgcaagcagcagattacgcgcagaaaaaaaggatctcaagaagatcctttgatcttttctacggggtct
gacgctcagtggaacgaaaactcacgttaagggattttggtcatgagattatcaaaaaggatcttcacctagatccttttaaattaaaa
atgaagttttaaatcaagcccaatctgaataatgttacaaccaattaaccaattctgattagaaaaactcatcgagcatcaaatgaaac
tgcaatttattcatatcaggattatcaataccatatttttgaaaaagccgtttctgtaatgaaggagaaaactcaccgaggcagttccat
aggatggcaagatcctggtatcggtctgcgattccgactcgtccaacatcaatacaacctattaatttcccctcgtcaaaaataaggttat
caagtgagaaatcaccatgagtgacgactgaatccggtgagaatggcaaaagtttatgcatttctttccagacttgttcaacaggccag
ccattacgctcgtcatcaaaatcactcgcatcaaccaaaccgttattcattcgtgattgcgcctgagcgagacgaaatacgcgatcgctg
ttaaaaggacaattacaaacaggaatcgaatgcaaccggcgcaggaacactgccagcgcatcaacaatattttcacctgaatcagga
tattcttctaatacctggaatgctgtttttccggggatcgcagtggtgagtaaccatgcatcatcaggagtacggataaaatgcttgatg
gtcggaagaggcataaattccgtcagccagtttagtctgaccatctcatctgtaacatcattggcaacgctacctttgccatgtttcagaa
acaactctggcgcatcgggcttcccatacaagcgatagattgtcgcacctgattgcccgacattatcgcgagcccatttatacccatataa
atcagcatccatgttggaatttaatcgcggcctcgacgtttcccgttgaatatggctcataacacccccttgtattactgtttatgtaagcag
acagttttattgttcatgatgatatatttttatcttgtgcaatgtaacatcagagattttgagacacgggccagagctgca

Figure B.1: Full sequence of Dα6 knock-in gene region. All elements added to the large, intracellular loop of Dα6, prior to Cre-mediated RFP removal, are shown and color coded. Sequence begins and ends with 5' and 3' ends of plasmid vector.

Appendix C

D. melanogaster Dα1* Regulatory region Genomic Relaxed *EvoPrint

Black capital letters represent bases conserved in all species;
Colored bases represent sequences present in all species except the one corresponding to that color here:

D.simulans, *D.sechellia*, *D.yakuba*, *D.erecta*, *D.ananassae* or *D.pseudoobscura*

Figure C.1: Full Dα1 sequence analyzed by BLAT. The conservation of each nucleotide is color coded. Sequence stretches containing highly conserved (i.e. capitalized) bases were manually selected for TF motif analysis.

Appendix D

D. melanogaster Dα6* Regulatory region Genomic Relaxed *EvoPrint

Black capital letters represent bases conserved in all species;
Colored bases represent sequences present in all species except the one corresponding to that color here:

D.simulans, *D.sechellia*, *D.erecta*, *D.yakuba*, *D.ananassae*,

D.pseudoobscura, *D.willistoni*, *D.virilis* or *D.grimshawi*

tcgaagggctcattgcgactgaggctggaatcgaattccgtgccatcgaccaggcgacccgtatagtgcaggg
acacagtgcatccgctgtgcggcgtctctgtgcccgtgccctctttcaggatctcctttaggacgccaccgtc
cccggacaagtcgattttattcccttccggcatttttggctgctgaactttaattcgcacgatgatggcagag
tgaccaagctcaagcacgttggaaagaccgtattgattattgggctcgtgcgtttttcagtcgcttaacagaa
ctgagttaacagtcagtgctaactaaagcgccatctatagtattaggacagttaaggcagtgggtacaaaaca
cagataactagctcggactcgaaccgtatcacatacctattaaaatggtttattagctagaatattgaaattt
cttgagctaattaacgataaaaacttgagaaatgctattagaaatacaaactttatttagttcgcatatgttt
caaaatgacgaacaagctaataggaataatttgttatatattaagttcggcactatgaataatattagctaa
aatgcatataccgttcattgtctatttggtacaattacaagtcattttcttgattaatccatttcggccgcaa
ttaatgatattaaaggatgtctgttgttcatttcattgtgttggcggctacaacaacaacacacacacacaca
cagtgctctccaaatgtaatctgcccagcggctttatgattgcatgtgcatccctataagtgtatgcatcaaa
tataatcctgttatcgtttttgttatatttgattattttgcccttggcttttggcagtgccaacttccaattt
cgtatgccagcgcaagagcaacagaaataaATTAATGCACTTAATTTTATTGGTTTctATaATTCATGctcgT
aAGCtcgtctgctataagctctcccgcacagtaggccaatttgggggattatcgcaatgggcattcaacgatt
ttttcaaggtcaactggaatgataaaaatgataagtgtgctcatgttgctggattcattcttcttcctaccag
ccagctgtgacattatttccttggaattccgcctgtgtctttataaatcgctgcagctgtcgctgtctcctcc
gcctactaaaatattagccagtcatccagcagcgtttcatcttcgagcttcggcaccaacttcataaaagccc
agagtctgggcgcgcacttgtcgctcattaattagggttcgtctacagggatgactacgctggaaaaatattg
tatattacaatattccttcaaaaaaaacgtagtttatttaataaatacatatacatagttaagaaataaattg
aacaaaagtaatcaaataatacacaatcaaactaactaaagggcttatatatgaatgacgtatacgcaatatt
attaagtatacgttagatgtattagaaacttatattattgtataataaaaaagattattaacttaattgtgag
aagtgtcaactgaaacgtttagaagtccattaagatgctattataaatggtgccacagggcttagactttcgc
ttcggtatgcaatagtcgtacttcttttgggcttaaagtatgtcagcatatgcgaatctccagatctccagag
attctagtgactccctcgaaagcagcatatatattttttttgagtgctccgagccgtgtccctgtccaggcc
cattATTTTTtCaggtataGTATAGAGACATTGACCAGCgacggacgcccacaatcacgctgcctcggctgct
gttggcgtctccgctggcagaggtcctgctgttgctcgctcgttaCTCgACTGTAAACATTCCAGggcAGCTT
TCACTCgtgcCAcagaataCACAggaccaaaacggactccctaacgcggtgactcaaaccgttcggctgcgcT
CggctggaagcttcgtttttcgttttccgtttcggattgagtcaaattgtggatgctgcgtggCTCgtGGTCC
ATGGcCGTGTGAAAAGCTGCGTTGAGCGCATTAAGTCGTTAGGGTACAACCAGACAGGACGCACTTacTCcgA
Gctgccgccattcgcc TGCCTTGgCGTgtgtgtaccgttagttcagctgtcccgtgcagagtgggaaaattag
cggggaagccccaacatcgaaccgaaatcgcaatcgaatcatagccaaatttaaagtcgctgactatcgaggt
gcataaaaagaaacttgctggctagtgcgtgaagaaaaaactgccaaaacaagaaaagtcaagaaaattcaaa
gaaaataaatactccaattccctctgtggcagctcccgcgcgTccaaGTGtgtgtaaGTGTcgtcTgTGCGTG
TGTGcGTGcgtttcCaaAAccttcagatcgaGTGTGTTCAtCAAcAACAAATAAgaTAAAAAAttcaaaaaaa
aaaaaaaaatatatatatattgaataaaatacaaaatgtatacaagcgacaagtagaagcaagtcgcattaaa
tcatagccAATTaaAAAtatttgcTTaaacgaacCAAGGTAAACAgAAcgagCAaAaattgttgctctctctt
cccaagcgcttttccaactttccgctttcctcccgaaattttgcccacaaaaaccaatgcactcgctacGGTG
CAACAGCTTAAAAGtaTgcTacGAttTTtCcCaCtcaatattttcgtgTAATTGTTGCGCcTgctgctgtgct

Figure D.1: Full Dα6 sequence analyzed by BLAT. The conservation of each nucleotide is color coded. Sequence stretches containing highly conserved (i.e. capitalized) bases were manually selected for TF motif analysis.

Appendix E

TF	#		TF	#		TF	#
Bap	1		dl	1		pdm2	1
Abd-A	1		Eip75B	2		peb	2
Abd-B	1		esm8	1		prd	2
Achi	1		Ets97D	1		repo	1
acj6	1		eve	1		run	1
ara	1		Exd	1		shn	1
bab1	1		fru	1		Six4	1
B-H1	1		Gce	1		slp1	2
bin	1		gl	1		slp2	1
btn	2		grh	1		Sna	1
cad	1		gt	1		sox15	2
caup	1		Hand	1		spl1	1
Cf2	1		Hbn	2		tap	1
CG16899	1		hth	4		Tin	2
CG32105	1		jigr1	1		tll	2
CG3407	1		jim	2		Trl	3
CG42234	1		lola	1		ttk	1
CG4328	2		Med	1		twist	1
Croc	2		Mes2	1		vis	4
D19A	2		mitf	1		vnd	1
deaf1	1		nub	2		zen	2
disco	2		Oncecut	2			

Figure E.1. Transcription factor consensus site count for Dα1 regulatory region. Table of transcription factors whose consensus sequence binding sites are found, and their frequency, in the region analyzed (listed in descending order of frequency).

Appendix F

TF	#	TF	#	TF	#	TF	#	TF	#
AbdA	6	ro	3	GATAe	2	BH-1	1	h	1
cad	5	slou	3	hbn	2	Bteb2	1	hkb	1
zen	5	so	3	Hmx	2	Caup	1	HLHm3	1
Br	4	Trl	3	inv	2	Cf2	1	Hmen	1
btn	4	Ubx	3	ken	2	CG11085	1	Hmin	1
CG15696	4	z	3	klu	2	CG11294	1	Hth	1
CG34031	4	Abd-B	2	knrl	2	CG11504	1	HunB	1
ems	4	Aef1	2	lbe	2	CG11617	1	jim	1
fru	4	al	2	lbl	2	CG12029	1	Kr	1
phdp	4	ap	2	Lim1	2	CG14962	1	lab	1
slp1	4	ara	2	Lim3	2	CG2052	1	lim	1
Antp	3	Awh	2	Mes2	2	CG3065	1	lmd	1
bin	3	bab1	2	Otp	2	CG3919	1	Mirr	1
C15	3	bap	2	pan	2	CG4360	1	Motif 8	1
CG13424	3	BH-2	2	Pph13	2	CG5953	1	odsh	1
CG32105	3	Bsh	2	prd	2	CG6276	1	PDHP	1
CG32532	3	CG11294	2	retn	2	chinmo	1	peb	1
CG42234	3	CG12236	2	Rx	2	cic	1	pnr	1
CG9437	3	CG18599	2	slp2	2	D19B	1	rn	1
en	3	CG33980	2	sna	2	da	1	scr	1
exd	3	CG4136	2	sqz	2	Dfd	1	sens-2	1
fd64A	3	CG4328	2	srp	2	DLL	1	shn	1
hb	3	CG7056	2	tin	2	E(spl)	1	Six4	1
HGTX	3	CG9876	2	tup	2	esm3	1	slbo	1
jigr1	3	croc	2	Unc4	2	esm5	1	sp1	1
kni	3	dati	2	unpg	2	esm8	1	Su(hw)	1
Lola	3	Dr	2	Vsx1	2	FBgn0000061	1	Tkr	1
Nk7.1	3	E5	2	Zen2	2	FBgn0030058	1	tll	1
pb	3	eve	2	Ap	1	FBgn0054031	1	ttk	1
Repo	3	ey	2	apte	1	Fer3	1	Vis	1
F1-3	2	ftz	2	Atf6	1	GATad	1		

Figure F.1: Transcription factor consensus site count for Dα6 regulatory region. Table of transcription factors whose consensus sequence binding sites are found, and their frequency, in the region analyzed (listed in descending order of frequency).

Bibliography

1. F. Madeira *et al.*, The EMBL-EBI search and sequence analysis tools APIs in 2019. *Nucleic Acids Res* **47**, W636-W641 (2019).
2. J. N. Langley, On the contraction of muscle, chiefly in relation to the presence of ;receptive' substances: Part IV. The effect of curari and of some other substances on the nicotine response of the sartorius and gastrocnemius muscles of the frog. *J Physiol* **39**, 235-295 (1909).
3. G. L. Brown, The actions of acetylcholine on denervated mammalian and frog's muscle. *J Physiol* **89**, 438-461 (1937).
4. J. P. Changeux, M. Kasai, M. Huchet, J. C. Meunier, [Extraction from electric tissue of gymnotus of a protein presenting several typical properties characteristic of the physiological receptor of acetylcholine]. *C R Acad Hebd Seances Acad Sci D* **270**, 2864-2867 (1970).
5. S. Bevan, J. H. Steinbach, The distribution of alpha-bungarotoxin binding sites of mammalian skeletal muscle developing in vivo. *J Physiol* **267**, 195-213 (1977).
6. R. Tarrab-Hazdai, B. Geiger, S. Fuchs, A. Amsterdam, Localization of acetylcholine receptor in excitable membrane from the electric organ of Torpedo: Evidence for exposure of receptor antigenic sites on both sides of the membrane. *Proc Natl Acad Sci U S A* **75**, 2497-2501 (1978).
7. J. R. Sanes, J. W. Lichtman, Development of the vertebrate neuromuscular junction. *Annu Rev Neurosci* **22**, 389-442 (1999).
8. J. R. Sanes, J. W. Lichtman, Induction, assembly, maturation and maintenance of a postsynaptic apparatus. *Nat Rev Neurosci* **2**, 791-805 (2001).
9. H. Wu, W. C. Xiong, L. Mei, To build a synapse: signaling pathways in neuromuscular junction assembly. *Development* **137**, 1017-1033 (2010).
10. L. A. Tintignac, H. R. Brenner, M. A. Ruegg, Mechanisms Regulating Neuromuscular Junction Development and Function and Causes of Muscle Wasting. *Physiol Rev* **95**, 809-852 (2015).
11. B. Zhang *et al.*, LRP4 serves as a coreceptor of agrin. *Neuron* **60**, 285-297 (2008).
12. N. Kim *et al.*, Lrp4 is a receptor for Agrin and forms a complex with MuSK. *Cell* **135**, 334-342 (2008).
13. S. D. Weatherbee, K. V. Anderson, L. A. Niswander, LDL-receptor-related protein 4 is crucial for formation of the neuromuscular junction. *Development* **133**, 4993-5000 (2006).
14. D. J. Glass *et al.*, Agrin acts via a MuSK receptor complex. *Cell* **85**, 513-523 (1996).
15. T. M. DeChiara *et al.*, The receptor tyrosine kinase MuSK is required for neuromuscular junction formation in vivo. *Cell* **85**, 501-512 (1996).
16. D. M. Valenzuela *et al.*, Receptor tyrosine kinase specific for the skeletal muscle lineage: expression in embryonic muscle, at the neuromuscular junction, and after injury. *Neuron* **15**, 573-584 (1995).
17. G. Jones *et al.*, Induction by agrin of ectopic and functional postsynaptic-like membrane in innervated muscle. *Proc Natl Acad Sci U S A* **94**, 2654-2659 (1997).
18. E. W. Godfrey, R. M. Nitkin, B. G. Wallace, L. L. Rubin, U. J. McMahan, Components of Torpedo electric organ and muscle that cause aggregation of acetylcholine receptors on cultured muscle cells. *J Cell Biol* **99**, 615-627 (1984).

19. R. M. Nitkin *et al.*, Identification of agrin, a synaptic organizing protein from Torpedo electric organ. *J Cell Biol* **105**, 2471-2478 (1987).
20. S. C. Froehner, C. W. Luetje, P. B. Scotland, J. Patrick, The postsynaptic 43K protein clusters muscle nicotinic acetylcholine receptors in Xenopus oocytes. *Neuron* **5**, 403-410 (1990).
21. S. J. Burden, R. L. DePalma, G. S. Gottesman, Crosslinking of proteins in acetylcholine receptor-rich membranes: association between the beta-subunit and the 43 kd subsynaptic protein. *Cell* **35**, 687-692 (1983).
22. D. E. Frail *et al.*, cDNAs for the postsynaptic 43-kDa protein of Torpedo electric organ encode two proteins with different carboxyl termini. *Proc Natl Acad Sci U S A* **84**, 6302-6306 (1987).
23. M. Gautam *et al.*, Failure of postsynaptic specialization to develop at neuromuscular junctions of rapsyn-deficient mice. *Nature* **377**, 232-236 (1995).
24. L. Jing, J. L. Lefebvre, L. R. Gordon, M. Granato, Wnt signals organize synaptic prepattern and axon guidance through the zebrafish unplugged/MuSK receptor. *Neuron* **61**, 721-733 (2009).
25. Y. Liu *et al.*, Essential roles of the acetylcholine receptor gamma-subunit in neuromuscular synaptic patterning. *Development* **135**, 1957-1967 (2008).
26. S. Lin, L. Landmann, M. A. Ruegg, H. R. Brenner, The role of nerve- versus muscle-derived factors in mammalian neuromuscular junction formation. *J Neurosci* **28**, 3333-3340 (2008).
27. X. Yang *et al.*, Patterning of muscle acetylcholine receptor gene expression in the absence of motor innervation. *Neuron* **30**, 399-410 (2001).
28. W. Lin *et al.*, Distinct roles of nerve and muscle in postsynaptic differentiation of the neuromuscular synapse. *Nature* **410**, 1057-1064 (2001).
29. K. Gundersen, J. R. Sanes, J. P. Merlie, Neural regulation of muscle acetylcholine receptor epsilon- and alpha-subunit gene promoters in transgenic mice. *J Cell Biol* **123**, 1535-1544 (1993).
30. M. G. Tansey, G. C. Chu, J. P. Merlie, ARIA/HRG regulates AChR epsilon subunit gene expression at the neuromuscular synapse via activation of phosphatidylinositol 3-kinase and Ras/MAPK pathway. *J Cell Biol* **134**, 465-476 (1996).
31. G. C. Chu, L. M. Moscoso, M. X. Sliwkowski, J. P. Merlie, Regulation of the acetylcholine receptor epsilon subunit gene by recombinant ARIA: an in vitro model for transynaptic gene regulation. *Neuron* **14**, 329-339 (1995).
32. S. A. Jo, X. Zhu, M. A. Marchionni, S. J. Burden, Neuregulins are concentrated at nerve-muscle synapses and activate ACh-receptor gene expression. *Nature* **373**, 158-161 (1995).
33. J. P. Merlie, J. R. Sanes, Concentration of acetylcholine receptor mRNA in synaptic regions of adult muscle fibres. *Nature* **317**, 66-68 (1985).
34. A. Klarsfeld *et al.*, Regulation of muscle AChR alpha subunit gene expression by electrical activity: involvement of protein kinase C and Ca2+. *Neuron* **2**, 1229-1236 (1989).
35. L. Adams, D. Goldman, Role for calcium from the sarcoplasmic reticulum in coupling muscle activity to nicotinic acetylcholine receptor gene expression in rat. *J Neurobiol* **35**, 245-257 (1998).
36. C. F. Huang, B. E. Flucher, M. M. Schmidt, S. K. Stroud, J. Schmidt, Depolarization-transcription signals in skeletal muscle use calcium flux through L channels, but bypass the sarcoplasmic reticulum. *Neuron* **13**, 167-177 (1994).

37. S. Burden, Development of the neuromuscular junction in the chick embryo: the number, distribution, and stability of acetylcholine receptors. *Dev Biol* **57**, 317-329 (1977).
38. D. Goldman, H. R. Brenner, S. Heinemann, Acetylcholine receptor alpha-, beta-, gamma-, and delta-subunit mRNA levels are regulated by muscle activity. *Neuron* **1**, 329-333 (1988).
39. H. J. Tsay, J. Schmidt, Skeletal muscle denervation activates acetylcholine receptor genes. *J Cell Biol* **108**, 1523-1526 (1989).
40. J. P. Merlie, K. E. Isenberg, S. D. Russell, J. R. Sanes, Denervation supersensitivity in skeletal muscle: analysis with a cloned cDNA probe. *J Cell Biol* **99**, 332-335 (1984).
41. R. J. Balice-Gordon, J. W. Lichtman, In vivo visualization of the growth of pre- and postsynaptic elements of neuromuscular junctions in the mouse. *J Neurosci* **10**, 894-908 (1990).
42. J. H. Steinbach, Developmental changes in acetylcholine receptor aggregates at rat skeletal neuromuscular junctions. *Dev Biol* **84**, 267-276 (1981).
43. M. J. Marques, J. A. Conchello, J. W. Lichtman, From plaque to pretzel: fold formation and acetylcholine receptor loss at the developing neuromuscular junction. *J Neurosci* **20**, 3663-3675 (2000).
44. J. Desaki, Y. Uehara, Formation and maturation of subneural apparatuses at neuromuscular junctions in postnatal rats: a scanning and transmission electron microscopical study. *Dev Biol* **119**, 390-401 (1987).
45. B. L. Patton, J. H. Miner, A. Y. Chiu, J. R. Sanes, Distribution and function of laminins in the neuromuscular system of developing, adult, and mutant mice. *J Cell Biol* **139**, 1507-1521 (1997).
46. P. T. Martin, S. J. Kaufman, R. H. Kramer, J. R. Sanes, Synaptic integrins in developing, adult, and mutant muscle: selective association of alpha1, alpha7A, and alpha7B integrins with the neuromuscular junction. *Dev Biol* **174**, 125-139 (1996).
47. G. S. Bewick, C. Young, C. R. Slater, Spatial relationships of utrophin, dystrophin, beta-dystroglycan and beta-spectrin to acetylcholine receptor clusters during postnatal maturation of the rat neuromuscular junction. *J Neurocytol* **25**, 367-379 (1996).
48. P. A. Redfern, Neuromuscular transmission in new-born rats. *J Physiol* **209**, 701-709 (1970).
49. M. C. Brown, J. K. Jansen, D. Van Essen, Polyneuronal innervation of skeletal muscle in new-born rats and its elimination during maturation. *J Physiol* **261**, 387-422 (1976).
50. J. L. Rosenthal, P. S. Taraskevich, Reduction of multiaxonal innervation at the neuromuscular junction of the rat during development. *J Physiol* **270**, 299-310 (1977).
51. J. C. Martinou, D. L. Falls, G. D. Fischbach, J. P. Merlie, Acetylcholine receptor-inducing activity stimulates expression of the epsilon-subunit gene of the muscle acetylcholine receptor. *Proc Natl Acad Sci U S A* **88**, 7669-7673 (1991).
52. M. Mishina *et al.*, Molecular distinction between fetal and adult forms of muscle acetylcholine receptor. *Nature* **321**, 406-411 (1986).
53. V. Witzemann *et al.*, Acetylcholine receptor epsilon-subunit deletion causes muscle weakness and atrophy in juvenile and adult mice. *Proc Natl Acad Sci U S A* **93**, 13286-13291 (1996).

54. A. C. Missias *et al.*, Deficient development and maintenance of postsynaptic specializations in mutant mice lacking an 'adult' acetylcholine receptor subunit. *Development* **124**, 5075-5086 (1997).
55. M. J. Niciu, B. Kelmendi, G. Sanacora, Overview of glutamatergic neurotransmission in the nervous system. *Pharmacol Biochem Behav* **100**, 656-664 (2012).
56. Y. N. Jan, L. Y. Jan, Branching out: mechanisms of dendritic arborization. *Nat Rev Neurosci* **11**, 316-328 (2010).
57. A. K. McAllister, Cellular and molecular mechanisms of dendrite growth. *Cereb Cortex* **10**, 963-973 (2000).
58. P. Garcia-Lopez, V. Garcia-Marin, M. Freire, The discovery of dendritic spines by Cajal in 1888 and its relevance in the present neuroscience. *Prog Neurobiol* **83**, 110-130 (2007).
59. J. DeFelipe, The dendritic spine story: an intriguing process of discovery. *Front Neuroanat* **9**, 14 (2015).
60. M. Sheng, E. Kim, The postsynaptic organization of synapses. *Cold Spring Harb Perspect Biol* **3** (2011).
61. J. E. Brenman *et al.*, Interaction of nitric oxide synthase with the postsynaptic density protein PSD-95 and alpha1-syntrophin mediated by PDZ domains. *Cell* **84**, 757-767 (1996).
62. Y. Hayashi *et al.*, Driving AMPA receptors into synapses by LTP and CaMKII: requirement for GluR1 and PDZ domain interaction. *Science* **287**, 2262-2267 (2000).
63. K. Prybylowski *et al.*, The synaptic localization of NR2B-containing NMDA receptors is controlled by interactions with PDZ proteins and AP-2. *Neuron* **47**, 845-857 (2005).
64. K. U. Bayer, P. De Koninck, A. S. Leonard, J. W. Hell, H. Schulman, Interaction with the NMDA receptor locks CaMKII in an active conformation. *Nature* **411**, 801-805 (2001).
65. K. Shen, T. Meyer, Dynamic control of CaMKII translocation and localization in hippocampal neurons by NMDA receptor stimulation. *Science* **284**, 162-166 (1999).
66. G. Wu, R. Malinow, H. T. Cline, Maturation of a central glutamatergic synapse. *Science* **274**, 972-976 (1996).
67. W. C. Sin, K. Haas, E. S. Ruthazer, H. T. Cline, Dendrite growth increased by visual activity requires NMDA receptor and Rho GTPases. *Nature* **419**, 475-480 (2002).
68. G. Y. Wu, D. J. Zou, I. Rajan, H. Cline, Dendritic dynamics in vivo change during neuronal maturation. *J Neurosci* **19**, 4472-4483 (1999).
69. T. V. Bliss, T. Lomo, Long-lasting potentiation of synaptic transmission in the dentate area of the anaesthetized rabbit following stimulation of the perforant path. *J Physiol* **232**, 331-356 (1973).
70. J. A. Kauer, R. C. Malenka, R. A. Nicoll, A persistent postsynaptic modification mediates long-term potentiation in the hippocampus. *Neuron* **1**, 911-917 (1988).
71. M. L. Mayer, G. L. Westbrook, P. B. Guthrie, Voltage-dependent block by Mg2+ of NMDA responses in spinal cord neurones. *Nature* **309**, 261-263 (1984).
72. R. C. Malenka, M. F. Bear, LTP and LTD: an embarrassment of riches. *Neuron* **44**, 5-21 (2004).
73. M. F. Bear, R. C. Malenka, Synaptic plasticity: LTP and LTD. *Curr Opin Neurobiol* **4**, 389-399 (1994).
74. S. F. Cooke, T. V. Bliss, Plasticity in the human central nervous system. *Brain* **129**, 1659-1673 (2006).

75. A. K. Jones, V. Raymond-Delpech, S. H. Thany, M. Gauthier, D. B. Sattelle, The nicotinic acetylcholine receptor gene family of the honey bee, Apis mellifera. *Genome Res* **16**, 1422-1430 (2006).
76. J. Dupuis, T. Louis, M. Gauthier, V. Raymond, Insights from honeybee (Apis mellifera) and fly (Drosophila melanogaster) nicotinic acetylcholine receptors: from genes to behavioral functions. *Neurosci Biobehav Rev* **36**, 1553-1564 (2012).
77. S. J. Lansdell, N. S. Millar, Dbeta3, an atypical nicotinic acetylcholine receptor subunit from Drosophila : molecular cloning, heterologous expression and coassembly. *J Neurochem* **80**, 1009-1018 (2002).
78. R. Schulz *et al.*, D alpha3, a new functional alpha subunit of nicotinic acetylcholine receptors from Drosophila. *J Neurochem* **71**, 853-862 (1998).
79. E. Sawruk, C. Udri, H. Betz, B. Schmitt, SBD, a novel structural subunit of the Drosophila nicotinic acetylcholine receptor, shares its genomic localization with two alpha-subunits. *FEBS Lett* **273**, 177-181 (1990).
80. E. Sawruk, P. Schloss, H. Betz, B. Schmitt, Heterogeneity of Drosophila nicotinic acetylcholine receptors: SAD, a novel developmentally regulated alpha-subunit. *EMBO J* **9**, 2671-2677 (1990).
81. M. Grauso, R. A. Reenan, E. Culetto, D. B. Sattelle, Novel putative nicotinic acetylcholine receptor subunit genes, Dalpha5, Dalpha6 and Dalpha7, in Drosophila melanogaster identify a new and highly conserved target of adenosine deaminase acting on RNA-mediated A-to-I pre-mRNA editing. *Genetics* **160**, 1519-1533 (2002).
82. B. Bossy, M. Ballivet, P. Spierer, Conservation of neural nicotinic acetylcholine receptors from Drosophila to vertebrate central nervous systems. *EMBO J* **7**, 611-618 (1988).
83. S. J. Lansdell, N. S. Millar, Molecular characterization of Dalpha6 and Dalpha7 nicotinic acetylcholine receptor subunits from Drosophila: formation of a high-affinity alpha-bungarotoxin binding site revealed by expression of subunit chimeras. *J Neurochem* **90**, 479-489 (2004).
84. L. Yu, R. J. LaPolla, N. Davidson, Mouse muscle nicotinic acetylcholine receptor gamma subunit: cDNA sequence and gene expression. *Nucleic Acids Res* **14**, 3539-3555 (1986).
85. A. Baumann, P. Jonas, E. D. Gundelfinger, Sequence of D alpha 2, a novel alpha-like subunit of Drosophila nicotinic acetylcholine receptors. *Nucleic Acids Res* **18**, 3640 (1990).
86. S. J. Lansdell, N. S. Millar, Cloning and heterologous expression of Dalpha4, a Drosophila neuronal nicotinic acetylcholine receptor subunit: identification of an alternative exon influencing the efficiency of subunit assembly. *Neuropharmacology* **39**, 2604-2614 (2000).
87. S. G. Kachalsky, B. S. Jensen, D. Barchan, S. Fuchs, Two subsites in the binding domain of the acetylcholine receptor: an aromatic subsite and a proline subsite. *Proc Natl Acad Sci U S A* **92**, 10801-10805 (1995).
88. D. B. Sattelle *et al.*, Edit, cut and paste in the nicotinic acetylcholine receptor gene family of Drosophila melanogaster. *Bioessays* **27**, 366-376 (2005).
89. E. X. Albuquerque, E. F. Pereira, M. Alkondon, S. W. Rogers, Mammalian nicotinic acetylcholine receptors: from structure to function. *Physiol Rev* **89**, 73-120 (2009).
90. N. Le Novere, M. Zoli, J. P. Changeux, Neuronal nicotinic receptor alpha 6 subunit mRNA is selectively concentrated in catecholaminergic nuclei of the rat brain. *Eur J Neurosci* **8**, 2428-2439 (1996).

91. J. A. Dent, Evidence for a diverse Cys-loop ligand-gated ion channel superfamily in early bilateria. *J Mol Evol* **62**, 523-535 (2006).
92. A. K. Jones, S. D. Buckingham, D. B. Sattelle, Proteins interacting with nicotinic acetylcholine receptors: expanding functional and therapeutic horizons. *Trends Pharmacol Sci* **31**, 455-462 (2010).
93. E. D. Gundelfinger, N. Hess, Nicotinic acetylcholine receptors of the central nervous system of Drosophila. *Biochim Biophys Acta* **1137**, 299-308 (1992).
94. Y. Xu *et al.*, Conformational dynamics of the nicotinic acetylcholine receptor channel: a 35-ns molecular dynamics simulation study. *J Am Chem Soc* **127**, 1291-1299 (2005).
95. V. Bondarenko, T. Tillman, Y. Xu, P. Tang, NMR structure of the transmembrane domain of the n-acetylcholine receptor beta2 subunit. *Biochim Biophys Acta* **1798**, 1608-1614 (2010).
96. F. J. Barrantes, Modulation of nicotinic acetylcholine receptor function through the outer and middle rings of transmembrane domains. *Curr Opin Drug Discov Devel* **6**, 620-632 (2003).
97. J. T. Littleton, B. Ganetzky, Ion channels and synaptic organization: analysis of the Drosophila genome. *Neuron* **26**, 35-43 (2000).
98. K. Chamaon, K. H. Smalla, U. Thomas, E. D. Gundelfinger, Nicotinic acetylcholine receptors of Drosophila: three subunits encoded by genomically linked genes can co-assemble into the same receptor complex. *J Neurochem* **80**, 149-157 (2002).
99. J. Boulter *et al.*, Alpha 3, alpha 5, and beta 4: three members of the rat neuronal nicotinic acetylcholine receptor-related gene family form a gene cluster. *J Biol Chem* **265**, 4472-4482 (1990).
100. B. K. Rana *et al.*, Natural variation within the neuronal nicotinic acetylcholine receptor cluster on human chromosome 15q24: influence on heritable autonomic traits in twin pairs. *J Pharmacol Exp Ther* **331**, 419-428 (2009).
101. A. K. Jones, M. Grauso, D. B. Sattelle, The nicotinic acetylcholine receptor gene family of the malaria mosquito, Anopheles gambiae. *Genomics* **85**, 176-187 (2005).
102. M. De Biasi, Nicotinic mechanisms in the autonomic control of organ systems. *J Neurobiol* **53**, 568-579 (2002).
103. D. Z. Faltine-Gonzalez, M. J. Layden, Characterization of nAChRs in Nematostella vectensis supports neuronal and non-neuronal roles in the cnidarian-bilaterian common ancestor. *Evodevo* **10**, 27 (2019).
104. E. Sawruk, I. Hermans-Borgmeyer, H. Betz, E. D. Gundelfinger, Characterization of an invertebrate nicotinic acetylcholine receptor gene: the ard gene of Drosophila melanogaster. *FEBS Lett* **235**, 40-46 (1988).
105. S. C. Wadsworth, L. S. Rosenthal, K. L. Kammermeyer, M. B. Potter, D. J. Nelson, Expression of a Drosophila melanogaster acetylcholine receptor-related gene in the central nervous system. *Mol Cell Biol* **8**, 778-785 (1988).
106. P. Jonas, A. Baumann, B. Merz, E. D. Gundelfinger, Structure and developmental expression of the D alpha 2 gene encoding a novel nicotinic acetylcholine receptor protein of Drosophila melanogaster. *FEBS Lett* **269**, 264-268 (1990).
107. F. Sgard, L. A. Obosi, L. A. King, J. D. Windass, ALS and SAD-like nicotinic acetylcholine receptor subunit genes are widely distributed in insects. *Insect Mol Biol* **2**, 215-223 (1993).

108. Y. Jin *et al.*, RNA editing and alternative splicing of the insect nAChR subunit alpha6 transcript: evolutionary conservation, divergence and regulation. *BMC Evol Biol* **7**, 98 (2007).
109. C. Dubowy, A. Sehgal, Circadian Rhythms and Sleep in Drosophila melanogaster. *Genetics* **205**, 1373-1397 (2017).
110. M. Dombrovski *et al.*, Cooperative Behavior Emerges among Drosophila Larvae. *Curr Biol* **27**, 2821-2826 e2822 (2017).
111. A. C. Keene *et al.*, Distinct visual pathways mediate Drosophila larval light avoidance and circadian clock entrainment. *J Neurosci* **31**, 6527-6534 (2011).
112. Q. Yuan *et al.*, Light-induced structural and functional plasticity in Drosophila larval visual system. *Science* **333**, 1458-1462 (2011).
113. C. Sheng *et al.*, Experience-dependent structural plasticity targets dynamic filopodia in regulating dendrite maturation and synaptogenesis. *Nat Commun* **9**, 3362 (2018).
114. J. Yin *et al.*, Brain-specific lipoprotein receptors interact with astrocyte derived apolipoprotein and mediate neuron-glia lipid shuttling. *Nat Commun* **12**, 2408 (2021).
115. J. Yin *et al.*, Transcriptional Regulation of Lipophorin Receptors Supports Neuronal Adaptation to Chronic Elevations of Activity. *Cell Rep* **25**, 1181-1192 e1184 (2018).
116. A. Dereeper *et al.*, Phylogeny.fr: robust phylogenetic analysis for the non-specialist. *Nucleic Acids Res* **36**, W465-469 (2008).
117. A. K. Jones, L. A. Brown, D. B. Sattelle, Insect nicotinic acetylcholine receptor gene families: from genetic model organism to vector, pest and beneficial species. *Invert Neurosci* **7**, 67-73 (2007).
118. J. A. Dani, D. Bertrand, Nicotinic acetylcholine receptors and nicotinic cholinergic mechanisms of the central nervous system. *Annu Rev Pharmacol Toxicol* **47**, 699-729 (2007).
119. S. Vernino, M. Amador, C. W. Luetje, J. Patrick, J. A. Dani, Calcium modulation and high calcium permeability of neuronal nicotinic acetylcholine receptors. *Neuron* **8**, 127-134 (1992).
120. P. Seguela, J. Wadiche, K. Dineley-Miller, J. A. Dani, J. W. Patrick, Molecular cloning, functional properties, and distribution of rat brain alpha 7: a nicotinic cation channel highly permeable to calcium. *J Neurosci* **13**, 596-604 (1993).
121. S. Fucile, Ca2+ permeability of nicotinic acetylcholine receptors. *Cell Calcium* **35**, 1-8 (2004).
122. A. Fayyazuddin, M. A. Zaheer, P. R. Hiesinger, H. J. Bellen, The nicotinic acetylcholine receptor Dalpha7 is required for an escape behavior in Drosophila. *PLoS Biol* **4**, e63 (2006).
123. M. C. Kremer *et al.*, Structural long-term changes at mushroom body input synapses. *Curr Biol* **20**, 1938-1944 (2010).
124. F. Leiss *et al.*, Characterization of dendritic spines in the Drosophila central nervous system. *Dev Neurobiol* **69**, 221-234 (2009).
125. C. Wegener, Y. Hamasaka, D. R. Nassel, Acetylcholine increases intracellular Ca2+ via nicotinic receptors in cultured PDF-containing clock neurons of Drosophila. *J Neurophysiol* **91**, 912-923 (2004).
126. S. E. Celniker *et al.*, Unlocking the secrets of the genome. *Nature* **459**, 927-930 (2009).
127. V. R. Chintapalli, J. Wang, J. A. Dow, Using FlyAtlas to identify better Drosophila melanogaster models of human disease. *Nat Genet* **39**, 715-720 (2007).

128. S. Nagarkar-Jaiswal *et al.*, A library of MiMICs allows tagging of genes and reversible, spatial and temporal knockdown of proteins in Drosophila. *Elife* **4** (2015).
129. P. T. Lee *et al.*, A gene-specific T2A-GAL4 library for Drosophila. *Elife* **7** (2018).
130. I. Larderet *et al.*, Organization of the Drosophila larval visual circuit. *Elife* **6** (2017).
131. K. J. Venken *et al.*, MiMIC: a highly versatile transposon insertion resource for engineering Drosophila melanogaster genes. *Nat Methods* **8**, 737-743 (2011).
132. G. B. Watson *et al.*, A spinosyn-sensitive Drosophila melanogaster nicotinic acetylcholine receptor identified through chemically induced target site resistance, resistance gene identification, and heterologous expression. *Insect Biochem Mol Biol* **40**, 376-384 (2010).
133. W. Lu, E. A. Bushong, T. P. Shih, M. H. Ellisman, R. A. Nicoll, The cell-autonomous role of excitatory synaptic transmission in the regulation of neuronal structure and function. *Neuron* **78**, 433-439 (2013).
134. S. Kondo *et al.*, Neurochemical Organization of the Drosophila Brain Visualized by Endogenously Tagged Neurotransmitter Receptors. *Cell Rep* **30**, 284-297 e285 (2020).
135. W. Xu *et al.*, Multiorgan autonomic dysfunction in mice lacking the beta2 and the beta4 subunits of neuronal nicotinic acetylcholine receptors. *J Neurosci* **19**, 9298-9305 (1999).
136. M. Nakayama, E. Suzuki, S. Tsunoda, C. Hama, The Matrix Proteins Hasp and Hig Exhibit Segregated Distribution within Synaptic Clefts and Play Distinct Roles in Synaptogenesis. *J Neurosci* **36**, 590-606 (2016).
137. S. V. Raghu, M. Joesch, S. J. Sigrist, A. Borst, D. F. Reiff, Synaptic organization of lobula plate tangential cells in Drosophila: Dalpha7 cholinergic receptors. *J Neurogenet* **23**, 200-209 (2009).
138. M. Tomizawa, B. Latli, J. E. Casida, Novel neonicotinoid-agarose affinity column for Drosophila and Musca nicotinic acetylcholine receptors. *J Neurochem* **67**, 1669-1676 (1996).
139. R. Schulz *et al.*, Neuronal nicotinic acetylcholine receptors from Drosophila: two different types of alpha subunits coassemble within the same receptor complex. *J Neurochem* **74**, 2537-2546 (2000).
140. I. Hermans-Borgmeyer *et al.*, Neuronal acetylcholine receptors in Drosophila: mature and immature transcripts of the ard gene in the developing central nervous system. *Neuron* **2**, 1147-1156 (1989).
141. P. E. Jonas, B. Phannavong, R. Schuster, C. Schroder, E. D. Gundelfinger, Expression of the ligand-binding nicotinic acetylcholine receptor subunit D alpha 2 in the Drosophila central nervous system. *J Neurobiol* **25**, 1494-1508 (1994).
142. N. Hess, B. Merz, E. D. Gundelfinger, Acetylcholine receptors of the Drosophila brain: a 900 bp promoter fragment contains the essential information for specific expression of the ard gene in vivo. *FEBS Lett* **346**, 135-140 (1994).
143. K. Chamaon, R. Schulz, K. H. Smalla, B. Seidel, E. D. Gundelfinger, Neuronal nicotinic acetylcholine receptors of Drosophila melanogaster: the alpha-subunit dalpha3 and the beta-type subunit ARD co-assemble within the same receptor complex. *FEBS Lett* **482**, 189-192 (2000).
144. P. Schloss, H. Betz, C. Schroder, E. D. Gundelfinger, Neuronal nicotinic acetylcholine receptors in Drosophila: antibodies against an alpha-like and a non-alpha-subunit recognize the same high-affinity alpha-bungarotoxin binding complex. *J Neurochem* **57**, 1556-1562 (1991).

145. R. Schuster, B. Phannavong, C. Schroder, E. D. Gundelfinger, Immunohistochemical localization of a ligand-binding and a structural subunit of nicotinic acetylcholine receptors in the central nervous system of Drosophila melanogaster. *J Comp Neurol* **335**, 149-162 (1993).
146. S. Y. Takemura *et al.*, Cholinergic circuits integrate neighboring visual signals in a Drosophila motion detection pathway. *Curr Biol* **21**, 2077-2084 (2011).
147. M. Tomizawa, J. E. Casida, Selective toxicity of neonicotinoids attributable to specificity of insect and mammalian nicotinic receptors. *Annu Rev Entomol* **48**, 339-364 (2003).
148. P. Wu *et al.*, The Drosophila acetylcholine receptor subunit D alpha5 is part of an alpha-bungarotoxin binding acetylcholine receptor. *J Biol Chem* **280**, 20987-20994 (2005).
149. S. I. Ashraf, A. L. McLoon, S. M. Sclarsic, S. Kunes, Synaptic protein synthesis associated with memory is regulated by the RISC pathway in Drosophila. *Cell* **124**, 191-205 (2006).
150. D. Owald *et al.*, A Syd-1 homologue regulates pre- and postsynaptic maturation in Drosophila. *J Cell Biol* **188**, 565-579 (2010).
151. F. Christiansen *et al.*, Presynapses in Kenyon cell dendrites in the mushroom body calyx of Drosophila. *J Neurosci* **31**, 9696-9707 (2011).
152. C. Kuehn, C. Duch, Putative excitatory and putative inhibitory inputs are localised in different dendritic domains in a Drosophila flight motoneuron. *Eur J Neurosci* **37**, 860-875 (2013).
153. J. M. Blagburn, D. B. Sattelle, Nicotinic acetylcholine receptors on a cholinergic nerve terminal in the cockroach, Periplaneta americana. *J Comp Physiol A* **161**, 215-225 (1987).
154. Y. Dudai, A. Amsterdam, Nicotinic receptors in the brain of Drosophila melanogaster demonstrated by autoradiography with [125I]alpha-bungarotoxin. *Brain Res* **130**, 551-555 (1977).
155. D. Lee, D. K. O'Dowd, Fast excitatory synaptic transmission mediated by nicotinic acetylcholine receptors in Drosophila neurons. *J Neurosci* **19**, 5311-5321 (1999).
156. H. Su, D. K. O'Dowd, Fast synaptic currents in Drosophila mushroom body Kenyon cells are mediated by alpha-bungarotoxin-sensitive nicotinic acetylcholine receptors and picrotoxin-sensitive GABA receptors. *J Neurosci* **23**, 9246-9253 (2003).
157. J. B. Thomas, R. J. Wyman, Mutations altering synaptic connectivity between identified neurons in Drosophila. *J Neurosci* **4**, 530-538 (1984).
158. J. R. Trimarchi, A. M. Schneiderman, Giant fiber activation of an intrinsic muscle in the mesothoracic leg of Drosophila melanogaster. *J Exp Biol* **177**, 149-167 (1993).
159. M. Mejia, M. D. Heghinian, F. Mari, T. A. Godenschwege, New tools for targeted disruption of cholinergic synaptic transmission in Drosophila melanogaster. *PLoS One* **8**, e64685 (2013).
160. J. M. Campusano, H. Su, S. A. Jiang, B. Sicaeros, D. K. O'Dowd, nAChR-mediated calcium responses and plasticity in Drosophila Kenyon cells. *Dev Neurobiol* **67**, 1520-1532 (2007).
161. D. Raccuglia, U. Mueller, Temporal integration of cholinergic and GABAergic inputs in isolated insect mushroom body neurons exposes pairing-specific signal processing. *J Neurosci* **34**, 16086-16092 (2014).

162. M. S. Murmu, J. Stinnakre, E. Real, J. R. Martin, Calcium-stores mediate adaptation in axon terminals of olfactory receptor neurons in Drosophila. *BMC Neurosci* **12**, 105 (2011).
163. I. Cervantes-Sandoval, A. Phan, M. Chakraborty, R. L. Davis, Reciprocal synapses between mushroom body and dopamine neurons form a positive feedback loop required for learning. *Elife* **6** (2017).
164. K. Ueno *et al.*, Coincident postsynaptic activity gates presynaptic dopamine release to induce plasticity in Drosophila mushroom bodies. *Elife* **6** (2017).
165. P. Pyakurel, M. Shin, B. J. Venton, Nicotinic acetylcholine receptor (nAChR) mediated dopamine release in larval Drosophila melanogaster. *Neurochem Int* **114**, 33-41 (2018).
166. O. Barnstedt *et al.*, Memory-Relevant Mushroom Body Output Synapses Are Cholinergic. *Neuron* **89**, 1237-1247 (2016).
167. Y. Ping, S. Tsunoda, Inactivity-induced increase in nAChRs upregulates Shal K(+) channels to stabilize synaptic potentials. *Nat Neurosci* **15**, 90-97 (2011).
168. A. Eadaim, E. T. Hahm, E. D. Justice, S. Tsunoda, Cholinergic Synaptic Homeostasis Is Tuned by an NFAT-Mediated alpha7 nAChR-Kv4/Shal Coupled Regulatory System. *Cell Rep* **32**, 108119 (2020).
169. H. Fotowat, A. Fayyazuddin, H. J. Bellen, F. Gabbiani, A novel neuronal pathway for visually guided escape in Drosophila melanogaster. *J Neurophysiol* **102**, 875-885 (2009).
170. T. M. Khuong *et al.*, Nerve injury drives a heightened state of vigilance and neuropathic sensitization in Drosophila. *Sci Adv* **5**, eaaw4099 (2019).
171. M. Ihara *et al.*, Cofactor-enabled functional expression of fruit fly, honeybee, and bumblebee nicotinic receptors reveals picomolar neonicotinoid actions. *Proc Natl Acad Sci U S A* **117**, 16283-16291 (2020).
172. P. Schloss, I. Hermans-Borgmeyer, H. Betz, E. D. Gundelfinger, Neuronal acetylcholine receptors in Drosophila: the ARD protein is a component of a high-affinity alpha-bungarotoxin binding complex. *EMBO J* **7**, 2889-2894 (1988).
173. T. Perry, J. A. McKenzie, P. Batterham, A Dalpha6 knockout strain of Drosophila melanogaster confers a high level of resistance to spinosad. *Insect Biochem Mol Biol* **37**, 184-188 (2007).
174. S. Kondo, R. Ueda, Highly improved gene targeting by germline-specific Cas9 expression in Drosophila. *Genetics* **195**, 715-721 (2013).
175. C. Sheng *et al.*, Time-lapse Live Imaging and Quantification of Fast Dendritic Branch Dynamics in Developing Drosophila Neurons. *J Vis Exp* 10.3791/60287 (2019).
176. L. A. Kelley, S. Mezulis, C. M. Yates, M. N. Wass, M. J. Sternberg, The Phyre2 web portal for protein modeling, prediction and analysis. *Nat Protoc* **10**, 845-858 (2015).
177. C. Brunet Avalos, G. L. Maier, R. Bruggmann, S. G. Sprecher, Single cell transcriptome atlas of the Drosophila larval brain. *Elife* **8** (2019).
178. M. D. Gordon, K. Scott, Motor control in a Drosophila taste circuit. *Neuron* **61**, 373-384 (2009).
179. M. Nakayama, F. Matsushita, C. Hama, The matrix protein Hikaru genki localizes to cholinergic synaptic clefts and regulates postsynaptic organization in the Drosophila brain. *J Neurosci* **34**, 13872-13877 (2014).
180. T. J. Mosca, L. Luo, Synaptic organization of the Drosophila antennal lobe and its regulation by the Teneurins. *Elife* **3**, e03726 (2014).

181. T. J. Mosca, D. J. Luginbuhl, I. E. Wang, L. Luo, Presynaptic LRP4 promotes synapse number and function of excitatory CNS neurons. *Elife* **6** (2017).
182. D. S. McGehee, L. W. Role, Physiological diversity of nicotinic acetylcholine receptors expressed by vertebrate neurons. *Annu Rev Physiol* **57**, 521-546 (1995).
183. D. Bertrand, J. L. Galzi, A. Devillers-Thiery, S. Bertrand, J. P. Changeux, Mutations at two distinct sites within the channel domain M2 alter calcium permeability of neuronal alpha 7 nicotinic receptor. *Proc Natl Acad Sci U S A* **90**, 6971-6975 (1993).
184. C. L. Morales-Perez, C. M. Noviello, R. E. Hibbs, X-ray structure of the human alpha4beta2 nicotinic receptor. *Nature* **538**, 411-415 (2016).
185. I. Hermans-Borgmeyer *et al.*, Primary structure of a developmentally regulated nicotinic acetylcholine receptor protein from Drosophila. *EMBO J* **5**, 1503-1508 (1986).
186. J. E. Dallman, J. Allopenna, A. Bassett, A. Travers, G. Mandel, A conserved role but different partners for the transcriptional corepressor CoREST in fly and mammalian nervous system formation. *J Neurosci* **24**, 7186-7193 (2004).
187. E. C. Pym, T. D. Southall, C. J. Mee, A. H. Brand, R. A. Baines, The homeobox transcription factor Even-skipped regulates acquisition of electrical properties in Drosophila neurons. *Neural Dev* **1**, 3 (2006).
188. I. Riede, Proliferative genes induce somatic pairing defects in Drosophila melanogaster and allow replication. *Cancer Genet Cytogenet* **97**, 143-154 (1997).
189. S. Nair, N. Agrawal, G. Hasan, Homeostasis of glutamate neurotransmission is altered in Drosophila Inositol 1,4,5-trisphosphate receptor mutants. *Invert Neurosci* **7**, 137-147 (2007).
190. H. R. Jensen, I. M. Scott, S. R. Sims, V. L. Trudeau, J. T. Arnason, The effect of a synergistic concentration of a Piper nigrum extract used in conjunction with pyrethrum upon gene expression in Drosophila melanogaster. *Insect Mol Biol* **15**, 329-339 (2006).
191. H. Wang, X. Chen, T. He, Y. Zhou, H. Luo, Evidence for tissue-specific Jak/STAT target genes in Drosophila optic lobe development. *Genetics* **195**, 1291-1306 (2013).
192. L. H. Zhan, K. A. Hanson, S. H. Kim, A. Tare, R. S. Tibbetts, Identification of Genetic Modifiers of TDP-43 Neurotoxicity in Drosophila. *Plos One* **8** (2013).
193. E. D. Hoopfer, A. Penton, R. J. Watts, L. Q. Luo, Genomic analysis of Drosophila neuronal remodeling: A role for the RNA-binding protein boule as a negative regulator of axon pruning. *Journal of Neuroscience* **28**, 6092-6103 (2008).
194. S. J. Lansdell *et al.*, Host-cell specific effects of the nicotinic acetylcholine receptor chaperone RIC-3 revealed by a comparison of human and Drosophila RIC-3 homologues. *J Neurochem* **105**, 1573-1581 (2008).
195. S. Halevi *et al.*, The C. elegans ric-3 gene is required for maturation of nicotinic acetylcholine receptors. *EMBO J* **21**, 1012-1020 (2002).
196. S. Halevi *et al.*, Conservation within the RIC-3 gene family. Effectors of mammalian nicotinic acetylcholine receptor expression. *J Biol Chem* **278**, 34411-34417 (2003).
197. S. J. Lansdell, T. Collins, J. Goodchild, N. S. Millar, The Drosophila nicotinic acetylcholine receptor subunits Dalpha5 and Dalpha7 form functional homomeric and heteromeric ion channels. *BMC Neurosci* **13**, 73 (2012).
198. S. J. Lansdell *et al.*, RIC-3 enhances functional expression of multiple nicotinic acetylcholine receptor subtypes in mammalian cells. *Mol Pharmacol* **68**, 1431-1438 (2005).

199. T. Dean, R. Xu, W. Joiner, A. Sehgal, T. Hoshi, Drosophila QVR/SSS modulates the activation and C-type inactivation kinetics of Shaker K(+) channels. *J Neurosci* **31**, 11387-11395 (2011).
200. M. Wu, J. E. Robinson, W. J. Joiner, SLEEPLESS is a bifunctional regulator of excitability and cholinergic synaptic transmission. *Curr Biol* **24**, 621-629 (2014).
201. Anonymous, (!!! INVALID CITATION !!! (Gundelfinger and Hess 1992, Broughton, Kane et al. 1996, Kabbani, Nordman et al. 2013)).
202. E. Demir, B. J. Dickson, fruitless splicing specifies male courtship behavior in Drosophila. *Cell* **121**, 785-794 (2005).
203. K. Sato, J. Goto, D. Yamamoto, Sex Mysteries of the Fly Courtship Master Regulator Fruitless. *Front Behav Neurosci* **13**, 245 (2019).
204. X. Chen, R. Rahman, F. Guo, M. Rosbash, Genome-wide identification of neuronal activity-regulated genes in Drosophila. *Elife* **5** (2016).
205. N. Fujita *et al.*, Visualization of neural activity in insect brains using a conserved immediate early gene, Hr38. *Curr Biol* **23**, 2063-2070 (2013).
206. E. Bullitt, Expression of c-fos-like protein as a marker for neuronal activity following noxious stimulation in the rat. *J Comp Neurol* **296**, 517-530 (1990).
207. S. Perez-Sieira, M. Lopez, R. Nogueiras, S. Tovar, Regulation of NR4A by nutritional status, gender, postnatal development and hormonal deficiency. *Sci Rep* **4**, 4264 (2014).
208. S. Gu *et al.*, Brain alpha7 Nicotinic Acetylcholine Receptor Assembly Requires NACHO. *Neuron* **89**, 948-955 (2016).
209. J. A. Matta *et al.*, NACHO Mediates Nicotinic Acetylcholine Receptor Function throughout the Brain. *Cell Rep* **19**, 688-696 (2017).
210. S. C. Vernes, Genome wide identification of fruitless targets suggests a role in upregulating genes important for neural circuit formation. *Sci Rep* **4**, 4412 (2014).
211. M. C. Neville *et al.*, Male-specific fruitless isoforms target neurodevelopmental genes to specify a sexually dimorphic nervous system. *Curr Biol* **24**, 229-241 (2014).
212. J. E. Dalton *et al.*, Male-specific Fruitless isoforms have different regulatory roles conferred by distinct zinc finger DNA binding domains. *BMC Genomics* **14**, 659 (2013).
213. D. H. Tran, G. W. Meissner, R. L. French, B. S. Baker, A small subset of fruitless subesophageal neurons modulate early courtship in Drosophila. *PLoS One* **9**, e95472 (2014).